

THE UNIVERSITY OF CALGARY

**Effects of Elliptical Nozzles on the Flame Stability and Combustion Characteristics  
in a Cross-Flow**

by

Guiping Song

A THESIS

SUBMITTED TO THE FACULTY OF GRADUATE STUDIES  
IN PARTIAL FULFILMENT OF THE REQUIREMENTS FOR THE  
DEGREE OF MASTER OF SCIENCE

DEPARTMENT OF MECHANICAL & MANUFACTURING ENGINEERING

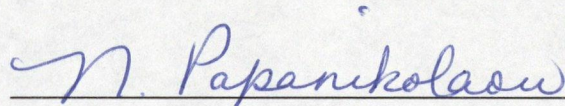
CALGARY, ALBERTA

DECEMBER, 2002

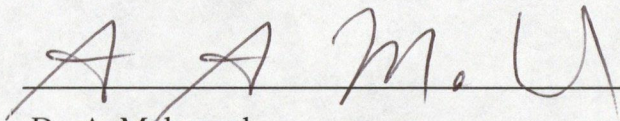
© Guiping Song 2002

UNIVERSITY OF CALGARY  
FACULTY OF GRADUATE STUDIES

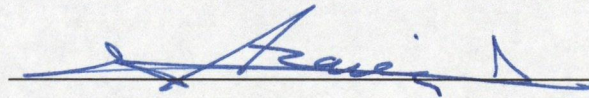
The undersigned certify that they have read, and recommend to the Faculty of Graduate Studies for acceptance, a thesis entitled "Effects of Elliptical Nozzles on the Flame Stability and Combustion Characteristics in a Cross-Flow" submitted by Guiping Song in partial fulfillment of the requirements for the degree of Master of Science in Mechanical Engineering.



Supervisor, Dr. N. Papanikolaou  
Department of Mechanical & Manufacturing  
Engineering



Dr. A. Mohamad  
Department of Mechanical & Manufacturing  
Engineering



Dr. J. Azaiez  
Department of Chemical & Petroleum  
Engineering

Jan. 20, 2003  
Date



## **Abstract**

A sub-scaled flaring system was set up to investigate the effects of elliptical nozzles on flame stability, characteristics, and trajectory of flares in a cross-flow for a range of operating conditions. The thesis presents the experimental results of natural gas flames issuing from circular and different aspect ratios (major axis/minor axis) elliptical nozzles with discharge areas of  $16.4 \text{ mm}^2$ ,  $30.4 \text{ mm}^2$ , and  $93.7 \text{ mm}^2$ . It was found that flames issuing from elliptical nozzles with the major axis perpendicular to the cross-flow have wider stability limits compared with flames issuing from circular nozzles or elliptical nozzles with the minor axis normal to the cross-flow. This is due to the larger recirculation zone on the leeside of the flare stack, counter-rotating vortices, and axis-switching. It was also found that flames from elliptical nozzles were slightly shorter but more yellowish than flames from circular nozzles. This may be an indication of more soot formation and incomplete combustion, which needs to be verified with emission measurements.

## **Acknowledgement**

The author wishes to acknowledge those who have contributed directly or indirectly to this work. The following list is not exhaustive, nor does it include all the contributions of the individuals named; it is a sincere attempt to at least identify the chief area in which each contributed.

Dr. N. Papanikolaou and Dr. A. Mohamad provided their invaluable supervision, guidance, advice, and sustained encouragement throughout the project. The author would like to express sincere appreciation to them.

The author would also like to thank Dr. J. Azaiez for serving on the thesis committee, for his time, consideration and interest in the project.

The author's grateful acknowledgement also goes to her friends who have helped her during the various stages of this work, especially her team worker Vivian Liu.

The financial supports of the University of Calgary, Natural Science and Engineering Research Council of Canada (NSERC), Coordination of University Research for Synergy and Effectiveness (COURSE), and Alberta Energy Research Institute (AERI) are gratefully acknowledged.

I wish to thank my family, particularly my husband, John and my son, Michael, for their love, devotion and unlimited support during my study and my life.

## Table of Contents

Approval Page .....	ii
Abstract .....	iii
Acknowledgement .....	iv
Table of contents .....	v
List of Tables .....	vii
List of Figures .....	viii
List of Symbols .....	xii
 CHAPTER ONE: INTRODUCTION	
1.1 Background and motivations .....	1
1.2 Objectives of the present work .....	4
1.3 Organization of the thesis .....	4
 CHAPTER TWO: LITERATURE REVIEW	
2.1 General .....	5
2.2 Experimental investigations on diffusion flames in a cross-flow .....	5
2.2.1 Stability limits studies .....	6
2.2.2 Flame shape and size studies .....	8
2.2.3 Concentration, velocity and temperature structure studies .....	12
2.2.4 Combustion efficiency and emission studies .....	13
2.2.5 Effects of the nozzle geometry .....	15
2.3 Theoretical investigations of diffusion flames in a cross-flow .....	19
2.4 Other research on combustion improvements by using noncircular jets .....	21
 CHAPTER THREE: EXPERIMENTAL APPARATUS AND PROCEDURES	
3.1 Experimental set up .....	24
3.1.1 Wind tunnel .....	24
Plenum chamber .....	27
Contraction .....	28
Test section .....	28
3.1.2 Fuel supply system .....	29
3.1.3 Nozzles and ignition system .....	31
Jet nozzles .....	31
Ignition system .....	33
3.2 Experimental procedures .....	35
3.2.1 Cross-wind measurements .....	35
3.2.2 Blowout limits measurements .....	35
3.2.3 Flame image collection and processing .....	36

3.3 Wind tunnel uniformity measurements .....	36
CHAPTER FOUR: RESULTS AND DISCUSSIONS	
4.1 Flame stability limits .....	45
4.1.1 General .....	45
4.1.2 Nozzles with discharge area of 16.4 mm <sup>2</sup> .....	46
4.1.3 Nozzles with discharge areas of 30.4 mm <sup>2</sup> and 93.7 mm <sup>2</sup> .....	47
4.1.4 Jet-to-wind momentum ratios at flame blowout as a function of cross-flow velocities .....	52
4.2 Flame visualizations .....	56
4.2.1 Images from nozzles with discharge area of 93.7 mm <sup>2</sup> .....	56
4.2.2 Images from nozzles with discharge area of 30.4 mm <sup>2</sup> .....	58
4.3 Flame trajectories .....	62
4.3.1 General .....	62
4.3.2 Nozzles with discharge area of 93.7 mm <sup>2</sup> .....	63
4.3.3 Nozzles with discharge area of 30.4 mm <sup>2</sup> .....	67
4.3.4 Comparison of the flame trajectories from different nozzles .....	71
Nozzles with discharge area of 93.7 mm <sup>2</sup> .....	71
Nozzles with discharge area of 30.4 mm <sup>2</sup> .....	75
4.4 Mean flame lengths .....	80
4.4.1 Nozzles with discharge area of 93.7 mm <sup>2</sup> .....	80
4.4.2 Nozzles with discharge area of 30.4 mm <sup>2</sup> .....	82
CHAPTER FIVE: CONCLUSIONS AND RECOMMENDATIONS	
5.1 Conclusions .....	84
5.2 Future recommendations .....	86
REFERENCES .....	88
APPENDIX A: Calibration of choked nozzles used in the experiments .....	99
APPENDIX B: Calculations of the major and minor diameter for elliptical nozzle .....	100
APPENDIX C: Results for the wind tunnel uniformity measurements .....	102

## **List of Tables**

<b>Table 3.1</b> Fuel supply capacity in the control panel .....	29
<b>Table 3.2</b> Circular and elliptical nozzles .....	32

## List of Figures

<b>Figure 2.1</b> A schematic of a diffusion flame in a cross-flow .....	10
<b>Figure 2.2</b> A sketch of axis-switching in the elliptic nozzle .....	17
<b>Figure 3.1</b> A schematic diagram of the apparatus .....	25
<b>Figure 3.2</b> The side view of the wind tunnel .....	26
<b>Figure 3.3</b> The plenum chamber and contraction .....	27
<b>Figure 3.4</b> A schematic diagram of fuel supply system .....	30
<b>Figure 3.5</b> A schematic diagram of cross-section of the nozzle tubes .....	31
<b>Figure 3.6</b> A schematic diagram of the ignition system .....	34
<b>Figure 3.7</b> Grids for wind uniformity measurements in the cross-section of the test chamber .....	37
<b>Figure 3.8</b> Velocity profiles at the average cross-wind velocity of 2.4 m/s .....	39
<b>Figure 3.9</b> Variance profiles at the average cross-wind velocity of 2.4 m/s, variance of 0.45 m/s .....	40
<b>Figure 3.10</b> Velocity profiles at the average cross-wind velocity of 6.7 m/s .....	41
<b>Figure 3.11</b> Variance profiles at the average cross-wind velocity of 6.7 m/s, variances of 0.52 m/s .....	42
<b>Figure 3.12</b> Velocity profiles at the average cross-wind velocity of 10.3 m/s .....	43
<b>Figure 3.13</b> Variance profiles at the average cross-wind velocity of 10.3 m/s, variance of 0.065 m/s .....	44
<b>Figure 4.1</b> Flame blowout limits of natural gas from nozzles with a discharge area of 16.4 mm <sup>2</sup> and a 0.89 mm wall thickness .....	49
<b>Figure 4.2</b> Flame blowout limits of natural gas from nozzles with a discharge area of 30.4 mm <sup>2</sup> and a 0.89 mm wall thickness .....	50
<b>Figure 4.3</b> Flame blowout limits of natural gas from nozzles with a discharge area of 93.7 mm <sup>2</sup> and a 0.89 mm wall thickness .....	51
<b>Figure 4.4</b> Jet-to-wind momentum flux ratios versus cross-wind velocities from nozzles with a discharge area of 16.4 mm <sup>2</sup> .....	53
<b>Figure 4.5</b> Jet-to-wind momentum flux ratios versus cross-wind velocities from nozzles with a discharge area of 30.4 mm <sup>2</sup> .....	54



<b>Figure 4.6</b> Jet-to-wind momentum flux ratios versus cross-wind velocities from nozzles with a discharge area of $93.7 \text{ mm}^2$ .....	55
<b>Figure 4.7</b> Long exposure images of diffusion flames in a cross-flow from nozzles with a discharge area of $93.7 \text{ mm}^2$ , ( $V_j = 4 \text{ m/s}$ ) .....	60
<b>Figure 4.8</b> Long exposure images of diffusion flames in a cross-flow from nozzles with a discharge area of $30.4 \text{ mm}^2$ , ( $V_j = 5.5 \text{ m/s}$ ) .....	61
<b>Figure 4.9</b> A sketch of the flame trajectory .....	62
<b>Figure 4.10</b> Flame trajectory from the circular nozzle with a discharge area of $93.7 \text{ mm}^2$ (fuel jet velocity of $4 \text{ m/s}$ ) .....	64
<b>Figure 4.11</b> Flame trajectory from the elliptical nozzle with aspect ratio of 2.4 (nozzle discharge area of $93.7 \text{ mm}^2$ , major axis normal to cross-flow, fuel jet velocity of $4 \text{ m/s}$ ) .....	65
<b>Figure 4.12</b> Flame trajectory from the elliptical nozzle with aspect ratio of 3.3 (nozzle discharge area of $93.7 \text{ mm}^2$ , major axis normal to cross-flow, fuel jet velocity of $4 \text{ m/s}$ ) .....	66
<b>Figure 4.13</b> Flame trajectory from the circular nozzle with a discharge area of $30.4 \text{ mm}^2$ , (fuel jet velocity of $5.5 \text{ m/s}$ ) .....	68
<b>Figure 4.14</b> Flame trajectory from the elliptical nozzle with aspect ratio of 2.5 (nozzle discharge area of $30.4 \text{ mm}^2$ , major axis normal to cross-flow, fuel jet velocity of $5.5 \text{ m/s}$ ) .....	69
<b>Figure 4.15</b> Flame trajectory from the elliptical nozzle with aspect ratio of 3.2 (nozzle discharge area of $30.4 \text{ mm}^2$ , major axis normal to cross-flow, fuel jet velocity of $5.5 \text{ m/s}$ ) .....	70
<b>Figure 4.16</b> Comparison of flame trajectories from different nozzles (discharge area of $93.7 \text{ mm}^2$ , fuel jet velocity $4 \text{ m/s}$ , cross-wind $3.1 \text{ m/s}$ ) .....	72
<b>Figure 4.17</b> Comparison of flame trajectories from different nozzles (discharge area of $93.7 \text{ mm}^2$ , fuel jet velocity $4 \text{ m/s}$ , cross-wind $3.5 \text{ m/s}$ ) .....	72
<b>Figure 4.18</b> Comparison of flame trajectories from different nozzles (discharge area of $93.7 \text{ mm}^2$ , fuel jet velocity $4 \text{ m/s}$ , cross-wind $4.6 \text{ m/s}$ ) .....	73

<b>Figure 4.19</b> Comparison of flame trajectories from different nozzles (discharge area of 93.7 mm <sup>2</sup> , fuel jet velocity 4 m/s, cross-wind 6.3 m/s) .....	73
<b>Figure 4.20</b> Comparison of flame trajectories from different nozzles (discharge area of 93.7 mm <sup>2</sup> , fuel jet velocity 4 m/s, cross-wind 7.8 m/s) .....	74
<b>Figure 4.21</b> Comparison of flame trajectories from different nozzles (discharge area of 93.7 mm <sup>2</sup> , fuel jet velocity 4 m/s, cross-wind 9.6 m/s) .....	74
<b>Figure 4.22</b> Comparison of flame trajectories from different nozzles (discharge area of 93.7 mm <sup>2</sup> , fuel jet velocity 4 m/s, cross-wind 10.3 m/s) .....	75
<b>Figure 4.23</b> Comparison of flame trajectories from different nozzles (discharge area of 30.4 mm <sup>2</sup> , fuel jet velocity 5.5 m/s, cross-wind 3.1 m/s) .....	76
<b>Figure 4.24</b> Comparison of flame trajectories from different nozzles (discharge area of 30.4 mm <sup>2</sup> , fuel jet velocity 5.5 m/s, cross-wind 3.5 m/s) .....	76
<b>Figure 4.25</b> Comparison of flame trajectories from different nozzles (discharge area of 30.4 mm <sup>2</sup> , fuel jet velocity 5.5 m/s, cross-wind 4.6 m/s) .....	77
<b>Figure 4.26</b> Comparison of flame trajectories from different nozzles (discharge area of 30.4 mm <sup>2</sup> , fuel jet velocity 5.5 m/s, cross-wind 6.3 m/s) .....	77
<b>Figure 4.27</b> Comparison of flame trajectories from different nozzles (discharge area of 30.4 mm <sup>2</sup> , fuel jet velocity 5.5 m/s, cross-wind 7.8 m/s) .....	78
<b>Figure 4.28</b> Comparison of flame trajectories from different nozzles (discharge area of 30.4 mm <sup>2</sup> , fuel jet velocity 5.5 m/s, cross-wind 9.6 m/s) .....	78
<b>Figure 4.29</b> Comparison of flame trajectories from different nozzles (discharge area of 30.4 mm <sup>2</sup> , fuel jet velocity 5.5 m/s, cross-wind 10.3 m/s) .....	79
<b>Figure 4.30</b> Flame lengths as a function of wind-to-jet velocity ratio $U_{\infty}/V_j$ (nozzle discharge area of 93.7 mm <sup>2</sup> , fuel jet velocity 4 m/s) .....	81
<b>Figure 4.31</b> Flame lengths as a function of wind-to-jet momentum flux ratio $R_{\infty}$ (nozzle discharge area of 93.7 mm <sup>2</sup> , fuel jet velocity 4 m/s) .....	81
<b>Figure 4.32</b> Flame lengths as a function of wind-to-jet velocity ratio $U_{\infty}/V_j$ (nozzle discharge area of 30.4 mm <sup>2</sup> , fuel jet velocity 5.5 m/s) .....	83
<b>Figure 4.33</b> Flame lengths as a function of wind-to-jet momentum flux ratio $R_{\infty}$ (nozzle discharge area of 30.4 mm <sup>2</sup> , fuel jet velocity 5.5 m/s) .....	83

<b>Figure A.1</b> Calibration curves for the choked nozzles used in the experiments .....	99
---	----

## List of Symbols

$A_c$	circular jet discharge area, (mm <sup>2</sup> )
$A_e$	elliptical jet discharge area, (mm <sup>2</sup> )
$a$	major axis half-width, (mm)
$a/b$	major axis to minor axis ratio
$b$	minor axis half-width, (mm)
$D$	distance downstream of the point of discharge for axis-switching, (mm)
$D_{eq}$	equivalent diameter, (mm)
$D_h$	horizontal direction half-width of the elliptical domain in the cross-section of the test chamber, (cm)
$D_i$	inner diameter of circular nozzle, (mm)
$D_o$	outer diameter of circular nozzle, (mm)
$D_v$	vertical direction half-width of the elliptical domain in the cross-section of the test chamber, (cm)
$M_j$	momentum flux of fuel jet, N
MV	metering valve
$M_v$	density weighted velocity ratio, $M_v = \left( \frac{\rho_j U_j^2}{\rho_\infty U_\infty^2} \right)^{0.5}$
$M_\infty$	momentum flux of cross-wind, N
$P_{abs}$	absolute pressure, (kPa)
PR	pressure regulator
PT	pressure transducer
Re	Reynolds number, $Re_j = V_j D_i / \nu_j$ , $Re_\infty = U_\infty D_{eq} / \nu_\infty$
$R_j$	jet-to-wind momentum flux ratio, $R_j = M_j / M_\infty$
$R_\infty$	wind-to-jet momentum flux ratio, $R_\infty = M_\infty / M_j$
S	solenoid valve
TC	thermocouple
$T$	temperature, (K)
$t$	time
$V_j$	jet velocity, (m/s)

$U_{\infty}$	cross-wind velocity, (m/s)
$X$	axial downstream distance from the nozzle exit, (cm)
$Y_c$	flame trajectory at downstream $X$ (cm) distance, (cm)
$Y_{CO}$	CO volume fraction, % in volume
$Y_{CO_2}$	CO <sub>2</sub> volume fraction, % in volume
$Y_{CH}$	CH volume fraction, % in volume
$\Delta$	lip thickness of the nozzle, (mm)
$\rho_j$	density of jet fuel, (kg/m <sup>3</sup> )
$\rho_{\infty}$	density of air, (kg/m <sup>3</sup> )
$\nu_j$	fuel kinematic viscosity, m <sup>2</sup> /s
$\nu_{\infty}$	air kinematic viscosity, m <sup>2</sup> /s
$\eta_c$	combustion efficiency

### **Subscripts**

abs	absolute
c	circular nozzle
e	elliptical nozzle
eq	equivalent
h	horizontal direction
i	inner
j	fuel jet
o	outer
v	vertical direction
$\infty$	ambient air

## CHAPTER ONE:

### INTRODUCTION

#### 1.1 Background and motivations

Flaring has long been used in the oil, natural gas, and petrochemical industries to manage the disposal of waste gaseous hydrocarbon products from production processes and for emergency use in operational upsets. In some situations gases are flared as a safety precaution during testing of initial well production rates and from wells with small gas production volumes. Therefore, three basic types of flares can be identified: flares at processing facilities, flares that are active for only a few days while testing a new well, and longer term flares used to burn "solution gases", which are light hydrocarbons that vaporize when crude oil is extracted from the high-pressure formation. In Alberta, the majority of flares are of the solution gas type, and there are now about 4,400 of these flares operating, which is a significant decrease from the 5,400 that existed in 1996 (EUB 1999). In 1998, about 93% of the solution gas produced in Alberta was "conserved" or captured for other uses and approximately 7-8% of produced solution gas was flared. More than 131 billion cubic meters of marketable natural gas were produced annually in Alberta, of which more than 22.5 billion cubic meters is solution gas. Approximately 1.8 billion cubic meters of this is flared, raising a number of environmental and health concerns, especially when recent research (e.g., Pohl et al., 1986; Strosher, 1996; Strosher, 2000) have found that some flares do not burn gases as completely as was once thought and the combustion efficiencies ranged from 65% to 85%.

At the same time, increasing societal pressure to reduce greenhouse gases has also directed attention at the flaring practice since on a mass basis, methane has a 21 times



greater global warming potential than carbon dioxide produced from flare combustion (Houghton, et al., 1996). Although there are efforts to reduce the need for flaring, the elimination of all flares is not currently realistic. Therefore, improvements in flaring technology and flare performance standards are required to alleviate at least some of the concerns associated with the flaring practice. To this end, the goal of this research is to develop technology that would ultimately improve the combustion efficiency of flares and reduce harmful emissions.

Flare systems are commonly designed to operate as diffusion type flames that involve the combustion of a non-premixed fuel in atmospheric air. Flame stability is strongly dependent on the fuel jet velocity. When the fuel jet velocity is sufficiently low, the diffusion flame anchors at the burner rim and this flame is called an attached flame. When the fuel jet velocity increases beyond a critical value, the flame base lifts off the burner rim and moves to a stable downstream region. This flame is called a lifted flame and the critical fuel jet velocity is called the lift-off velocity. When the fuel jet velocity is further increased, the flame will eventually extinguish at the blowout limit.

Although extensive studies have been conducted on lift-off and blowout limits and combustion characteristics of diffusion flames, they have been conducted in quiescent (e.g., Kalghatgi, 1981; Pohl, et al., 1986) and co-flow environments (e.g., Gollahalli, et al. 1992; Papanikolaou and Wierzb, 1996, 1997). Research has been conducted in cross-flow but the studies were limited to flames issuing from circular nozzles (e.g., Brzustowski, et al., 1975; Gollahalli, et al., 1975; Birch, et al., 1989; Huang and Chang, 1994; Huang and Yang, 1996; Yoo and Shin, 1994; Bourguignon, et al., 1999; Johnson and Kostiuk, 1999; Majeski, et al., 1999; Poudenx and Kostiuk, 1999;

Bandaru and Turns, 2000; Johnson and Kostiuk, 2000). Flare systems commonly used in flaring operations at oilfield battery sites in Alberta involve a simple circular pipe system with the top two to three meters usually being constructed from stainless steel, and have been associated with inefficient combustion and long, smoky flames (Stroscher, 1996). Since the combustion of such flames is governed by mixing of fuel and air, ensuring adequate air entrainment into the fuel stream can be a means of improving the combustion characteristics of flares.

A simple modification of flare nozzles can be a practical and cost-effective way to improve flare efficiency at oilfield battery sites since near-field mixing can play a significant role in the stability and efficiency of diffusion flames (e.g., Ho and Gutmark, 1987; Schadow et al., 1987; Schadow et al., 1988; Hussain and Husain, 1989; Gutmark et al., 1989; Quinn, 1991; Gollahalli et al., 1992; Zaman et al., 1997).

In the present research, passive flow control methods were studied experimentally as a possible combustion enhancing method for flares under cross-flow conditions. Asymmetric nozzle-tips were designed and their effectiveness on flame stability and combustion characteristics were examined. Elliptical nozzles were employed since they have been known to increase the air entrainment rate, suppress certain harmful emissions, and enhance combustion intensity and efficiency under the certain operating conditions (Ho and Gutmark, 1983, 1985, 1987; Schadow et al., 1987; Hussain and Husain, 1989; Gutmark et al., 1989; Gollahalli et al., 1992; Papanikolaou, N. and Wierzbza, 1996, 1997; Papanikolaou, 1998). Despite the success of this technique in quiescent and co-flow diffusion flames, to the knowledge of the author, it has not been applied to diffusion flames under cross-flow conditions

## **1.2. Objectives of the present work**

The present research is experimental in nature. A sub-scaled flaring system was set up to investigate the flame stability and combustion characteristics of flares in cross-flow for a range of operating conditions. Specific goals of the current research include:

- The design and construction of a sub-scaled flaring system,
- The design of elliptical nozzle tips with different aspect ratios,
- The investigation of the flame stability and combustion characteristics of flares burning natural gas,
- The verification of the effectiveness of the designed devices by testing the flame blowout limits and conducting flame visualization studies, and
- The optimization of the designed nozzle tips.

## **1.3 Organization of the thesis**

The contents of the remaining chapters of this thesis are as follows:

Chapter 2: A literature review of the experimental and theoretical studies on diffusion flames in a cross-flow and the effects of the nozzle geometries are presented.

Chapter 3: The experimental methods and apparatus used in the present work are described.

Chapter 4: The results of the research including the stability limits, flame visualization, and flame trajectory analyses of diffusion flames in a cross-flow under different operating conditions are presented and discussed.

Chapter 5: Concluding remarks are summarized and recommendations for future work are suggested. This is followed by the references used in this thesis, and appendices.

## **CHAPTER TWO:**

### **LITERATURE REVIEW**

#### **2.1 General**

Numerous studies on diffusion flames have been reported in open literature. Some of these investigations were experimental while the others were theoretical in nature. The following sections present previous research on diffusion flames.

#### **2.2 Experimental investigations on diffusion flames in a cross-flow**

Diffusion flames in a quiescent atmosphere (e.g., Kalghatgi, 1981; Pohl, et al., 1986) or co-flowing stream of air (e.g., Gollahalli, et al. 1992; Papanikolaou and Wierzbza, 1996, 1997) have been studied in the past. Several researchers (e.g., Kamotani and Greber, 1972; Stoy and Ben-Haim, 1973; Fearn and Weston, 1974; Crabb, et al., 1981; Fric and Roshko, 1994) have studied isothermal non-reacting systems in which the same fluid, usually air, has been used in both the jet and the cross-flow, and buoyant heated jets have been studied by Ramsey and Goldstein (1971), Kamotani and Greber (1972), and Ayoub (1973). Research has also been conducted on reacting diffusion flames in a cross-flowing air or cross-wind. For example, Brzustowski, et al. (1975) investigated the flame length and trajectory of a turbulent hydrogen diffusion flame in a cross-flow while Gollahalli, et al. (1975) studied the characteristics, such as flame size, length, and trajectory of a turbulent propane diffusion flame in a cross-wind. Birch, et al. (1989) measured the concentration and temperature fields of a non-reacting turbulent natural gas jet in a cross flow and found that the presence of the counter-rotating vortices caused the jet to be of a kidney-shaped cross-section.

Yoo and Shin (1994) employed direct color and reactive Mie scattering techniques for visualizing the flow of jet-diffusion flames in cross winds. Bourguignon, et al. (1999), Johnson, et al. (1998, 1999a, b), Johnson and Kostiuk (1999), Majeski, et al. (1999a, b), Poudenx and Kostiuk (1999), Bandaru and Turns (2000), Johnson and Kostiuk (2000) have done extensive studies on the combustion efficiency, emissions, flame structures, and size and trajectory of diffusion flames in cross flow. These studies were conducted on circular jets in reacting diffusion flames, and none of them were involved in elliptical jets in a cross-wind.

### **2.2.1 Stability limits studies**

Kalghatgi (1981b) conducted extensive stability limits research on diffusion flames in a cross-flow using a variety of gases, such as, propane (99% purity), methane (99% purity), ethylene (95% purity) and commercial butanes (28% isobutene, 42% n-butane, 26% propane, and 4% other hydrocarbons). He concluded that for a given burner and gas, a stable flame was not possible if the cross-wind velocity was greater than a limiting value (depending on the diameter of the nozzles); however, for the cross-flow velocity lower than that limit, there were two blow-out limits. Kalghatgi pointed out that the lower and upper blowout limits of the flames in a cross-wind were much lower and higher than those in the quiescent air environment, respectively. In other words, the flame stability range is wider for the flame in a cross-flow compared with a flame in quiescent air. At the upper stability limit, the intensity of turbulence was larger in a jet in a cross-wind than that in a jet in still air, and hence the turbulent burning velocity increased and improved the stability limit. Kalghatgi also correlated experimental data and reported a non-dimensional stability curve for diffusion flames in a cross-wind for various fuels.

The results were limited to jet diameters ranging from 2 mm to 20 mm under cross-wind velocities ranging from 3 m/s to 8 m/s, and high jet-to-crosswind momentum flux ratios.

Kibrya (1987) conducted experimental investigations on the blowout characteristics of a jet diffusion flame in a co- and cross-flowing air. The experiments were carried out with and without the introduction of an auxiliary fuel through a number of small pilot jets uniformly distributed around the main central fuel jets with diameters ranging from 1.0 mm to 2.5 mm. The tests were conducted in a 150 mm diameter vertical chamber for the co-flowing air study and a 500 mm diameter horizontal chamber for the cross-flowing air study. The majority of the tests were performed with methane of commercial purity ( $> 96\%$ ). He observed that the blowout limits of flames in a cross-flowing stream of air were higher than those in a co-flowing air. However, all the experiments were performed using small diameter nozzles; the largest diameter was 2.5 mm.

Huang and Chang (1994) investigated propane diffusion flames in a cross-flow with a low momentum flux ratios. They conducted the experiments in a small wind tunnel with a test section of 30 cm x 30 cm x 110 cm; the nozzle was a stainless steel tube with an inner diameter of 5 mm and outer diameter of 6.4 mm. The wind velocity varied from 4 m/s to 18 m/s. The gas used was commercial grade propane with compositions of 95% propane, 3.5% ethane, and 1.5% butane. They also concluded that there were two blowout limits, lower and upper stability limits, for a jet flame in a cross-flow. However, they categorized the stability domain into three regimes: *subcritical regime*, where the upper stability limit increased as the cross-wind velocity increased; *critical regime*, where the upper stability limit decreased as the cross-wind velocity increased; *supercritical*



*regime*, where the upper stability limit again increased with an increase in the cross-wind velocity.

## 2.2.2 Flame shape and size studies

The flame size and shapes have been extensively studied by many researchers (e.g., Brzustowski, et al., 1975; Gollahalli, et al., 1975; Becker et al., 1981; Kalghatgi, 1983; Birch, et al., 1989; Huang and Chang, 1994; Yoo and Shin, 1994; Majeski, et al., 1999a, b; Huang and Wang, 1999).

Gollahalli, et al. (1975) investigated the characteristics of a turbulent propane diffusion flame in a cross-flowing air stream. The experiments were carried out in an open-jet wind tunnel with a 5 mm diameter fuel nozzle. It was observed that the main parameter influencing the trajectory, size, and length of turbulent hydrocarbon flames in a cross-wind was the momentum flux ratio of the jet to the cross-wind,  $R_j$ .

$$R_j = M_j / M_\infty = (\rho_j V_j^2) / (\rho_\infty U_\infty^2)$$

Where  $M_j$  and  $M_\infty$  are the momentum flux of fuel jet and cross-wind, respectively;  $\rho_j$  and  $V_j$  are the density and velocity of fuel jet; and  $\rho_\infty$  and  $U_\infty$  are the density and velocity of the cross-flowing air, respectively. Similar results were obtained by Brzustowski, et al. (1975) with turbulent hydrogen flames in a cross-wind and by researchers in the Combustion and Environment Group at the University of Alberta in their flare research project (Interim report, Dec. 2000). Urson et al. (2001) reported similar conclusions from numerical analysis for non-reacting and reacting turbulent jets in a cross-flow.

It was observed that with a low momentum flux ratio  $R_j$ , “downwash” occurs as a portion of the combusting gases is drawn into the low-pressure region on the leeside of

the stack. The flames were bent over in the downstream direction of the cross-wind and were stabilized in the wake of the stack. The overall flame appeared blue due to the intense mixing of the fuel jet and ambient air, except in the vicinity of the stack, where a planar vortex was attached to the burner tube and a small luminous yellow region, defined as “recirculation zone”, was observed. With an increase in  $R_j$  (or increase in the jet velocity), this luminous yellow region moved closer to the tip of the stack and increased in size as the flame length became longer. Above a certain  $R_j$  value, the flame detached from the stack and stabilized above and downstream of the stack. Accordingly, the flame was categorized into three color regions: the *initial blue region*, where intense mixing of the fuel and air occurs, followed by the *luminous yellow region*, where fuel pyrolysis take place, followed by the *orange-red region*, where unburned carbon particulates radiate (**Figure 2.1**). These researchers also observed the kidney-shaped counter-rotating vortices by immersing a painted wire mesh into the cross section of the flames. Similar observations were also obtained by Birch, et al. (1989) in the experimental study of a turbulent natural gas jet in a cross-flow.

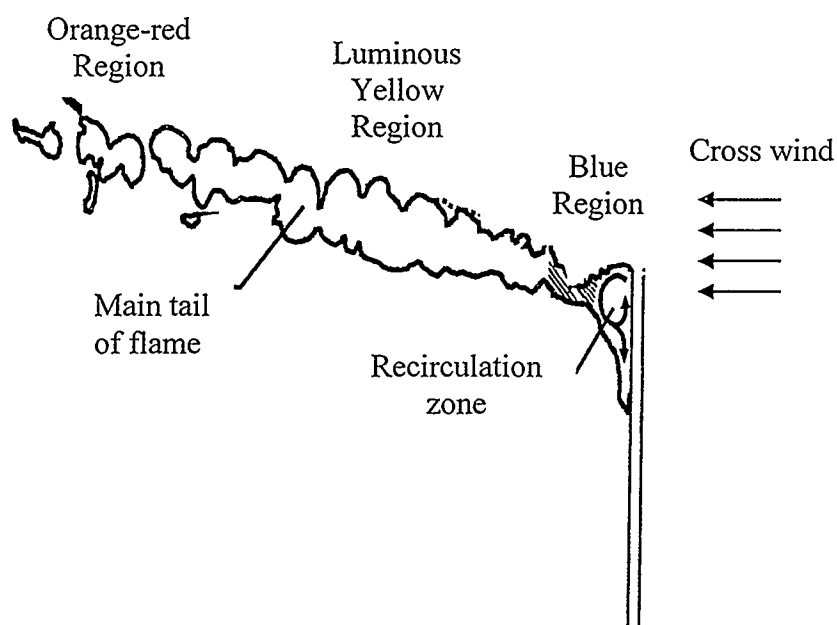


**Figure 2.1** A schematic of a diffusion flame in a cross-flow

Kalghalgi (1983) investigated the visible shape and size of a turbulent hydrocarbon diffusion flame in a cross-wind by using a large wind tunnel with a cross-section of 2 m by 2.65 m. The cross-wind velocity ranged from 2.7 m/s to 8.1 m/s and burners of 6, 10, 12, 14 and 22 mm diameters were used. The flame shape and size were obtained with the burners in different angles to the wind direction in the wind tunnel. With burners normal to the cross-wind direction, the shape and size of the flames were correlated with the burner diameter, the burner exit velocity, the cross-wind velocity, and the density of the burning gas. However, these results were limited to high jet-to-wind momentum ratios, and hence are not applicable for solution gas flare situations in which the velocity ratio is approximately unity.

Huang and Chang (1994), Huang and Wang (1999), and Majeski et al. (1999 a, b) studied flame size and trajectory in a reacting flow. Huang and Chang (1994) and Huang

and Wang (1999) conducted flame visualization studies to document the flow structures of a combustng jet in the cross-flow. They identified the flame configuration in each stability regime (i.e., *sub-critical*; *critical*; and *supercritical*) by direct visual inspection and by short and long exposure photographs. Six characteristic modes in sub-critical and critical regimes and five modes in the supercritical regime were identified by changing the jet-to-wind momentum ratios from low to high in the different regime. The flames were characterized as *down-washed*, *flashing*, *developing*, *dual*, *flickering*, and *pre-blowoff flames* in the sub-critical regime. They also pointed out that in the supercritical regime, the recirculating blue flame around the leeside of the stack always existed. The burner served as a flame holding device forming a recirculation zone, resulting in an upper flame stability limit to increasing with an increase in the cross-wind velocities.

Majeski et al. (1999 a, b) carried out the experiment on the size and trajectory of a flare in a cross-flow. The experiments were operated in a closed-loop wind tunnel with a cross-section of 2.4 m by 1.2 m. The fuel was commercial grade propane with the purity of 98%. The nozzle was a circular tube with inner and outer diameters of 22.1 mm and 24.7 mm, respectively. The cross-wind velocity ranged from 0.8 m/s to 1.2 m/s. The jet-to-wind velocity ratio ranged from 0.29 to 1.3. The mean length and angle of the visible flames were presented as functions of the wind speed ( $U_\infty$ ), velocity ratio ( $V_j/U_\infty$ ), and density weighted velocity ratio ( $M_v$ )

$$M_v = [(\rho_j V_j^2) / (\rho_\infty U_\infty^2)]^{0.5}$$

Based on the relative magnitude of buoyant forces associated with the hot products of combustion and the momentum flux of the cross-flow, the flames were categorized as: *trapped in the recirculation zone*, *deflected downward*, and *above the stack tip*.

### 2.2.3 Concentration, velocity and temperature structure studies

A number of researchers (e.g. Birch, et al., 1989; Botros and Brzustowski, 1989; Askari, et al., 1990; Huang and Yang, 1996; Smith and Mungal, 1998; Poudenx and Kostiuk, 1999) have focused on the investigations of the concentration, velocity and temperature structures of diffusion flames in a cross-flow.

Birch, et al. (1989) carried out the experimental work on the jet concentration of non-reacting turbulent natural gas jets, as well as jet ignitability, jet flame temperature and radiation of reacting jets in cross flows. They observed the kidney-shaped cross-section, which arises through the presence of the counter-rotating vortices in both the non-reacting and reacting jets. However, their study was based on one jet geometry (10.26 mm ID circular pipe, 76.2 m/s mean jet exit velocity, and 5 m/s cross-wind velocity). Further studies are required over a wide range of operating conditions to verify their conclusions.

Askari, et al. (1990) carried out a field scale experiment on a test site using a 5 m high steel vent stack with a nominal internal diameter of 300 mm. The fuel used was natural gas containing between 92% to 95% methane by volume. The concentration of natural gas in the surrounding ambient air was measured in order to assess the effect of atmospheric venting of flammable gas. The trajectory of the fuel was affected by the changes of the wind directions which were governed by convective mass transfer in the near-field of the jet, but diffusive mass transfer in the far-field.

Huang and Yang (1996) investigated the temperature and concentration fields of burner attached flames in cross-flow. They pointed out that the temperature and CO, CO<sub>2</sub> and O<sub>2</sub> concentration structures of the burner-attached jet flames in cross flow were

closely related to the characteristic flame modes which were categorized by Huang and Chang (1994) due to the complicated interaction among the cross flow, fuel jet and burner tube.

Recently, Poudenx and Kostiuk (1999) investigated plume structures of a flare in a cross-flow. The experiment was conducted in a low-speed, closed-loop wind tunnel facility. Two-dimensional mappings of mean temperatures at various downstream positions were reported. The plume structures were categorized into three shapes: *kidney shaped*, *double peaked*, and *single peaked plumes* which were the result of the flame interacting with the counter-rotating vortices associated with the bending of the jet and the vortices shed from the wake of the flare stack.

#### **2.2.4 Combustion efficiency and emission studies**

Many researchers (e.g. Gollahali, 1978; Ellzey, et al., 1990; Stroscher, 1996; Johnson et al., 1998; Bourguignon et al., 1999; Johnson et al., 1999a, b; Johnson and Kostiuk, 1999; Poudenx and Kostiuk, 1999; Bandaru and Turns, 2000; Johnson and Kostiuk, 2000; U of A, 2000; Prybysh, 2002) have investigated the combustion efficiencies and emissions from diffusion flames in a cross-flow. Gollahali (1978) investigated the aerodynamic and diluent effects on the emissions of nitrogen oxides from hydrocarbon diffusion flames. He pointed out that the quantities of NO and NO<sub>2</sub> generated in a diffusion flame was strongly influenced by the structure of flame. Ellzey, et al. (1990) studied the total soot yield from a propane diffusion flame in cross-flow. They found that the orientation of the fuel jet relative to the air stream had a significant effect on the flame shape and soot yield, and the jet diameter did not affect the soot yield when the velocity was held constant. Bandaru and Turns (2000) investigated the effects



of jet, cross-flow and pilot-flame parameters on emissions from a turbulent jet in a cross-flow. They concluded that high levels of unburned hydrocarbons and CO emissions, along with high ratios of NO<sub>x</sub> were obtained from cross-flow flames possibly due to local flame quenching brought by the rapid mixing of fuel with the cross-flow air. Prybysh (2002) studied the production of toxic emissions of stripped fuel (e.g. methane, propane), gaseous compounds (e.g. aldehydes, PAHs), and particulate matters (e.g. soot, smoke) from diffusion flames in a cross-flow. The results showed that no gaseous compounds were found in detectable quantities, however, particulate compounds were found in propane jets. Stroscher (1996) found more than 150 kinds of poly-nuclear aromatic hydrocarbon (PAH) emitted from flares and combustion efficiencies were as low as 64%. These findings raised concerns and drew more attentions to the flare practice.

Researchers in the Combustion and Environment Group at the University of Alberta (e.g. Johnson et al., 1998; Bourguignon et al., 1999; Johnson et al., 1999a, b; Johnson and Kostiuk, 1999; Matthew et al., 1999; Poudenx and Kostiuk, 1999; Johnson and Kostiuk, 2000) conducted experiments on the combustion efficiencies of hydrocarbons in diffusion flames. Bourguignon et al. (1999) used a closed-loop wind tunnel to collect products of combustion for the purpose of measuring the combustion efficiency of flames in a cross-flow. They defined combustion efficiency as:

$$\eta_c = \frac{\frac{d}{dt} \left( \frac{Y_{CO_2}}{T} \right)}{\frac{d}{dt} \left( \frac{Y_{CO_2}}{T} \right) + \frac{d}{dt} \left( \frac{Y_{CO}}{T} \right) + \frac{d}{dt} \left( \frac{Y_{HC}}{T} \right)}$$

Where  $Y$  is volume fraction,  $T$  is temperature,  $t$  is time and the subscripts identify the various species. They claimed that their method was a more accurate and robust approach

than the typical methodologies, such as, single point sampling, line of sight measurement, and plume collection methods in open atmospheric flares. However, the method was limited to the combustion products of gaseous fuels and little or no soot concentrations were assumed.

Johnson et al. (1998, 1999a, 1999b) used the same set-up as Bourguignon et al. (1999) to investigate flare combustion efficiencies in cross-flow. They pointed out that the combustion efficiency of a propane flame was strongly dependent on the cross flow velocity. In addition, Johnson and Kostiuk (1999) investigated the effects of fuel diluents on the efficiencies of diffusion flames in a cross flow. A variety of natural gas/carbon dioxide fuel mixtures were used in the experiments. They concluded that the increased CO<sub>2</sub> fraction and cross-flow had a significant adverse effect on the efficiency of the combustion process. Johnson and Kostiuk (2000) also investigated the efficiencies of low-momentum diffusion flames in cross flows. In their study, propane, natural gas, and propane/CO<sub>2</sub> were used as fuels. They found that increasing cross-wind velocities affected the combustion efficiency adversely, whereas when the jet velocities were increased, the flames were less susceptible to the effects of the cross flow. However, because these studies were undertaken in the closed-loop wind tunnel, there were questions of relevancy to practical situations since the accumulation of the combustion products or the depletion of oxygen in the tunnel during the test altered combustion characteristics.

#### **2.2.5 Effects of the nozzle geometry**

There are a number of parameters that affect flare combustion in a cross-flowing air stream including but not limited to, cross-wind velocity, jet velocity, fuel density, fuel

compositions, temperature, and nozzle geometry. The mixing of the fuel and ambient air is a key role in flare combustion. Much effort has been spent to control the flow actively or passively for mixing augmentation. Active control involves external acoustical or mechanical forcing of the flow, and passive control is based on changing the initial conditions of the jet by changing the nozzle geometry, for example, by using noncircular nozzles. As a passive flow control method, asymmetric nozzle tips have been studied extensively in still air or co-flow conditions by researchers, such as Gutmark and his colleagues (1985, 1987, 1989); Schadow et al. (1987); Hussain and Husain (1989); Quinn (1991); Verma and Rathakrishnan (1996); Zaman (1996, 1997). To the knowledge of author, no studies have been reported on noncircular nozzles in a cross flow. Therefore, the following literature review documents the characteristics of flames issuing from noncircular nozzles in quiescent or co-flow environments.

There have been many experimental studies (Ho and Gutmark, 1985; Ho and Gutmark, 1987; Schadow et al., 1987; Hussain and Husain, 1989; Quinn, 1991; Verma and Rathakrishnan, 1996; Zaman, 1996; Zaman et al., 1997; Gutmark and Grinstein, 1999) focused on the flow structure of cold three-dimensional jets such as rectangular, triangular and elliptical jets. Of these irregular jets, an elliptical jet was the least complex because of the smooth variation in the azimuthal curvature, which prompted authors to conduct research using elliptical nozzles. Ho and Gutmark (1983) found that an elliptical jet with a small aspect ratio (2:1) could substantially increase the entrainment by three to eight times (depending on the axial locations) higher than that of a circular jet, suggesting that an asymmetric nozzle jet with a small aspect ratio could be an effective passive enhancement device for entrainment. Later, Ho and Gutmark (1985, 1987) carried out

experiments on a submerged forced elliptical water jet and on an unforced elliptical cold air jet with major-to-minor diameter ratio of 2:1. They found that the coherent structure switched axis due to the self-induction of the asymmetric distribution of vorticity. The vortex near the minor axis spread greater than that of the major axis. Eventually, the jet became wider in the minor axis plane (the plane containing the minor axis of the nozzle) than in the major axis plane (the plane containing the major axis of the nozzle). The jet cross-section appeared to have switched at some distance  $D$  downstream of the point of discharge (see **Figure 2.2**, Hussain and Husain, 1989).

The azimuthal distortions were responsible for engulfing large amounts of surrounding fluid into the jet. This characteristic made the noncircular jets superior to the conventional circular jet in terms of the enhancement of mixing.

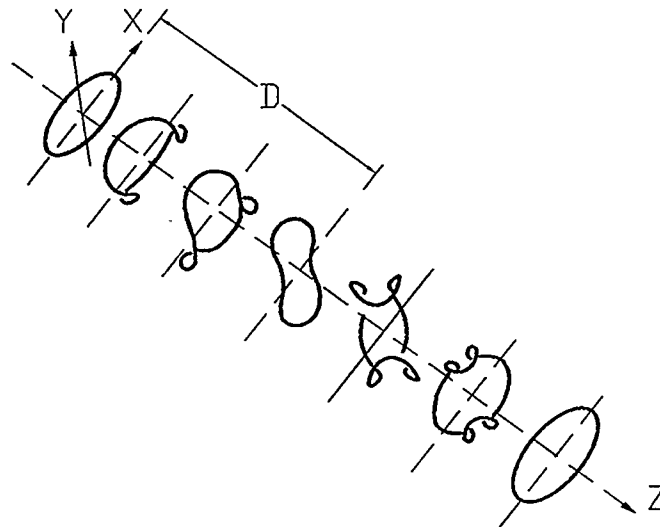


**Figure 2.2** A sketch of axis-switching in the elliptic nozzle

Schadow et al. (1987) investigated the enhancement of mixing in non-reacting and combustion jets with circular and elliptical nozzles. It was found that the jet from elliptical nozzles mixed faster with the co-flowing ducted stream than that from circular nozzles. However, the results were limited to high Reynolds number. It was also reported that the switching of the axes in an initially turbulent jet occurred at a location farther downstream than that in an initially laminar jet (Hussain and Husain, 1989).

The results from these cold flow studies could not always be easily extrapolated to flames and hence necessitated the investigation of three-dimensional jet flames (Gollahalli and Prabhu, 1990; Prabhu and Gollahalli, 1991; Gollahalli et al., 1992; Gollahalli, 1999). These studies were focused on the velocity and temperature fields, and emission indices of ignited elliptical jets. Elliptical nozzle flames were reported to have higher temperatures and concentrations of carbon dioxide and nitrogen oxide, but lower flame radiation and concentrations of soot and carbon monoxide than for circular flames.

The stability limits of lifted flames issuing from elliptical nozzles (with a discharge area of  $71 \text{ mm}^2$ ) into a low co-flowing stream velocity (of  $0.66 \text{ m/s}$ ) were adversely affected by the ellipticity of the nozzle geometry (Prabhu and Gollahalli, 1991). The reduced stability for nozzles of higher aspect ratios (of greater than 2) was attributed to the development of the azimuthal deformations and higher turbulence levels that had a tendency to dilute the flame base region in lifted flames due to intense small-scale fluctuations. However, Schadow et al. (1984), who employed large elliptical nozzles in ducted rockets, reported the existence of an optimum aspect ratio. They found that a jet with an aspect ratio of 3 yields a greater jet spread and higher combustion efficiency than jets with aspect ratios of 2 and 3.5. Another researcher (Papanikolaou, 1998) reported that

the optimum aspect ratio with respect to the blowout limits for attached flames was 1.4 for a 28 mm<sup>2</sup> jet. The blowout limits of lifted flames were not affected by varying the aspect ratio; this was because the flame stabilization region was too far downstream of the jet rim for a change in the nozzle configuration to exert a visible effect on the blowout limits (Papanikolaou and Wierzb, 1996, 1997). Such contradictory behavior may have been the result of the scaling (Chen, 1981).

### **2.3 Theoretical investigations of diffusion flames in a cross-flow**

A number of investigators have studied jet flames in a cross-flow through semi-empirical modeling or computation. For example, Escudier (1972) developed simple integral models, while Botros and Brzustowski (1979) based predictions of the structure of a turbulent reacting jet in a cross-flow on finite-difference solutions of the three-dimensional elliptical equations of fluid flow. Adler and Baron (1979) used a quasi-three-dimensional integral method to solve the problem of the isothermal incompressible turbulent jet. In 1986, Karagozian developed a two-dimensional model for a turbulent jet injected normally into a uniform cross flow. In this study, emphasis was placed on the counter-rotating vortex pair associated with the jet and the prediction of the flame length and shape based on the entrainment of the oxidizer into the fuel jet. Karagozian and Nguyen (1986) also investigated the effects of the heat release and flame distortion in a transverse fuel jet by using an analytical model. Results indicated that the heat release in the reaction reduced the degree of cross flow penetration by the flame, and buoyancy played a lesser role in the flame development than that of the jet momentum.

Cook (1990) presented an integral model for calculating the structure of turbulent diffusion jet flames in a cross-flow. The results were in good agreement with



experimental data in the prediction of flame trajectory and length. However, numerical models developed by Fairweather et al. (1991) in predictions of flame trajectory and length were only in reasonable qualitative agreement with experimental studies by Birch et al. (1989); Fairweather et al. (1992) also developed a numerical model for predictions of radiative heat transfer from a turbulent reacting jet in a cross-wind.

Hernandez et al. (1995) applied a numerical model in a co-flow and cross-flow situation to predict the temperature distribution, which was verified by experimental data. Urson, et al. (2001) employed a numerical model to study the interaction of radial jets with a reacting and non-reacting cross-flow in a confined round pipe and results were compared to the experimental studies by Popovic, et al. (2000). The two results were not in agreement and an advanced model was required to predict the combustion more precisely.

Escudier (1972) presented a theoretical treatment of the motion of a turbulent gas jet burning in an oxidizing cross-flow. He suggested that the influence on the motion of thermal-radiation losses to the surroundings was likely to be one of secondary importance. Also, buoyancy forces, generated by the release of thermal energy during the combustion process, had a negligible effect on the motion until far downstream. Escudier also concluded that species concentrations were strongly coupled with the plume temperature. However, these conclusions were based on the following assumptions: the cross-flow velocity was steady and non-turbulent; the fluid entrainment rates were proportional to the magnitudes of the velocity differences between the plume velocity and cross-flow velocity; and the combustion of a gaseous hydrocarbon fuel was complete

with no consideration to dissociation or the production of intermediate species, such as CO and NO<sub>x</sub>.

In the study by Fairweather et al. (1991), they predicted the trajectory and length of the reacting jet in a cross-flow taking the influence of the cross-flow-to-jet velocity ratio into consideration. Later, they predicted the flame temperature distribution using one cross-flow-to-jet velocity ratio ( $V_j/U_\infty=15.2$ ). Both predictions were compared with the results from experimental work. The prediction of the mean temperature field for one particular velocity ratio agreed closely with the experimental results while the prediction of trajectory and length of flame were in reasonable qualitative agreement with experimental data. However, these predictions were limited to flame lift-off and radiative heat loss which was discussed in another study by Fairweather et al. (1992).

In summary, there is no experimental investigation on non-circular nozzles in a cross flow and three dimensional, unsteady flows.

## **2.4 Other research on combustion improvements by using noncircular jets**

There have been investigations of fuel combustion under various environments. Gutmark et al. (1989) studied the growth and turbulent characteristics of subsonic and supersonic circular and small-aspect-ratio ( $a/b = 3$ ) elliptical and rectangular jets in cold and hot flows. They pointed out that the introduction of sharp corners in, for example, triangular or square nozzles could increase significantly the small-scale turbulence intensity at these corners relative to the flat segments of the nozzle. The coexistence of regions with large-scale structures and others with fine-scale structures in the same flow of triangular and square jets was advantageous for combustion. Gutmark et al. (1991) also investigated non-reacting and ignited flows under subsonic, sonic, and supersonic

conditions using noncircular injectors. The results from square, equilateral, and isosceles-triangular nozzles were compared to the result from the circular nozzle and they concluded that the combination of large-scale mixing at the flat sides with fine-scale mixing at the vertices was beneficial for combustion. Large-scale structures provided bulk mixing between the fuel and air; whereas fine-scale mixing contributed to the reaction rate and to better flame-holding characteristics.

Attention was raised on the application of vortex generators. Different azimuthal perturbation methods, including corrugated, lobed, or indented nozzle edges, vortex generators, or other nozzle shaping concepts were used to achieve the controlled stream-wise vortex generation. For instance, Zaman (1994) conducted experiments on axisymmetric jets with vortex generators, while Zaman (1996) investigated axis switching and spreading of an asymmetric jet and the role of coherent structure dynamics. Reeder and Samimy (1996) investigated the evolution of a jet with vortex-generation tabs using real-time visualization and quantitative measurements. Reeder, et al. (1996) also conducted the investigation of the effect of tabs on supersonic jets using advance diagnostics. Their results showed an influence on both the convection of the shear layer eddies and the characteristics of the upstream bow shock and separation region. This information could be used as the theoretical foundations for the future investigation of the elliptical nozzles with tabs (e.g. delta tabs) in the cross flow.

There have been no experimental investigations reported on the effects of the elliptical nozzle on the flame stability and combustion characteristics of flares in a cross flow. Most of the studies have used either circular nozzles in a co- or cross-flow or elliptical nozzles in still air or co-flow conditions. Experimental investigations on the

effects of an elliptical nozzle as a passive flow control method in a cross-flowing air stream have been lacking. Flame stability limit and flame visualization and trajectory analyses would be necessary to verify the effectiveness of any designed elliptical nozzles in the flaring process.

## CHAPTER 3

### EXPERIMENTAL APPARATUS AND PROCEDURES

#### 3.1 Experiment set-up

The experiments were conducted in the combustion laboratory at the Department of Mechanical & Manufacturing Engineering. The main components of the set-up consist of the following:

- Wind tunnel
- Fuel supply system
- Nozzle and ignition system

A schematic diagram of the apparatus is shown in **Figure 3.1**.

##### 3.1.1 Wind tunnel

One of the objectives of this research is to quantify the influence of the wind on the performance and emissions of flares in a cross-flow. Atmospheric winds are highly variable in direction, speed, and turbulence intensity. Hence, it is very difficult to duplicate all the features of the atmosphere in a wind tunnel facility. The approach adopted in this research was to create a uniform cross-flow in one direction in a scaled down wind tunnel facility.

The wind tunnel was designed to simulate a flare in an unconstrained wind flow and to ensure that the wind flow was uniform across the test section. This process was labor intensive since the design of the wind tunnel was an iterative process. The design process was based on the published works of Bossel, 1969; Morel, 1976; Mehta and Bradshaw, 1979; Mikhail, 1979; Barrett, 1984; Albayrak, 1991 and by personal communications with faculty members in the Department of Mechanical & Manufacturing Engineering. A

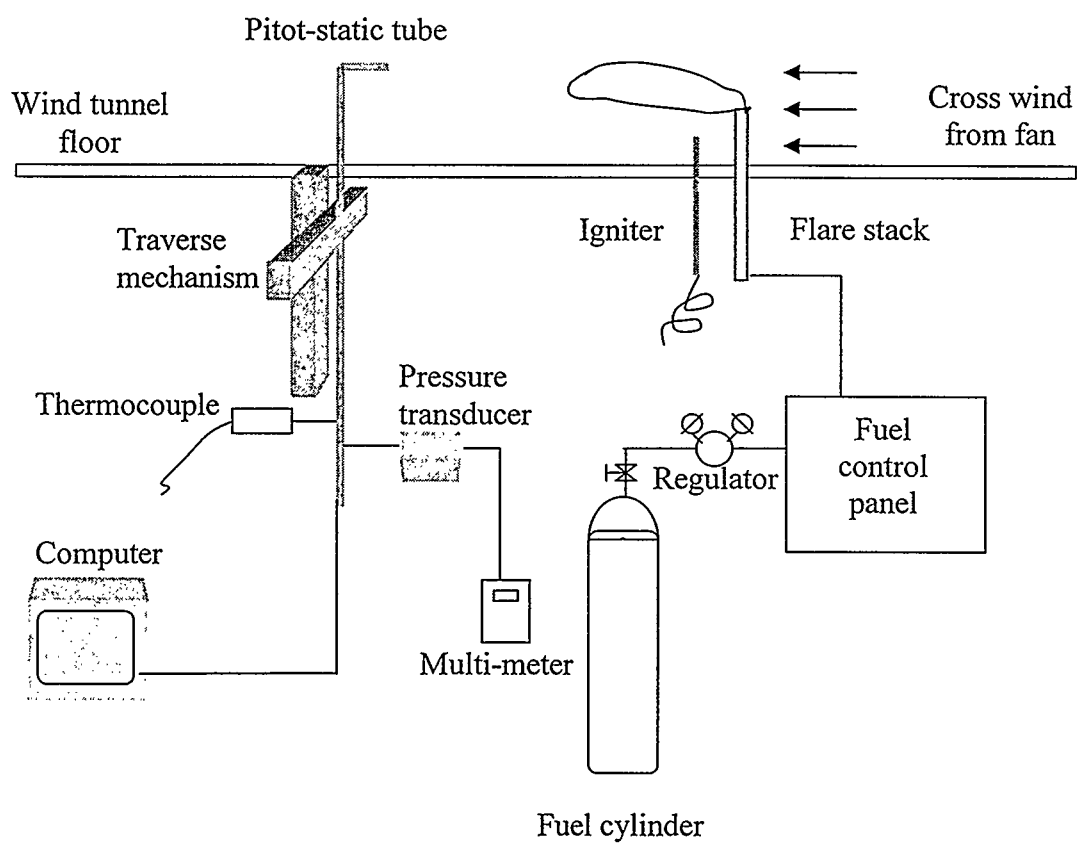


**Figure 3.1** A schematic diagram of the apparatus.

low speed wind tunnel with an air blower, butterfly valve, plenum chamber, contraction and test section was built for the laboratory. The side view of the wind tunnel is shown in **Figure 3.2**.

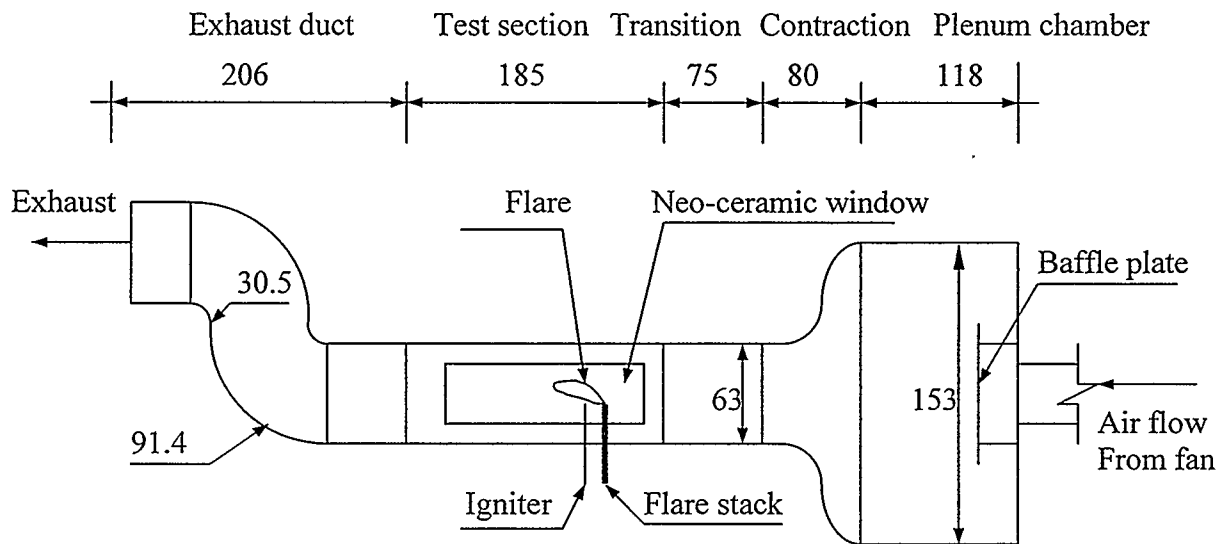


**Figure 3.2** The side view of the wind tunnel (all dimensions are in centimeters)

Air was driven by a centrifugal blower into a 1.3 x 1.53 x 1.18 m plenum chamber. The volumetric flow rate was controlled by the butterfly valve fixed at the inlet of the plenum chamber. The contraction section bridged the plenum chamber of cross-section of 1.3 x 1.53 m with the test section of cross-section of 0.4 m x 0.63 m which had a contraction ratio of 8. The contraction contours in the two axis planes were profiled with third-order polynomials curves. The approaching cross-flow velocities in the testing section ranged from 2.3 to 10.3 m/s. For the range of flow velocities considered, the average cross-flow turbulence level was less than 5%. During the experiments, velocity maps of the cross-flow were measured with a Pitot-static tube on a traversing mechanism.

**Plenum chamber.** The plenum chamber was manufactured by using 14 gauge galvanized steel. The uniformity of the flow inside the test section was achieved by inserting a baffle plate, perforated sheet, honeycomb air straightener, and two mesh screens into the plenum chamber to reduce the turbulence intensity of the flow in the testing section. A side view of the plenum chamber is shown in **Figure 3.3**.

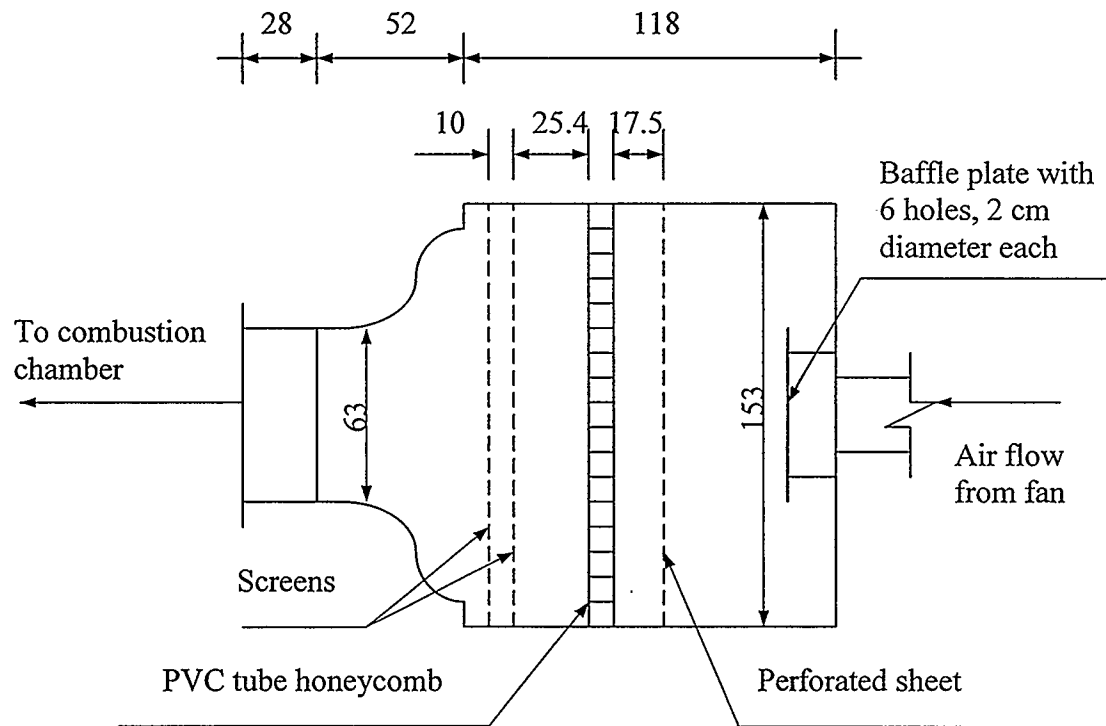


**Figure 3.3** The plenum chamber and contraction (all dimensions are in centimeters).

A 0.5 x 0.5 m metal baffle plate was fixed at the inlet of the plenum chamber to disperse the air inside the chamber. The perforated sheet was manufactured from 18 gauge steel with holes of 6.35 mm in diameter, spaced 6.35 mm apart. The main intention of using the perforated sheet was to break down the large scale vorticities into small scale



vorticities. The honeycomb air straightener was made of PVC tube, glued with high duty PVC glue, with each cell size 38.1 mm in diameter and 152.4 mm in depth. The main purpose of the honeycomb was to reduce swirl and lateral mean velocity variation, and hence straighten the flow. Two screens with a mesh size of 20 were tacked on the metal frames and used for the reduction of spatial non-uniformity of velocity and eliminating any remaining large scale turbulence.

**Contractions.** A contraction with a third-order polynomial contour in the two axis planes was built to connect the plenum chamber to the test section. A contraction ratio of 8 was used to increase the mean velocity in the test section. This allowed the honeycomb and screens to be placed in the low speed region, thus reducing pressure losses and spatial non-uniformity of the velocity field. The contraction was used to maintain a uniform flow and prevent flow separation.

**Test section.** The tests were conducted in a square cross section of 0.4 m x 0.63 m and 2 m long chamber made from 14 gauge galvanized steel, equipped with a neo-ceramic window (0.8 m x 0.3 m) on one side for flame visualization studies. The test section was fully contained and exhausted directly to the exterior of the building.

The fuel jet was inserted through a hole at the bottom of the test section. The fuel was discharged into the test section from nozzles with various geometries in the middle of the test section. Several small slots were drilled at the bottom of the test section for taking various measurements in different positions. The first slot was 10 cm from the fuel jet, followed by others at intervals of 5 cm for the first 120 cm, then at intervals of 10 cm for the rest of the test section. Wall effects were negligible at the operating conditions

employed in this study because the boundary layers in the test section were less than 5 cm all around the test section walls.

### 3.1.2 Fuel supply system

Sales grade natural gas with a purity of 96% was used in the experiments. A schematic diagram of the fuel supply system is shown in **Figure 3.4**. Fuel was supplied from cylinders. Their pressures were regulated by two-stage regulators to approximately 600 kPa (gauge) delivery pressure. The volumetric flow rate was measured by a metering valve (choked nozzle) on a fuel control panel. The fuel control panel consisted of three lines fitted with different range flow rate measuring systems. Each of the lines consisted, in series, of a solenoid valve, pressure transducer, thermocouple, and metering valve. The calibration was required to be unaffected by any downstream disturbances, such as pressure pulsation, temperature rise etc. Choked nozzles have been found to fulfill this condition, since the downstream disturbances can not propagate against the flow through the nozzle throat. For choked nozzles, the mass flow rate depends only on the upstream pressure and temperature (Karim and Klat). The fuel delivery capacity of each line is shown in **Table 3.1**

**Table 3.1** Fuel supply capacity in the control panel

Fuel delivery capacity	For air (m <sup>3</sup> /h)	For methane (m <sup>3</sup> /h)	For propane (m <sup>3</sup> /h)
Line One	0.09-0.37	0.12-0.49	0.07-0.28
Line Two	0.13-0.45	0.17-0.59	0.10-0.34
Line Three	0.71-3.32	0.93-4.36	0.53-2.50

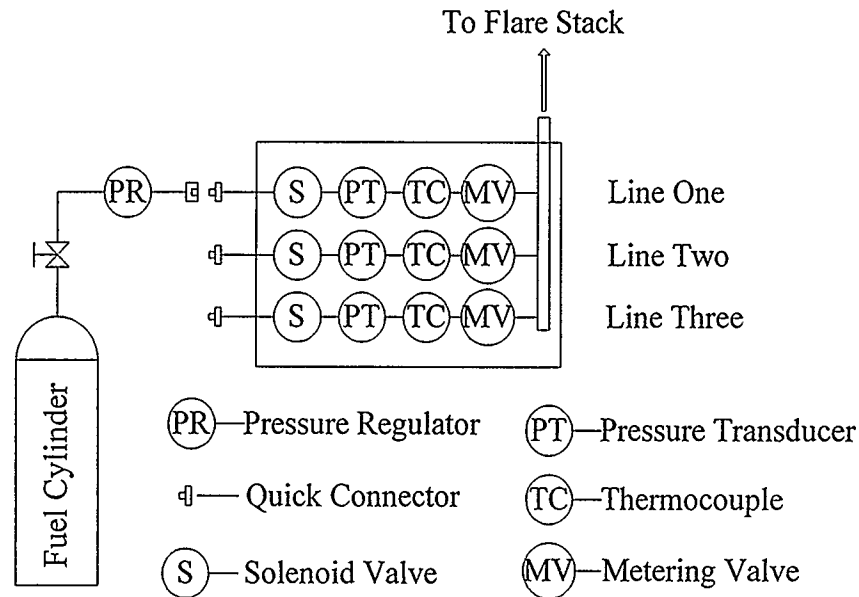


**Figure 3.4** A schematic diagram of fuel supply system.

The solenoid valves were controlled by LabVIEW software. The metering valve was calibrated before it was used for fuel control using a wet test meter. A stopwatch provided the time for the volume transferred. Since the volume resolution on the meter was 0.01 liter and the stopwatch resolution was 0.01 second, long duration samples were taken to minimize errors associated with the activating and deactivation of the timer. The primary source of error was the starting and stopping of the watch. The estimated error in the maximum flow rate was less than 3%. For a calibration test that ran for several minutes (usually 3 to 5 minutes), this error (usually a few seconds) was minute.

In some experiments, the fuel flow rate on the control panel was not enough and another series of choked nozzles were added for the fuel delivery capacity needed. These choked nozzles were calibrated by using orifice plates. The choked nozzle sizes used

were 0.64 mm, 0.91 mm, 1.09 mm, 1.32 mm, and 2.26 mm, which could deliver a fuel flow rate ranging from 0.41 m<sup>3</sup>/hr to 8.66 m<sup>3</sup>/hr and a gauge pressure ranging from 100 kPa to 600 kPa. The calibration curves and respective fuel flow rate for each choked nozzle are presented in **Appendix A**.

### 3.1.3 Nozzles and ignition system

**Jet nozzles.** The fuel was discharged into the test section with circular and non-circular nozzles of three different discharge areas. The jet nozzles protruded 16.5 cm above the chamber floor. The nozzle mouth and the flame were within the uniform cross-flow area. The cross-section of the non-circular nozzles was not truly an ellipse but will be referred to as such for simplicity (**Figure 3.5**).

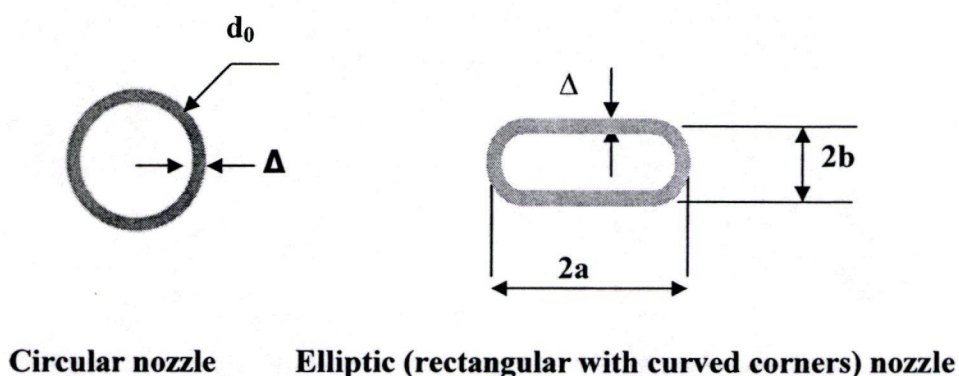


**Figure 3.5** A schematic diagram of cross-section of the nozzle-tubes.

Three series of stainless steel nozzles with different discharge areas of 16.4 mm<sup>2</sup>, 30.4 mm<sup>2</sup>, and 93.7 mm<sup>2</sup>, and a nozzle wall thickness of 0.89 mm were used in the experiments. The geometrical calculations are presented in **Appendix B**, and summarized in **Table 3.2**. The size of the nozzles used was depended on the type of experiments involved, i.e., blowout limits or flame visualization studies. For the stability limit experiments, all of the nozzles were used to determine the maximum fuel velocity beyond

which the flame blows out. However, for flame visualization investigations, the small nozzle (discharge area of  $16.4 \text{ mm}^2$ ) issued a much smaller flame. For increased accuracy in flame trajectory and length measurements, the first two large nozzles were used in the flame visualization studies.

**Table 3.2** Circular and elliptical nozzles

Stainless steel tube		Major Diameter 2a (mm)	Minor Diameter 2b (mm)	Aspect ratio	Discharge area ( $\text{mm}^2$ )
Series one	Circular nozzle	12.7	12.7	1	93.7
	Elliptical nozzle	20.4	8.2	2.5	93.7
		23.4	7.3	3.2	93.7
Series two	Circular nozzle	8.00	8.00	1	30.4
	Elliptical nozzle	12.7	5.3	2.4	30.4
		15.3	4.6	3.3	30.4
Series three	Circular nozzle	6.35	6.35	1	16.4
	Elliptical nozzle	7.3	5.6	1.3	16.4
		8.1	5.1	1.6	16.4

The elliptical nozzles were made by pressing circular pipes into elongated shapes. For example, elliptical nozzles with major-to-minor axes ratios of 1.3 and 1.6 were manufactured by pressing 4.6 mm ID circular tubes into elongated shapes (with discharge area of  $16.4 \text{ mm}^2$ ). The elliptical jets with major-to-minor axes ratios of 2.4 and 3.3 were made by pressing 7.0 and 7.7 mm ID circular tubes into elongated shapes (with discharge areas of  $30.4 \text{ mm}^2$ ), respectively. The elliptical jets with major-to-minor axes ratios of 2.5

and 3.2 were made by pressing 12.6 and 13.4 mm ID circular tubes into elongated shapes (with discharge areas of 93.7 mm<sup>2</sup>), respectively. The areas of the circular and elliptical nozzles remained approximately unchanged ( $\pm 5\%$ ). The length of the nozzles was fifty times the diameter of the circular jets and at least seven times the major axis of the elliptical jets to ensure a fully developed flow at the nozzle exit.

**Ignition system.** The igniter and stack are shown in the **Figure 3.6**. The fuel was delivered to the fuel jet and ignited with a spark igniter, mounted on the floor in the downwind side near the burner tube. The igniter consisted of two Nichrome wires in quartz sleeves installed in a stainless steel tube. The wires were connected to a 5 kV source, which caused an arc at the wire tips. It was retractable and could be withdrawn after ignition, so that it would not disturb the air flow in the test section.

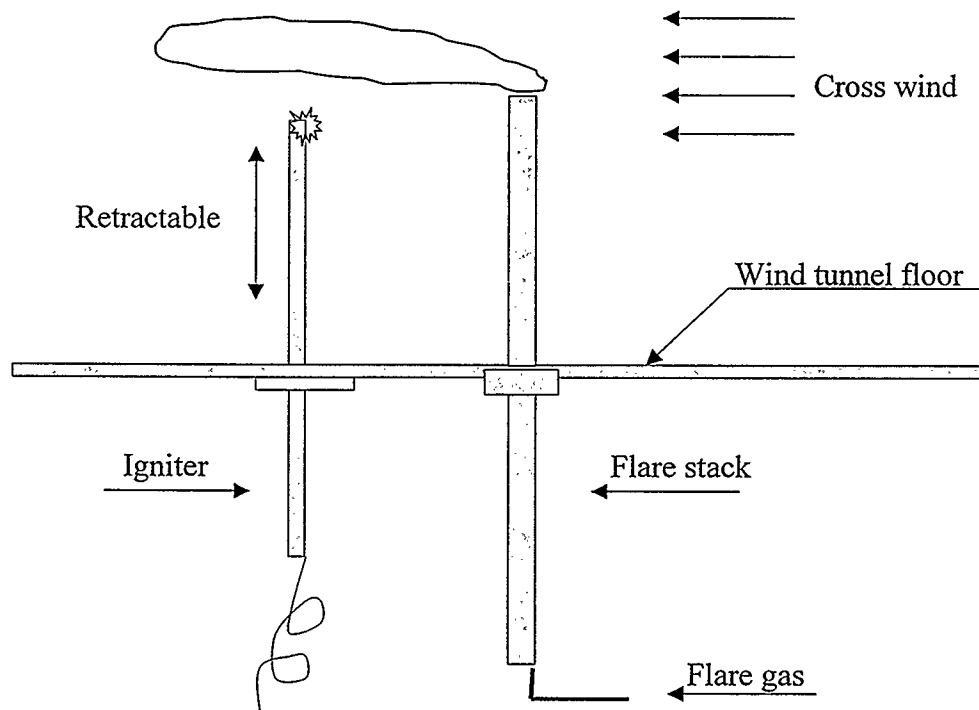


**Figure 3.6** A schematic diagram of the ignition system.

### **3.2 Experimental procedures**

#### **3.2.1 Cross-wind measurements**

The velocities of the cross-flow were measured using a Pitot-static tube over a range of 2.3 m/s to 10.3 m/s. A differential pressure transducer (OMEGA PX277) with a selectable measurement range of  $-12.7$  to  $25.4$  mm of water column was used to measure the differential pressure inside the chamber. A K-type thermocouple was used for temperature measurements inside the test chamber. A three component traversing mechanism was installed at the bottom of the test chamber for positioning various probes downstream of the flare stack. Movements in the vertical and cross-stream directions were controlled through stepper motors in increments of 3.81 cm. The movement in the stream-wise direction was done manually on tracks in increments of 5 cm, or 10 cm over the length of 2 m depending on the downstream position. The cross-section of the test chamber was scanned at 16 (horizontal) by 10 (vertical) points (160 points in total) not including the 2.54 cm boundary layer at the perimeter. The scan rate was 1000/s, and data was collected for 30 seconds at each point; therefore, the total data collected at each point was 30000. The average velocity was calculated by using LabVIEW software, and the data was processed using MatLAB software.

#### **3.2.2 Blowout limits measurements**

The blowout limits of the diffusion flame were measured by first setting the cross-flow stream and jet velocity at low values. The jet was then ignited with the igniter which was then retracted to avoid disturbances to the air flow. Two procedures can be followed to measure the blowout limits. The first is by gradually increasing the jet discharge velocity while maintaining a constant cross-flow stream velocity. The second is



by gradually increasing the cross-flow stream velocity while maintaining a constant jet discharge velocity. The first procedure was used due to the greater accuracy and ease that the fuel control panel offered. The blowout limits of the jet flames were observed visually. The measured volumetric flow rate or velocity of the jet at which the flame suddenly blew out of the test chamber was deemed the blowout limit. The experiments were repeated to establish repeatability.

### **3.2.3 Flame image collection and processing**

The luminous flames were photographed using a digital camera with a 1600 x 1200 pixel resolution. The lens (12.5 mm, f 2.8) and camera were placed normal to the cross flow at a distance of 1.3 m from the ceramic chamber window. A field of view of 0.75 m x 0.25 m was achieved with this arrangement, capturing the entire flame under the range of operating conditions. A shutter speed of 1/500s was used to record “instantaneous” flame images. In this study, pictures were taken several times at each operating condition, and typical images at each operating condition are shown in **Subsection 4.2**. The flame trajectories were derived from the pictures taken at each point by taking vertical slices across the flame images and determining the visible limits of the flame. Midpoints were found from these limits. The path following the midpoints of each slice was used to define the flame trajectory.

### **3.3 Wind tunnel uniformity measurements**

A high-pressure plenum chamber was designed and built (see **Figure 3.2**). The cross-wind uniformity was measured under the conditions and procedure discussed in **Subsection 3.2.1**. **Figure 3.7** shows the cross section of the wind tunnel with measurement locations. As reported before, 160 measurement locations were used to

evaluate the flow uniformity in the testing section. Three velocities, 2.4 m/s, 6.7 m/s, and 10.3 m/s were chosen to test the uniformity of the cross flow. The data is listed in **Appendix C. Figure 3.8 to Figure 3.13** show the details of the measurement contours of different cross-flow velocities. These figures were plotted with the left-bottom corner of the test section as the point of origin when looking upwind.

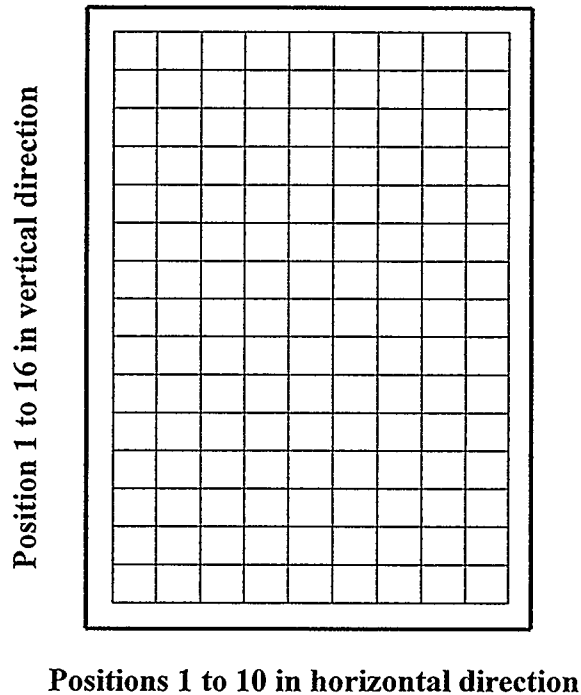


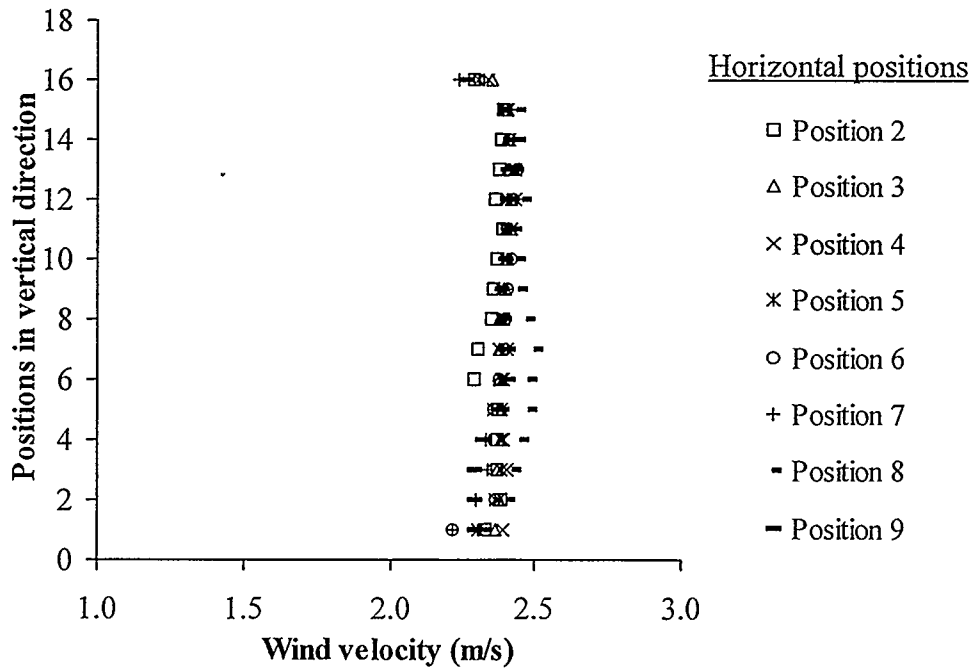
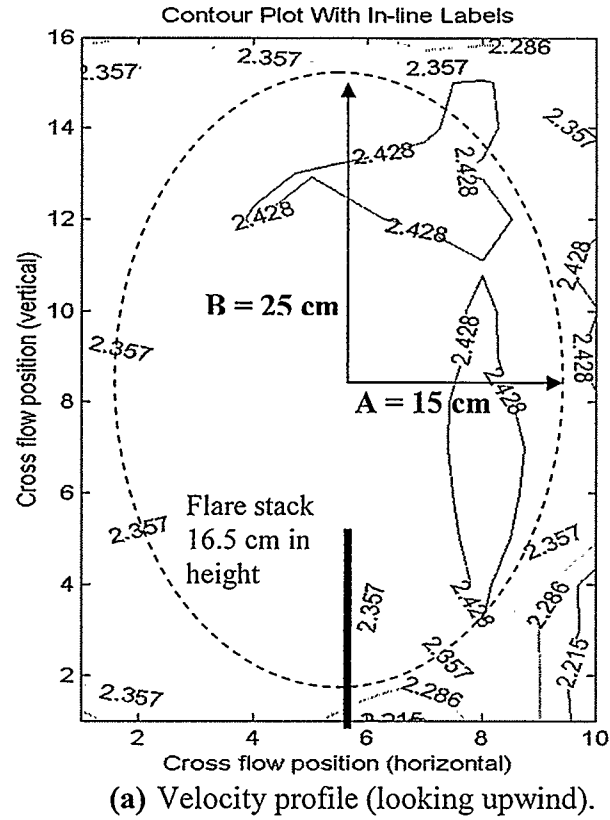
**Figure 3.7** Grids for wind uniformity measurements in the cross-section of the test chamber.

Velocity profiles of the cross-flow in the test section were projected onto topographical maps in **Figure 3.8(a)**, **Figure 3.10(a)** and **Figure 3.12(a)**. For the range of the cross-flow velocities of 2.3 m/s to 10.3 m/s, the velocity profiles were observed to be uniform inside a 15 cm by 25 cm elliptical domain with the current configuration. The flame size and shape were within this domain at all times. Therefore, uniformity was considered to be achieved in all the experiments even though the flow was non-uniform

at the corners of the test section. At lower cross-flow velocities, the velocity distribution in the right middle area of the maps was higher than that in other area due to the butterfly valve position and design at the inlet of the plenum chamber. An increase in the valve opening and hence the wind velocity reduced non-uniformities across the entire test section. Therefore, the experiments were conducted in moderate cross-wind velocities, within the range of 2.3 m/s to 10.3 m/s.

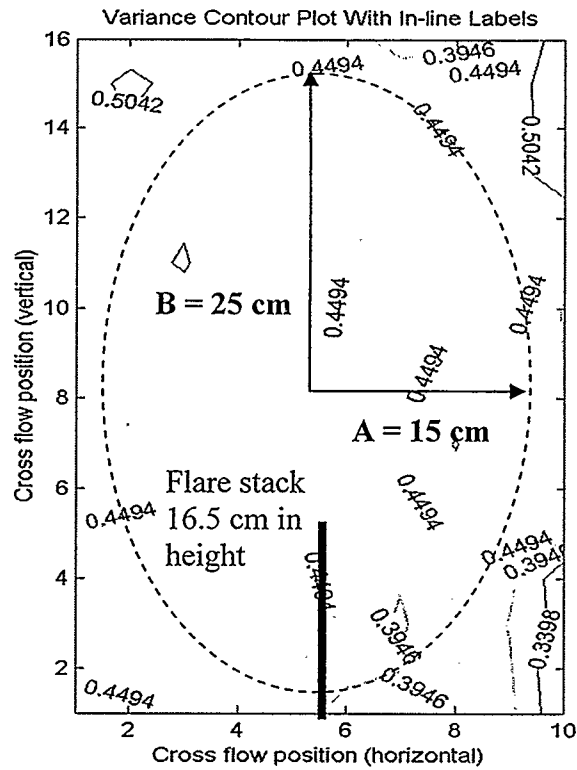
The side-views of the velocity profiles in the test section are presented in **Figure 3.8(b)**, **Figure 3.10(b)**, and **Figure 3.12(b)**. From these figures, it can be seen that uniformity inside the domain was achieved.

Similarly, the results of variances for the different test velocities are presented in **Figure 3.9 (a)**, **Figure 3.11 (a)**, and **Figure 3.13 (a)**. Variances of 0.45 m/s, 0.52 m/s, and 0.065 m/s were obtained and turbulence intensities of 18.75%, 7.76%, and 0.63% were obtained for the wind velocities of 2.4 m/s, 6.7 m/s, and 10.3 m/s, respectively. The higher turbulence intensity of the low wind velocity can be due to the effects of the position of the butterfly valve in the inlet of the plenum chamber and the result of small, low-frequency oscillations of the mean wind speed associated with the control circuitry of the wind tunnel fan. With an increase of the valve openings, the turbulence intensity was improved drastically. Also, the variance profiles located inside the 15 cm by 25 cm elliptical domain were improved. In order to visualize the uniformity of the turbulence intensity the side-views of the variance profiles for the test velocities are presented in **Figure 3.9 (b)**, **Figure 3.11 (b)**, and **Figure 3.13 (b)**.

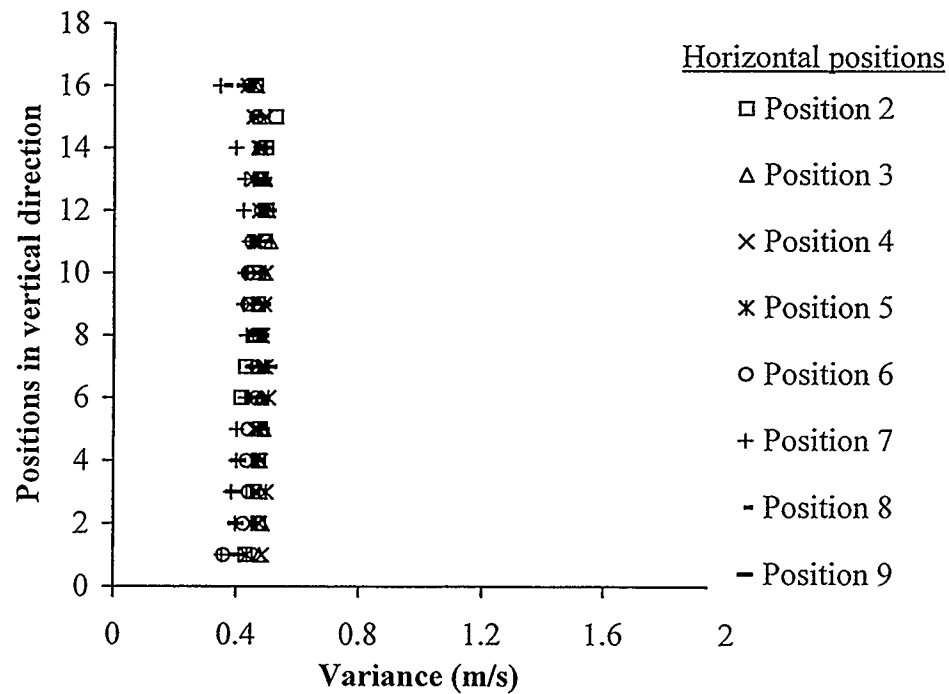


(b) Velocity profile (side-view).

Figure 3.8 Velocity profiles at the average crosswind velocity of 2.4 m/s.

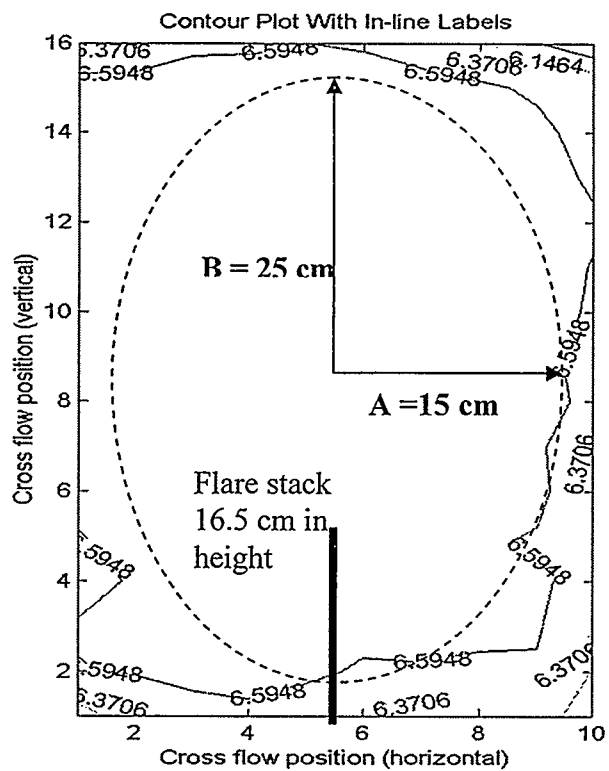


(a) Variance profile (looking upwind).

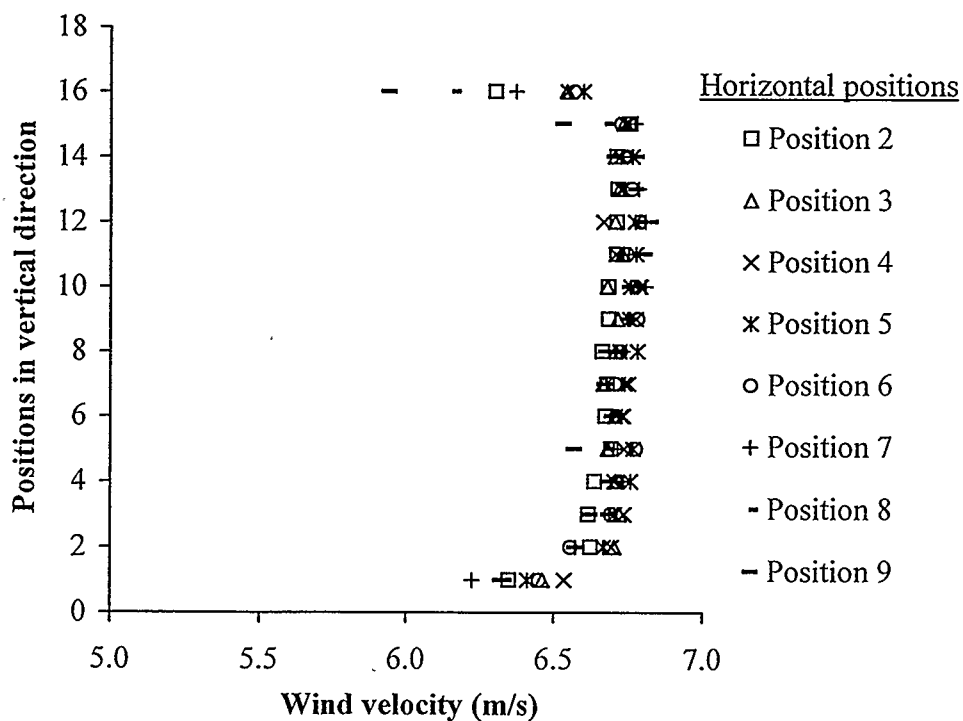


(b) Variance profile (side-view).

**Figure 3.9** Variance profiles at the average crosswind velocity of 2.4 m/s, variance of 0.45 m/s.

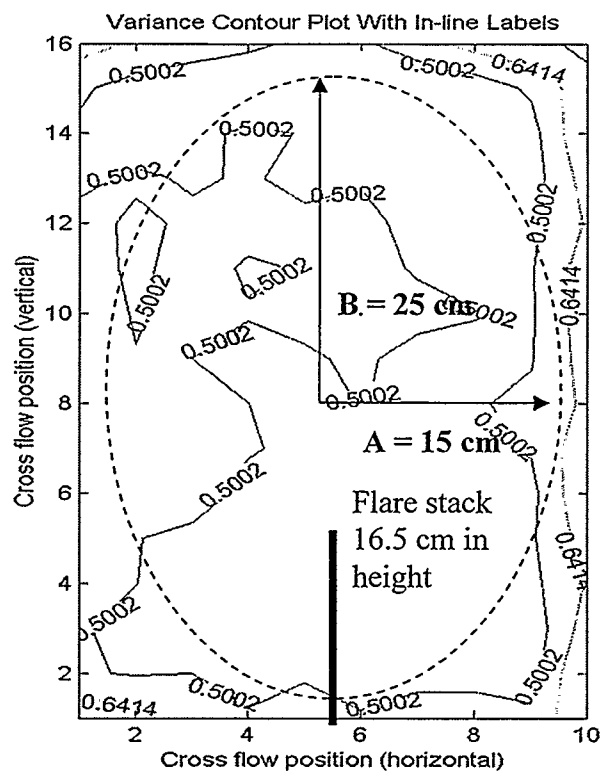


(a) Velocity profile (looking upwind).

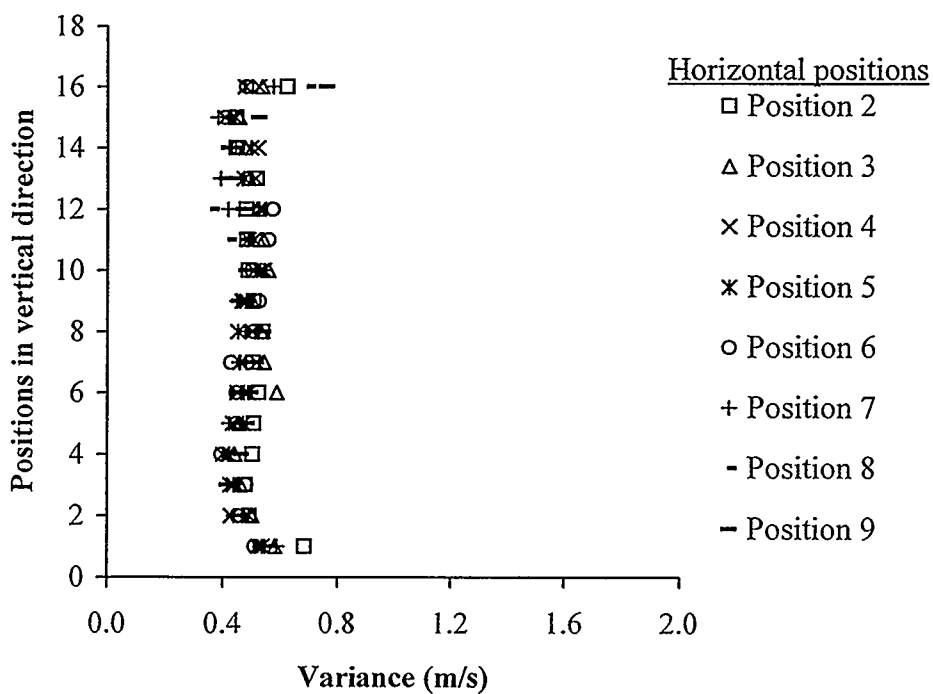


(b) Velocity profile (side-view).

Figure 3.10 Velocity profiles at the average crosswind velocity of 6.7 m/s.

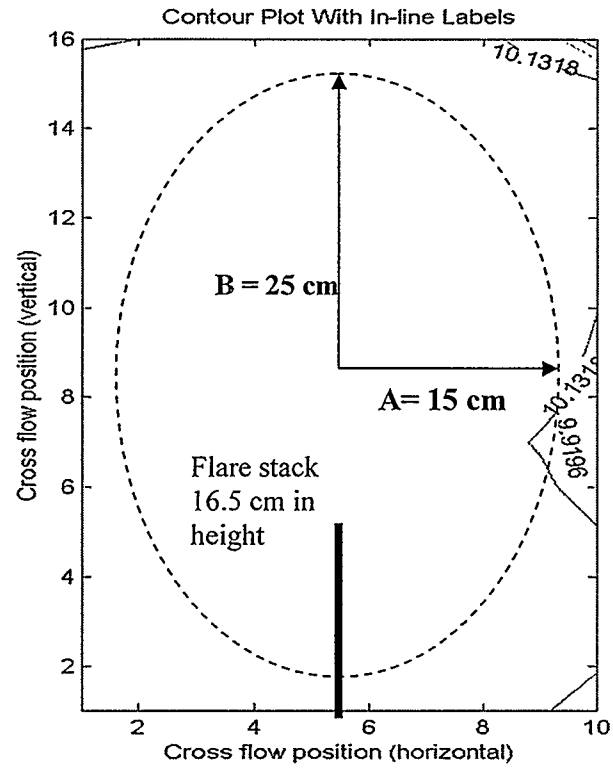


(a) Variance profile (looking upwind).

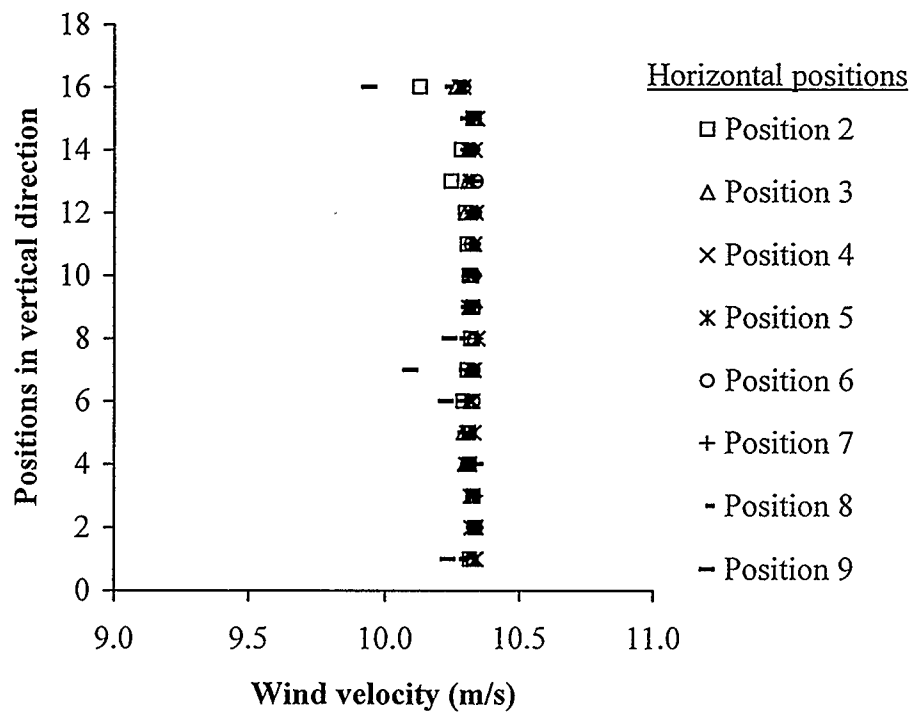


(b) Variance profile (side-view).

**Figure 3.11** Variance profiles at the average crosswind velocity of 6.7 m/s, variances of 0.52 m/s.



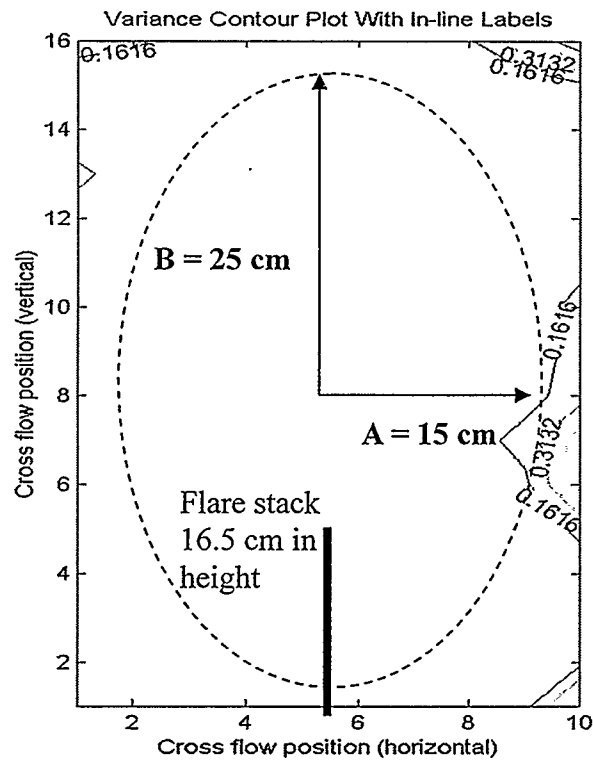
(a) Velocity profile (looking upwind).



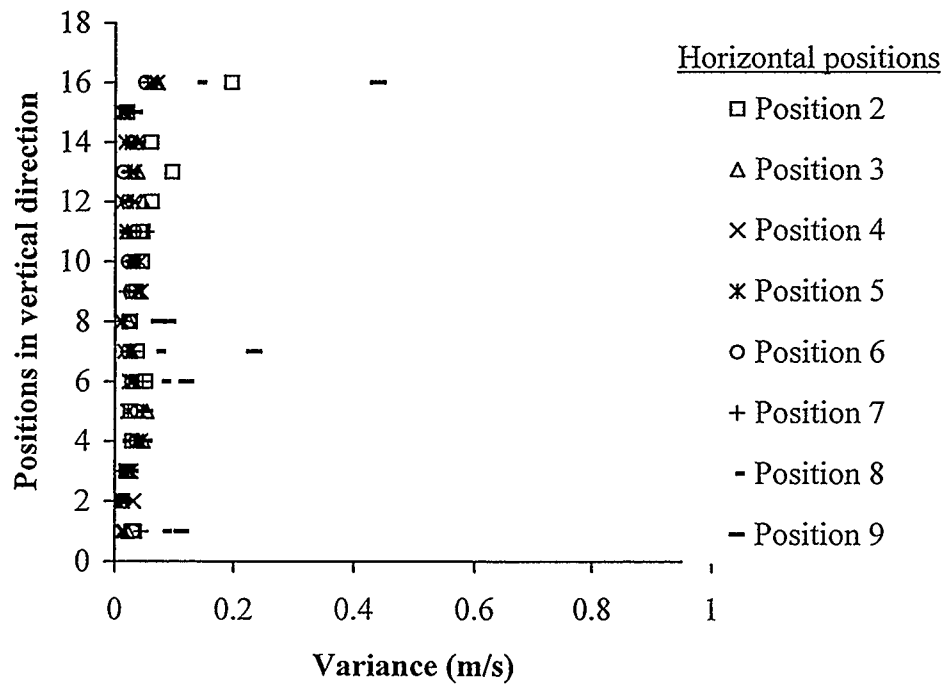
(b) Velocity profile (side-view).

**Figure 3.12** Velocity profiles at the average crosswind velocity of 10.3 m/s.





(a) Variance profile (looking upwind).



(b) Variance profile (side-view).

**Figure 3.13** Variance profiles at the average crosswind velocity of 10.3 m/s, variance of 0.065 m/s.

## CHAPTER FOUR: RESULTS AND DISCUSSIONS

The effects of elliptical nozzles on the stability limits and flame trajectories of diffusion flames in a cross-flow were investigated and are discussed below.

### 4.1 Flame stability limits

#### 4.1.1 General

The effect of elliptical nozzles on the blowout limits of diffusion flames in a cross flow was investigated for velocities ranging from 2.3 m/s to 10.3 m/s and the results are shown in **Figure 4.1** to **Figure 4.3**. To ensure repeatability, experiments were repeated at least three times. The solid lines in the figures were the average values of all the trials for each different nozzle and operating condition. Elliptical nozzles with a discharge area of 16.4 mm<sup>2</sup>, 30.4 mm<sup>2</sup> and 93.7 mm<sup>2</sup> were employed and their respective blowout limits were compared with their circular counterparts (6.4 mm, 8 mm, and 12.7 mm (OD)). The flame extinguished if the jet flow rate exceeded a critical value. The area under the curves represents the region in which flames were stabilized, and above this region, a stable flame could not be obtained. Generally, the blowout limits of a jet issuing from elliptical nozzles were greater than those of the circular jet with the same discharge area as long as the major axis was perpendicular to the cross-flowing air. This is most likely due to the greater recirculation zone, in which a flammable fuel/air mixture exists immediately downstream of the stack but the axis-switching phenomenon reported by Ho and Gutmark (1987) may have played a role as well.

#### 4.1.2 Nozzles with discharge area of $16.4 \text{ mm}^2$

It can be seen in **Figure 4.1** that the elliptical nozzle with an aspect ratio of 1.6 had higher blowout limits than those of the elliptical nozzle with an aspect ratio of 1.3 (when the major axis was normal to the flow). However, the blowout limits decreased significantly with an increase in the nozzle aspect ratio when the nozzle was oriented with the minor axis normal to the airflow. For the nozzle dimensions and geometries shown in **Figure 4.1**, the blowout limits increased with increasing cross-wind (or cross-flow) velocities when the wind velocity was relatively low (for circular nozzle, less than 4.2 m/s; for elliptical nozzles, less than 4.6 m/s). At such low cross-wind velocities, the intense mixing of the fuel jet and cross-flow caused the blowout limits to increase with an increase of the wind velocity. However, the blowout limits reached their peak values at 4.2 m/s for the circular nozzle and 4.6 m/s for the elliptical nozzles, and then decreased drastically as the wind velocity was further increased. For a stable, stationary flame to exist, two criteria need to be met. Firstly, the local burning velocity should equal or exceed the fuel discharge and cross-wind velocities. A flame can not be sustained if either, or the combination of the fuel and cross-wind velocities exceeds the local burning velocity. Furthermore, a flame can only exist when the local fuel/air ratio is within the lower and upper flammability limits. Consequently, when the cross-wind velocity was further increased, the local burning velocity could not match the fuel and cross-wind velocities and the increased degree of mixing between the fuel and air caused the diluted fuel/air ratio to drop below the lower flammability limits, resulting in flame blow out. Under even higher wind velocities exceeding 5.1 m/s, the fuel jet could not be ignited

since a fuel/air ratio above the lower flammability limit could not be obtained. These results are in good agreement with the results of Huang and Chang (1994).

Also in **Figure 4.1**, it can be seen that the peak blowout limits were at higher wind velocities with the use of the elliptical nozzles with their major axes normal to the cross-flow. Throughout these tests, it was observed that the flames were attached prior to blowout. With the major axis normal to the flow, there is a larger recirculation zone than that of circular jets or an elliptical jet with the minor axis perpendicular to the cross-flow. The nozzle itself becomes an effective flame holder since the flame attachment area in the vicinity of the nozzle rim is larger. When the minor axis of the elliptical nozzle was normal to the cross-wind, the recirculation zone and nozzle rim to which the flame could attach was even smaller than that in the circular nozzle. Therefore, the blowout limits of the elliptical nozzles with the minor axis perpendicular to the cross-flow were much lower than those in the circular nozzle as shown in the figures.

#### **4.1.3 Nozzles with discharge areas of 30.4 mm<sup>2</sup> and 93.7 mm<sup>2</sup>**

In order to verify the reliability of the results, another two series of nozzles with discharge area of 30.4 mm<sup>2</sup> and 93.7 mm<sup>2</sup> were used to test the blowout limits. The results are shown in **Figure 4.2** and **Figure 4.3**. The range of cross-wind velocities in which a flame can be sustained was increased with increasing nozzle discharge area as long as the elliptical jet was oriented with its major axis normal to the cross-wind. The cross-wind velocity ranged from 2.3 m/s to 10.3 m/s for the 30.4 mm<sup>2</sup> and 93.7 mm<sup>2</sup> nozzles compared with 2.3 m/s to 5.1 m/s for the 16.4 mm<sup>2</sup> nozzles. This is because with an increased discharge area, the recirculation zone was increased allowing the flame to stabilize on the leeside of the nozzle. At the same time, a greater discharge of fuel would

require a higher cross-wind velocity to dilute the fuel/air mixture to the point of extinguishment.

**Figure 4.2** shows that when the wind velocity was further increased beyond another critical value (6.7 m/s for 8 mm (OD) circular nozzle; 9.9 m/s for 2.4:1 elliptical nozzles with major diameter normal to the air flow), the blowout limits gradually increased with an increase in the wind velocity, and the flame was bent over severely in the direction of the cross-wind. The fuel jet stack served as a flame holder which generated a flammable region on its leeside. This recirculation zone was reported to be the major source for stabilization of the flame. Therefore, the stability domain is categorized into three regimes: *sub-critical regime*, where the upper blowout limit increased as the cross-wind velocity increased; *critical regime*, where the upper blowout limit decreased as the cross-wind velocity increased; *supercritical regime*, where the upper blowout limit again increased with an increase in the cross-wind velocity (Huang and Chang, 1994).

**Figure 4.2** also shows that the elliptical nozzle with an aspect ratio of 3.3 had higher blowout limits than the elliptical nozzle with an aspect ratio of 2.4 (when the major axes were normal to the cross-flow), which had a higher blowout limit than those of the circular jet. This again is due to the greater recirculation zone that developed on the leeside of the stack.

Similar trends are shown in **Figure 4.3**; however, the blowout limits of flames issuing from nozzles with discharge area of  $93.7 \text{ mm}^2$  were higher than their counterparts with discharge area of  $30.4 \text{ mm}^2$  and  $16.4 \text{ mm}^2$  under the same operating conditions. Also

the critical values for the different regimes were extended to higher wind velocities (i.e., 6.7 m/s for circular nozzle; 8.5 m/s for the elliptical nozzles).

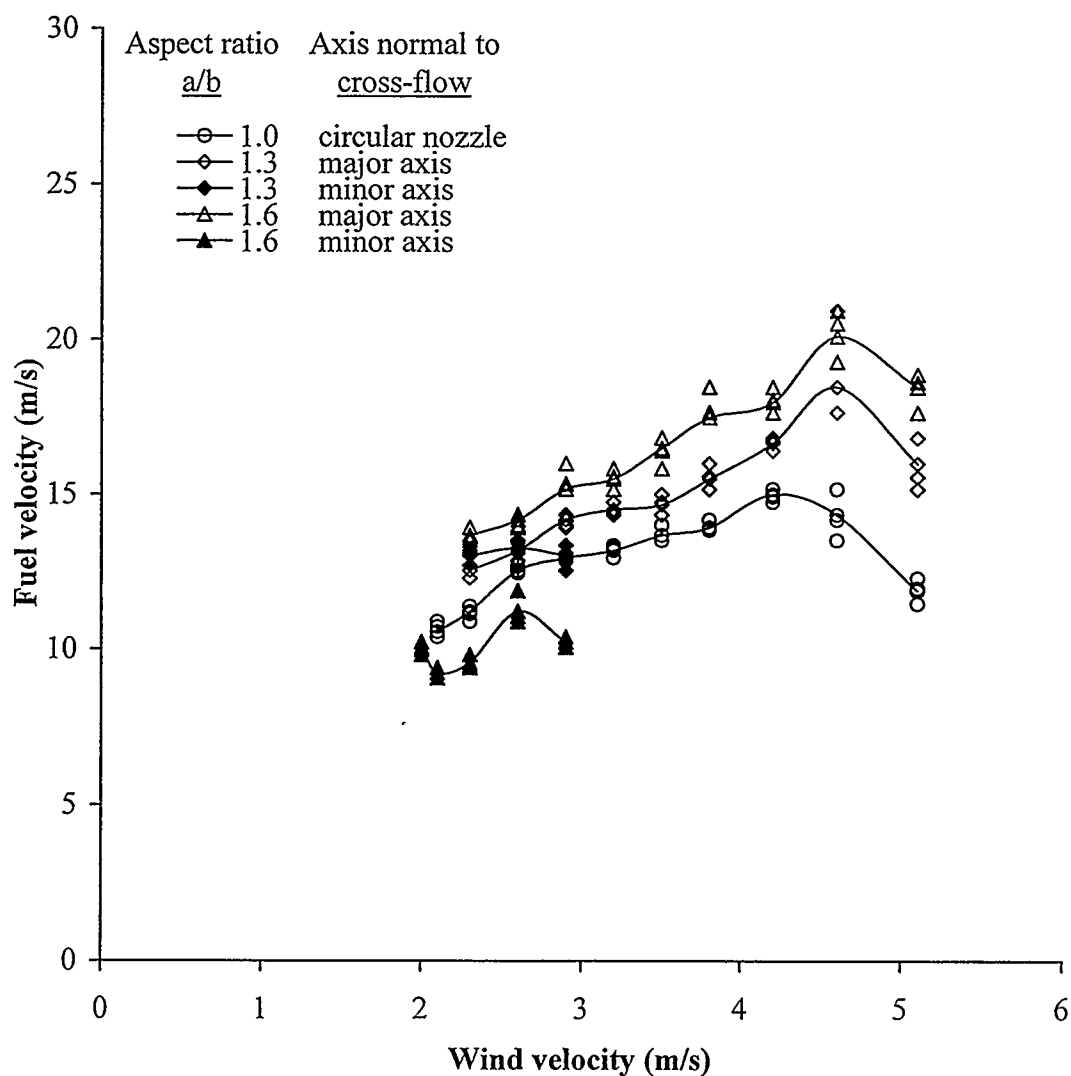


**Figure 4.1** Flame blowout limits of natural gas from nozzles with a discharge area of  $16.4 \text{ mm}^2$  and a  $0.89 \text{ mm}$  wall thickness.

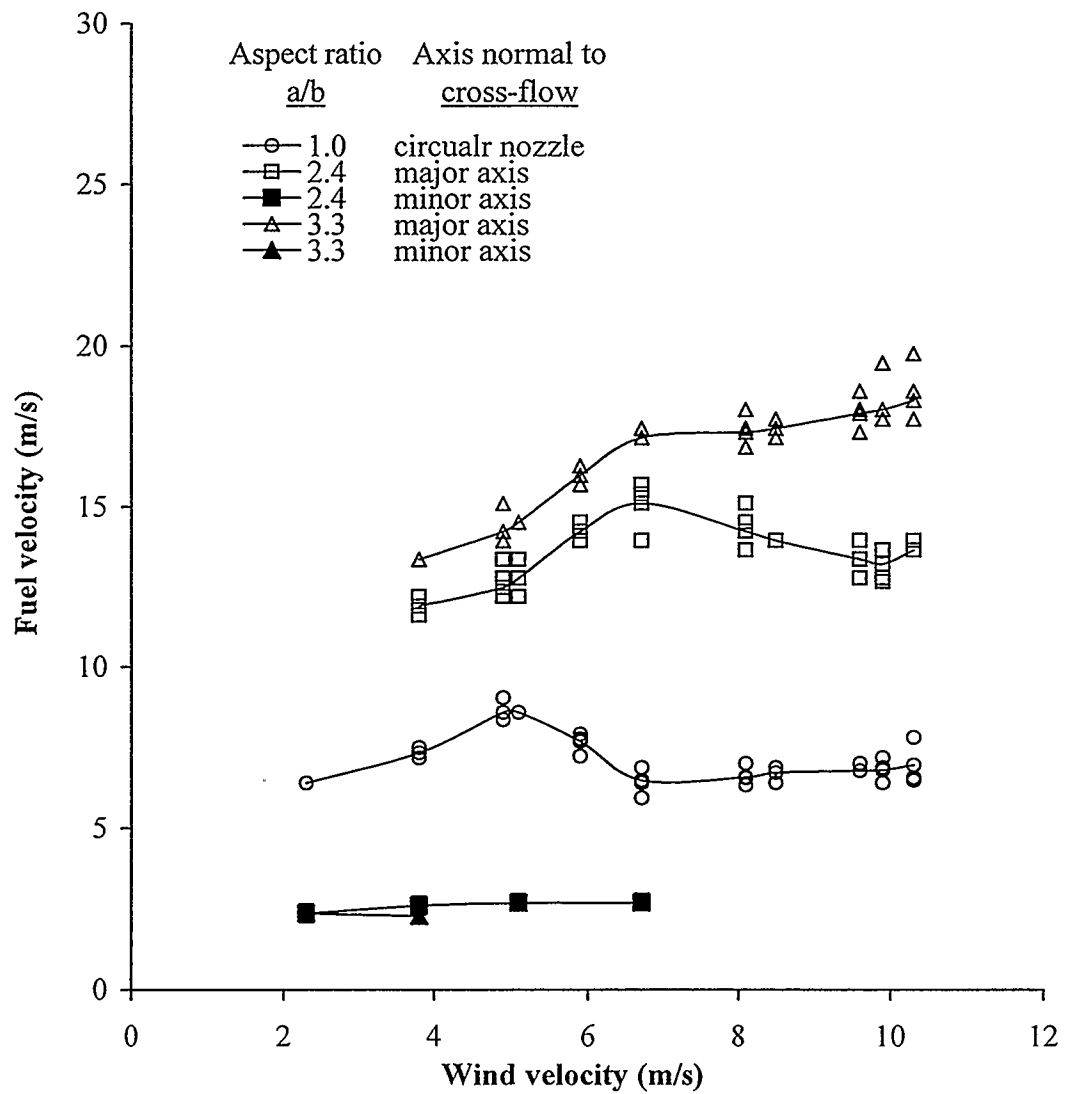


**Figure 4.2** Flame blowout limits of natural gas from nozzles with a discharge area of  $30.4 \text{ mm}^2$  and a  $0.89 \text{ mm}$  wall thickness.

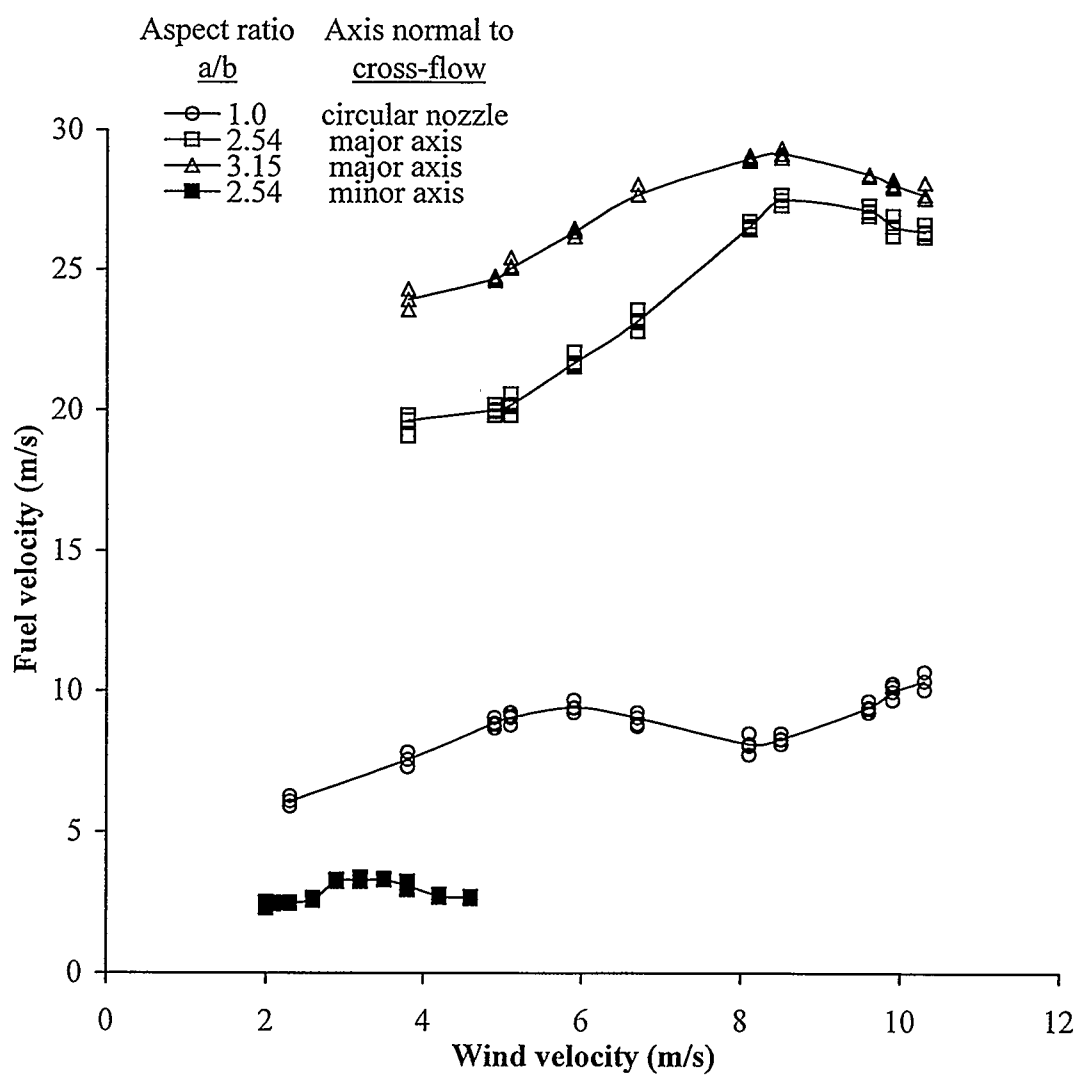


**Figure 4.3** Flame blowout limits of natural gas from nozzles with a discharge area of  $93.7 \text{ mm}^2$  and a  $0.89 \text{ mm}$  wall thickness.



#### 4.1.4 Jet-to-wind momentum ratios at flame blowout as a function of cross-flow velocities

Figure 4.4 to Figure 4.6 show the jet-to-wind momentum flux ratio  $R_j$  as a function of the cross-wind velocity at blowout for different nozzles. The definition of  $R_j$  is taken from Gollahalli et al. (1975) and expressed as  $R_j = M_j/M_\infty = (\rho_j u_j^2) / (\rho_\infty u_\infty^2)$ , where  $M_j$  and  $M_\infty$  are the momentum flux of fuel jet and cross-wind, respectively;  $\rho_j$  and  $u_j$  are the density and velocity of fuel jet; and  $\rho_\infty$  and  $u_\infty$  are the density and velocity of the cross-flowing air, respectively. It was observed that in all three cases: the jet-to-wind momentum flux ratios at blowout decreased with an increase in the wind velocity in a nonlinear manner. Data could not be obtained at higher cross-wind velocities; however a decrease in the jet-to-wind momentum flux ratios was observed in this super-critical regime. These results are consistent with Huang and Chang's (1994), however, more data needs to be collected in higher wind velocities to verify the trend observed.

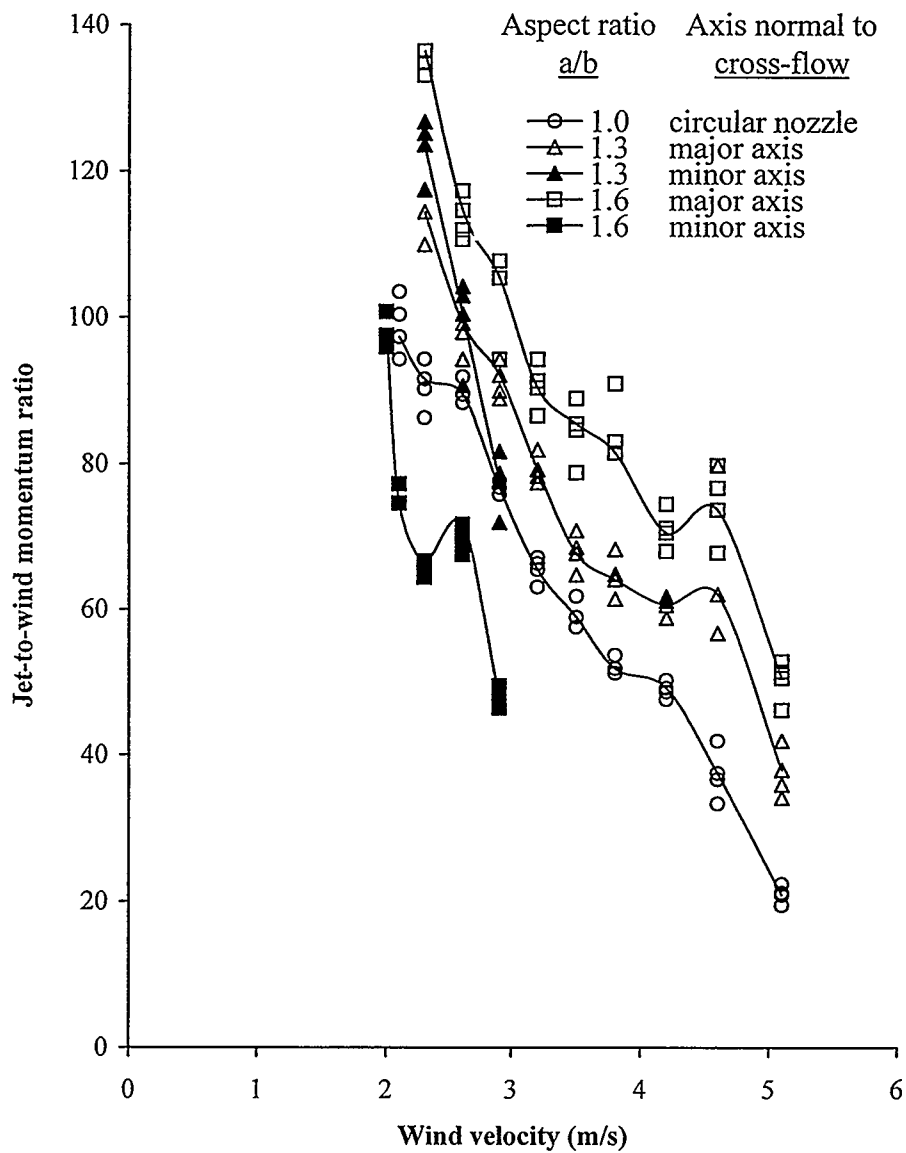


**Figure 4.4** Jet-to-wind momentum ratios versus cross-wind velocities from nozzles with a discharge area of  $16.4 \text{ mm}^2$ .

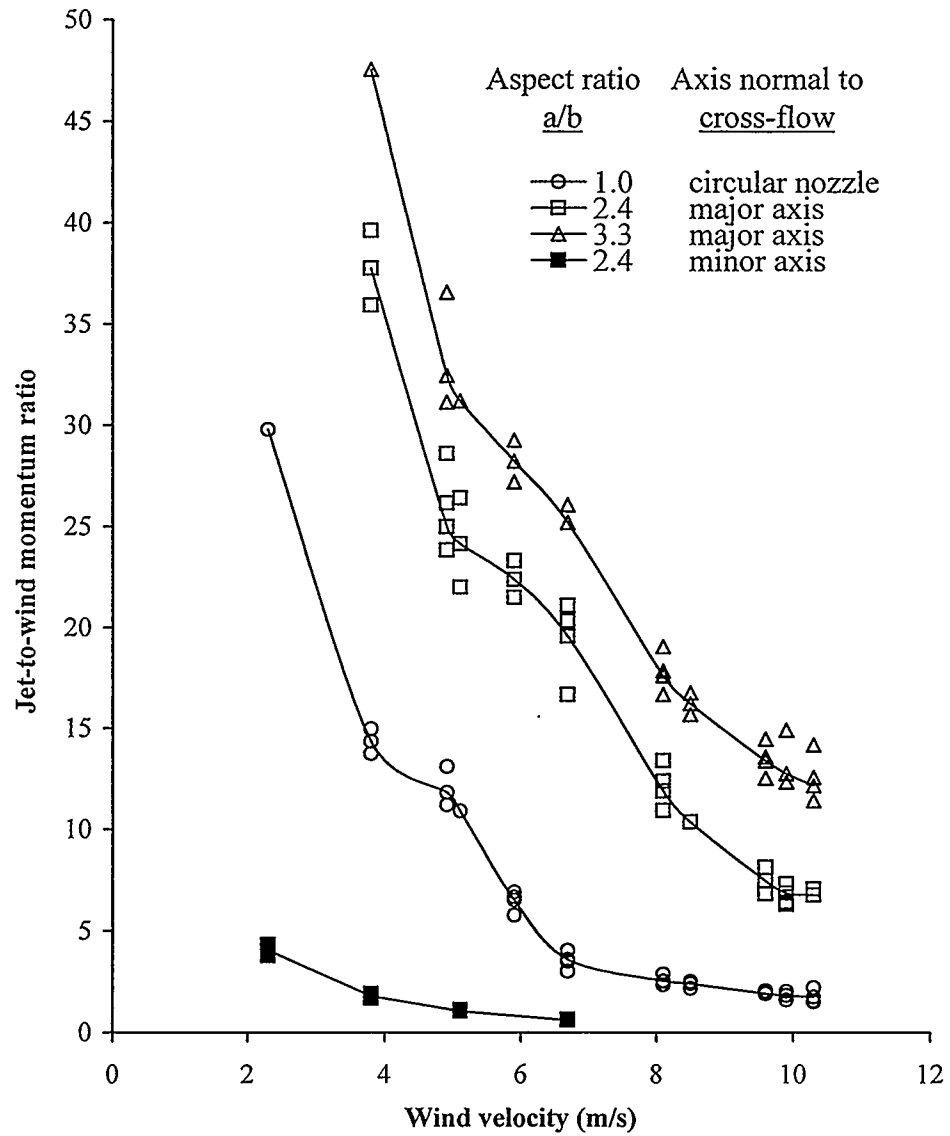


**Figure 4.5** Jet-to-wind momentum ratios versus cross-wind velocities from nozzles with a discharge area of  $30.4 \text{ mm}^2$ .

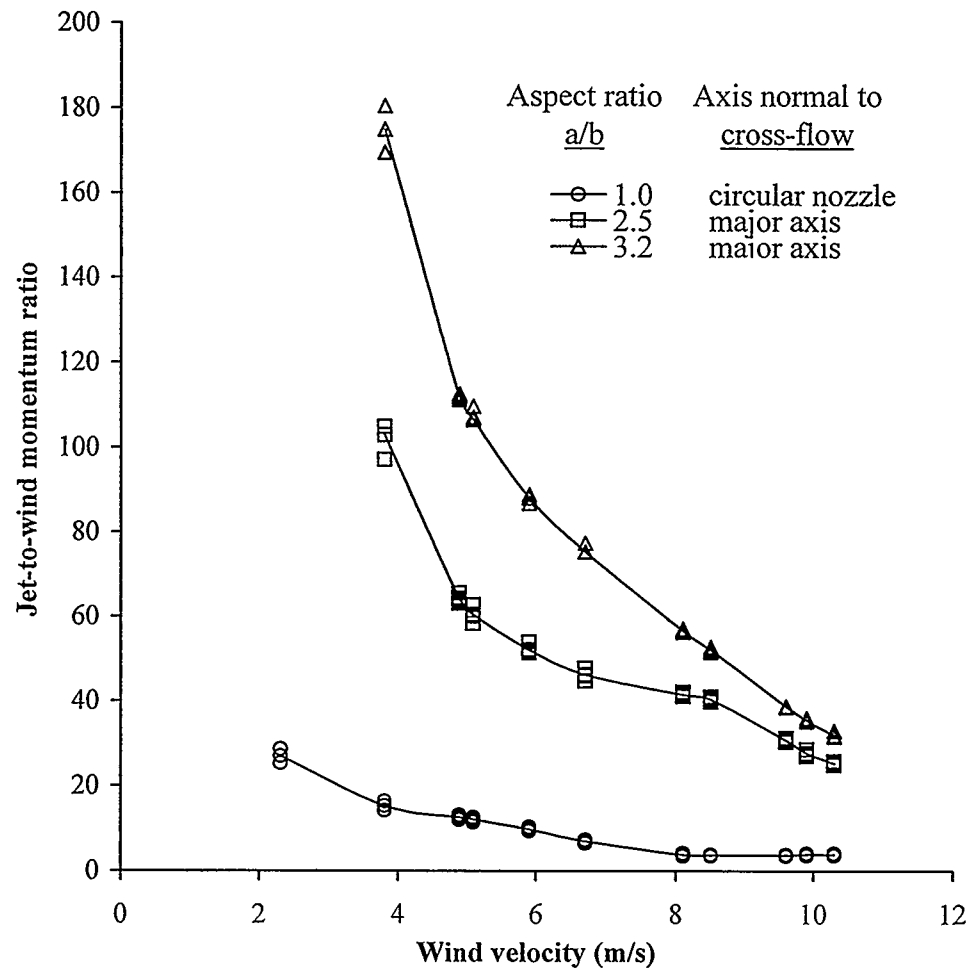


**Figure 4.6** Jet-to-wind momentum ratios versus cross-wind velocities from nozzles with a discharge area of  $93.7 \text{ mm}^2$ .

## 4.2 Flame visualizations

Two series of long exposure side-view photographs of natural gas flames with different nozzles are shown in **Figure 4.7** and **Figure 4.8**. These photographs show the overall position and size of the flame.

### 4.2.1 Images from nozzles with discharge area of $93.7 \text{ mm}^2$

In **Figure 4.7**, attached flames were issued from circular and elliptical nozzles with a discharge area of  $93.7 \text{ mm}^2$ . The jet exit velocity of the fuel,  $V_j$ , was held constant at 4 m/s and the cross-wind speed,  $U_\infty$ , was varied from 3.1 m/s to 10.3 m/s. Images from the circular nozzle with an outer diameter of 12.7 mm are shown in the first column (denoted as column 1), while images from elliptical nozzles with aspect ratios of 2.5 and 3.2 (with the major axis normal to the cross-flow) are shown in columns 2 and 3, respectively.

As seen in row **A** of **Figure 4.7**, at a high momentum flux ratio,  $R_j$ , the attached flames were stabilized above the stack and angled towards the downstream direction. The flames were highly radiative and sooty. The side of the flame facing into the cross-wind was diluted by the air and the base of the flame was partially quenched on upwind side of the nozzle. The flame was blue in color in the near-field region of the nozzle, with a luminous yellow color region in mid-flame and an orange-red region in the far-field. This observation is in agreement with the results reported by Gollahalli and Sullivan (1975) and Birch, et al. (1989). However, the flames from the elliptical nozzles (images **A2** and **A3**) were wider and more yellowish than those from the circular nozzle (image **A1**) under the same conditions and similar flame lengths. Furthermore, the flame from the elliptical nozzle with an aspect ratio of 3.2 (image **A2**) was even more yellowish than that from

elliptical nozzle with an aspect ratio of 2.5 (image **A3**). This is an indirect indication of high soot formation from flames issuing from elliptical nozzles. The elliptical nozzles enhanced the flame blowout limits compared with those from the circular nozzle under the same operating conditions. This could be due to better fuel-air mixing as a result of axis-switching and the larger recirculation zone in elliptical nozzles. However, this does not explain what appears to be a greater formation of soot. Emission measurements of flames under these operating conditions would give insight to the phenomena.

As the cross-wind velocity was increased and the  $R_j$  value was decreased, the length of the flame was increased and the flame was stabilized in the wake of the stack (images in row **B**). A further decrease in  $R_j$  resulted in a portion of the fuel being drawn into the low-pressure region on the downwind side of the stack and a small luminous yellow region was observed (image **C1** for the circular nozzle). This luminous region appeared earlier in the elliptical nozzles (images **A2** and **A3** for elliptical nozzles with aspect ratios of 2.5 and 3.2, respectively) and the size of the luminous region increased with an increase of the aspect ratios of the nozzles. A further increase in the cross-flow velocity pushed the flame further in the downstream direction but the flame remained anchored at the wake of the stack. The luminous regions at the lee-side of the stacks became larger and moved further down the stacks, especially in the case of elliptical nozzles. At this point, the length of the flame began to shorten and the color of the flames was predominantly blue due to the intensive mixing of the air and fuel (images in row **D**). The shape of the flame from the circular nozzle changed, and necking of the flame was observed near the stack (image **D1**), which is in good agreement with the observations by Kibrya (1987) and University of Alberta Combustion Project Group (2000); however,

this characteristic is not seen in flames from elliptical nozzles. At a high cross-wind velocity, the main tail of the flame is extinguished and only a combusting recirculating vortex on the downstream side of the flare stack remains (images in row **G**).

#### 4.2.2 Images from nozzles with discharge area of $30.4 \text{ mm}^2$

Diffusion flames issuing from circular and elliptical nozzles with a discharge area of  $30.4 \text{ mm}^2$  were photographed and are presented in **Figure 4.8**. The jet exit velocity of the fuel,  $V_j$ , was held constant at 5.5 m/s and the cross-wind speed,  $U_\infty$ , was varied from 3.1 m/s to 10.3 m/s. Images from the circular nozzle with an outer diameter of 8 mm are shown in the first column (denoted as column 4), while images from elliptical nozzles with aspect ratios of 2.4 and 3.3 (with the major normal to the cross-flow) are shown in columns 5 and 6, respectively.

The overall appearances of flames issuing from different nozzles are similar to those from the nozzles with a discharge area of  $93.7 \text{ mm}^2$  and flame necking phenomena are seen in images from both circular and elliptical nozzles (images in rows **D**, **E**, and **F**). However, the differences between flame images from circular and elliptical nozzles are not as significant as those in **Figure 4.7** due to the smaller nozzle discharge area.

From the discussions in this section, the following conclusions could be made:

- Flames from elliptical nozzles are wider and sootier than those from circular nozzles under the same operating conditions.
- The flares are affected severely by the recirculation zone in the lee-side of the nozzles under cross-wind conditions.
- The larger the aspect ratio, the greater the recirculation zone.

- The flame necking appears under high cross-wind velocities when the aspect ratio is small.



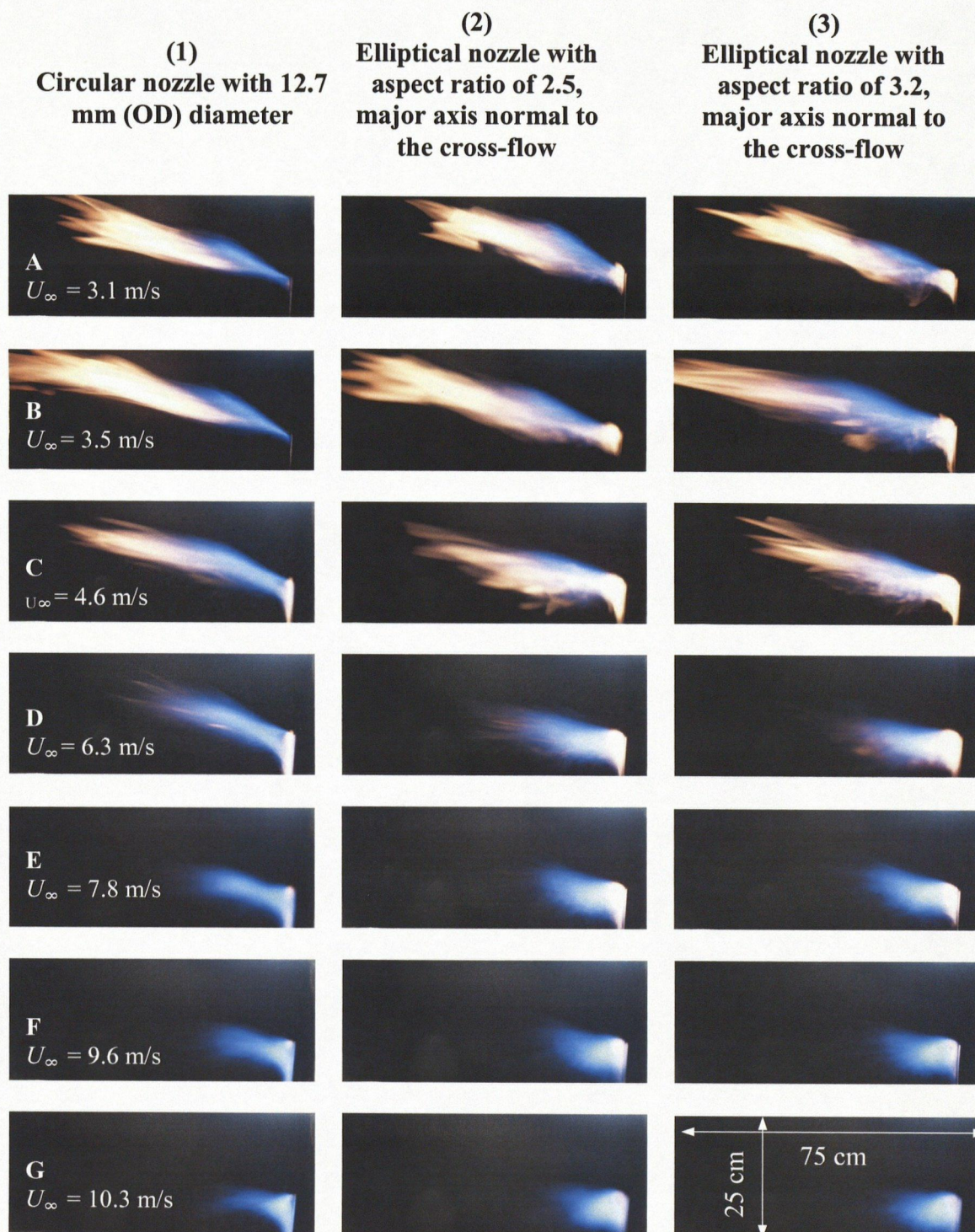


**Figure 4.7** Long exposure images of diffusion flames in a cross-flow from nozzles with a discharge area of  $93.7 \text{ mm}^2$  ( $V_j = 4 \text{ m/s}$ ).



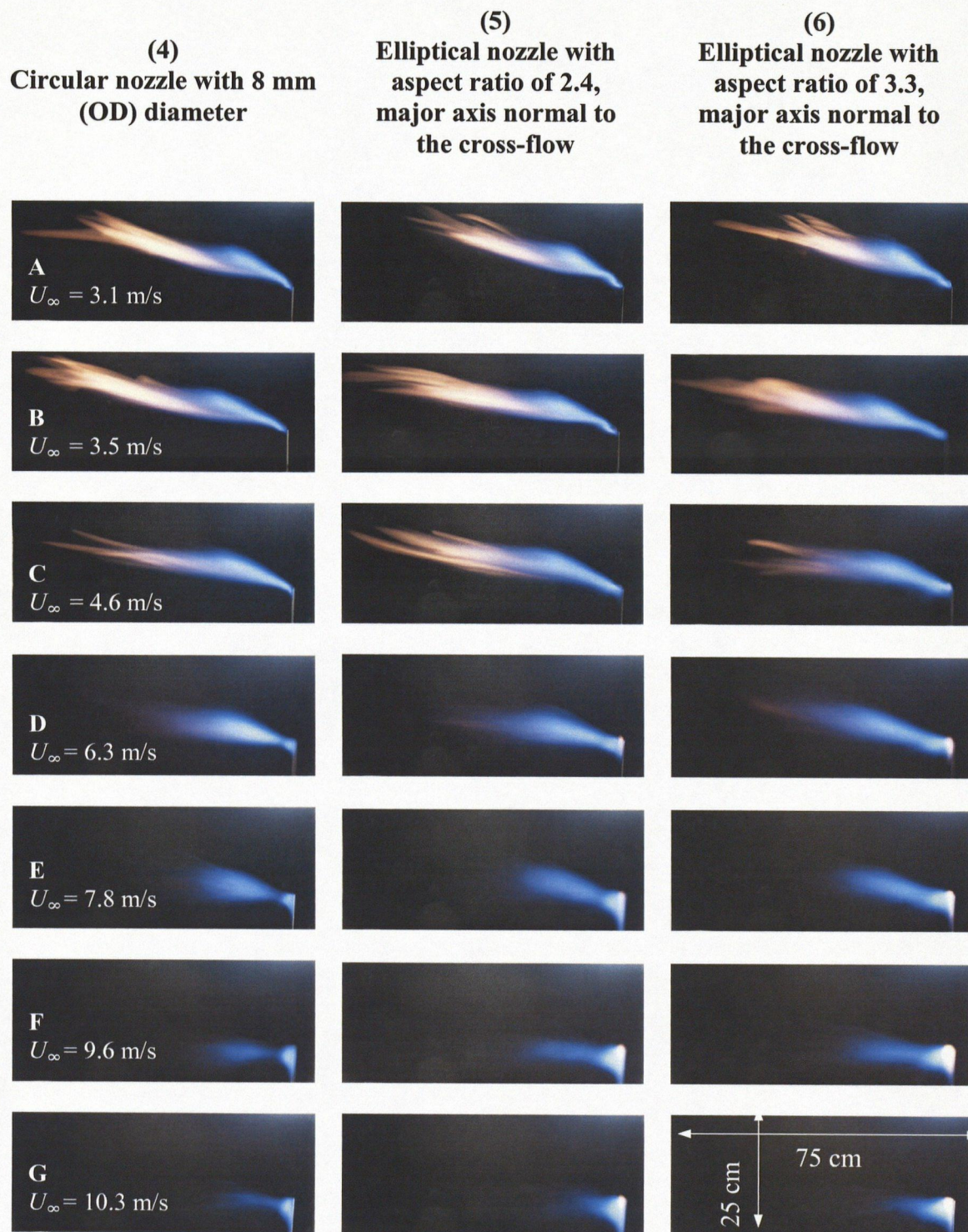


**Figure 4.8** Long exposure images of diffusion flames in a cross-flow from nozzles with a discharge area of  $30.4 \text{ mm}^2$  ( $V_j = 5.5 \text{ m/s}$ ).

### 4.3 Flame trajectories

#### 4.3.1 General

Flare trajectory is a parameter commonly used to characterize a diffusion flame in a cross-flow. It has been defined by different researchers in different forms. For example, in the study of the characteristics of a turbulent propane flame in a cross-wind, Gollahalli et al. (1975) defined the flame trajectory using the locus of the center point of the shortest section through the visible-light image of the flame photographed from a distant point at the side. Rao and Brzustowski (1982) defined the flame trajectory as the locus of centroids of the area enclosed by the tracer concentration contour measured in the plane of symmetry. In Yoo and Shin's (1994) study, the flame trajectory was defined by the mean of heights of the upper and lower boundaries of the flame which were calculated from photographic measurements. This definition is used in the present study, and a sketch of the flame trajectory is shown in **Figure 4.9**.

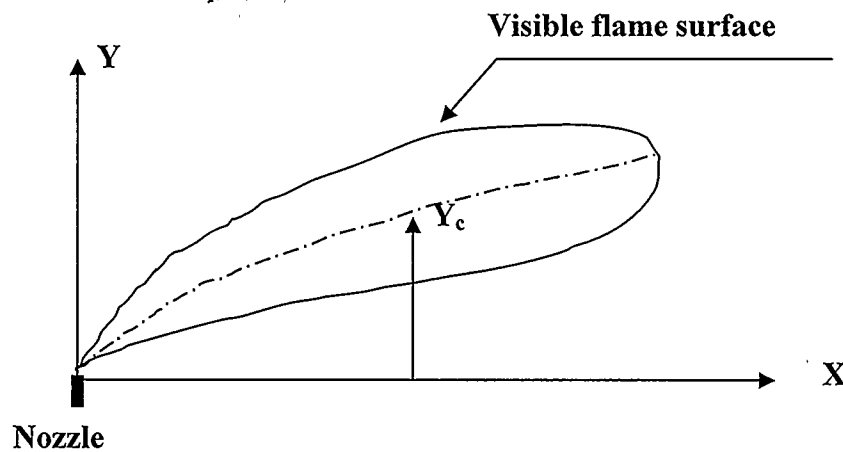


**Figure 4.9** A sketch of the flame trajectory.

### 4.3.2 Nozzles with discharge area of 93.7 mm<sup>2</sup>

The results of the trajectories for nozzles with discharge areas of 93.7 mm<sup>2</sup> are plotted in **Figure 4.10** to **Figure 4.12**. From these figures, it can be seen that the flame trajectories are affected by the cross-flow velocity ( $U_{\infty}$ ) and fuel jet velocity ( $V_j$ ). At low wind-to-jet velocity ratios ( $U_{\infty}/V_j < 1$ ), the flames were bent downstream in the direction of the cross-flow and the flame trajectories were dominated by the initial jet momentum. In the near-nozzle region of the flame, the flow patterns were governed by the momentum of the jet and cross-flow; while further downstream, buoyancy effects were coming into play. When the wind-to-jet velocity ratios were close to unity ( $U_{\infty}/V_j = 1$ ), part of the fuel stream was captured into the immediate wake of the stack where it continued to burn. Within the recirculation zone, buoyancy effects were not significant. With an increase of the wind-to-jet velocity ratios ( $U_{\infty}/V_j > 1$ ), the flame trajectories were dominated by the cross-wind and the recirculation zone became more apparent. With a further increase of the wind-to-jet ratios ( $U_{\infty}/V_j = 1.87$  for circular nozzle;  $U_{\infty}/V_j = 1.75$  for elliptical nozzle with aspect ratio of 2.4;  $U_{\infty}/V_j = 1.42$  for elliptical nozzle with aspect ratio of 3.3), the flames were predominantly in the recirculation zone, in the wake of the stack. It was observed that the recirculation zone increased with an increase of the aspect ratios of the nozzles as long as the major axis was normal to the cross-wind. These observations are in agreement with the results of Escudier (1972) and Majeski, et. al (1999a, b).



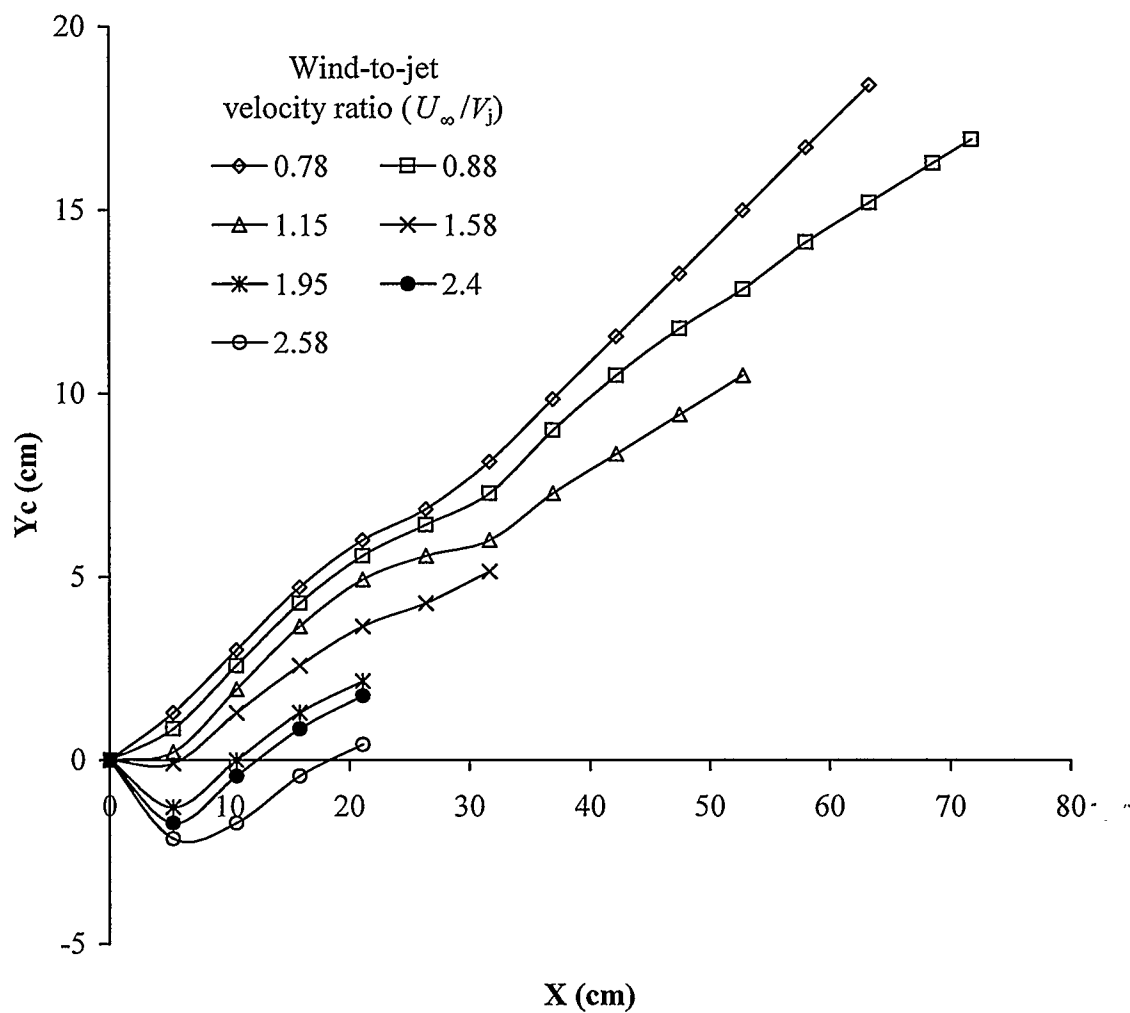


**Figure 4.10** Flame trajectory from the circular nozzle with a discharge area of  $93.7 \text{ mm}^2$  (fuel jet velocity of  $4 \text{ m/s}$ ).

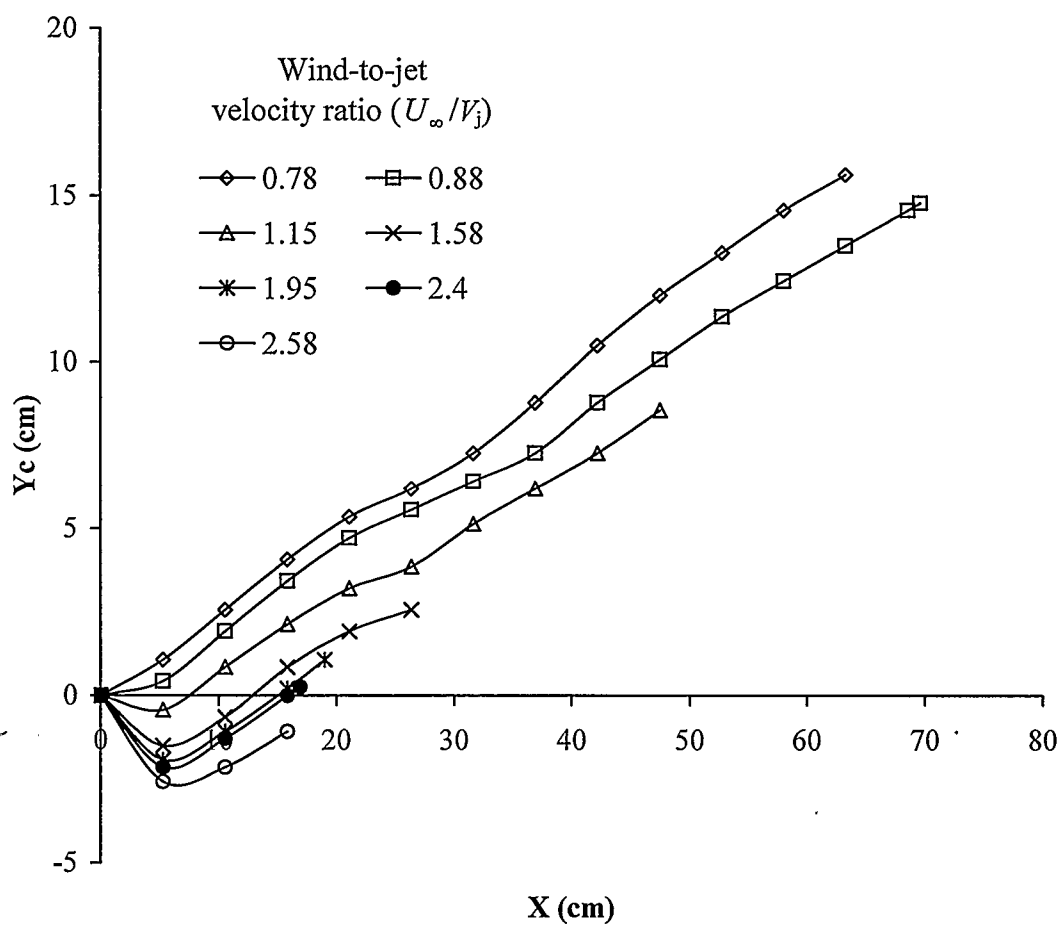


**Figure 4.11** Flame trajectory from the elliptical nozzle with aspect ratio of 2.4 (nozzle discharge area of 93.7 mm<sup>2</sup>, major axis normal to cross wind, fuel jet velocity of 4 m/s).

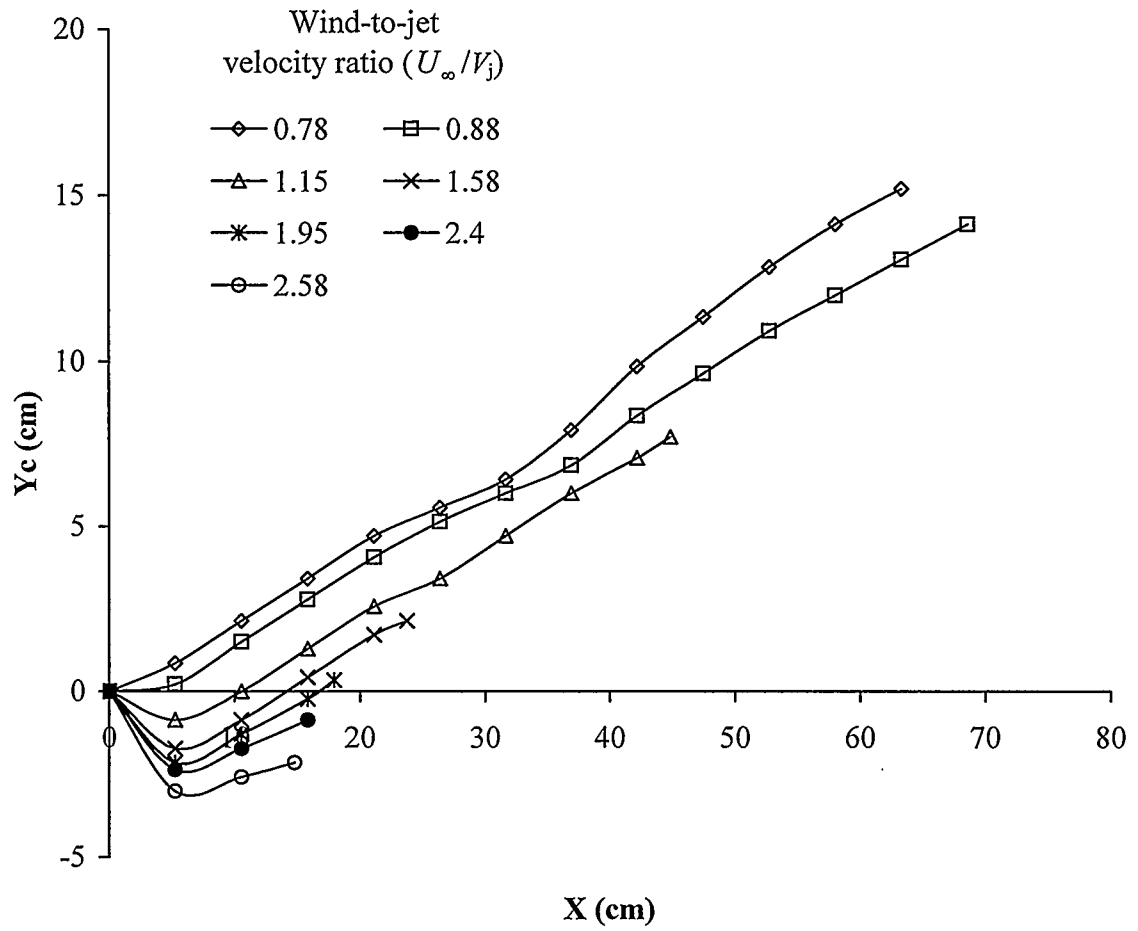


**Figure 4.12** Flame trajectory from the elliptical nozzle with aspect ratio of 3.3 (nozzle discharge area of  $93.7 \text{ mm}^2$ , major axis normal to the cross wind, fuel jet velocity of 4 m/s).

#### 4.3.3 Nozzles with discharge area of $30.4 \text{ mm}^2$

The results of the trajectories for nozzles with discharge areas of  $30.4 \text{ mm}^2$  are plotted in **Figure 4.13** to **Figure 4.15**. The flame trajectories followed the same trends as the nozzles with discharge areas of  $93.7 \text{ mm}^2$ . However, the recirculation zone was smaller for the smaller discharge area nozzles because of the smaller projected area in the lee-side of the stack in the cross-flow. Therefore, the effects of nozzle shape on flame trajectory were not as significant for the nozzle with a discharge area of  $30.4 \text{ mm}^2$  as those with a discharge area of  $90.7 \text{ mm}^2$ . The flame trajectories from the 2.5 aspect ratio nozzle behaved similar to those from the circular nozzle. Also, the 3.2 aspect ratio jet had a more pronounced recirculation zone than the 2.5 aspect ratio jet.



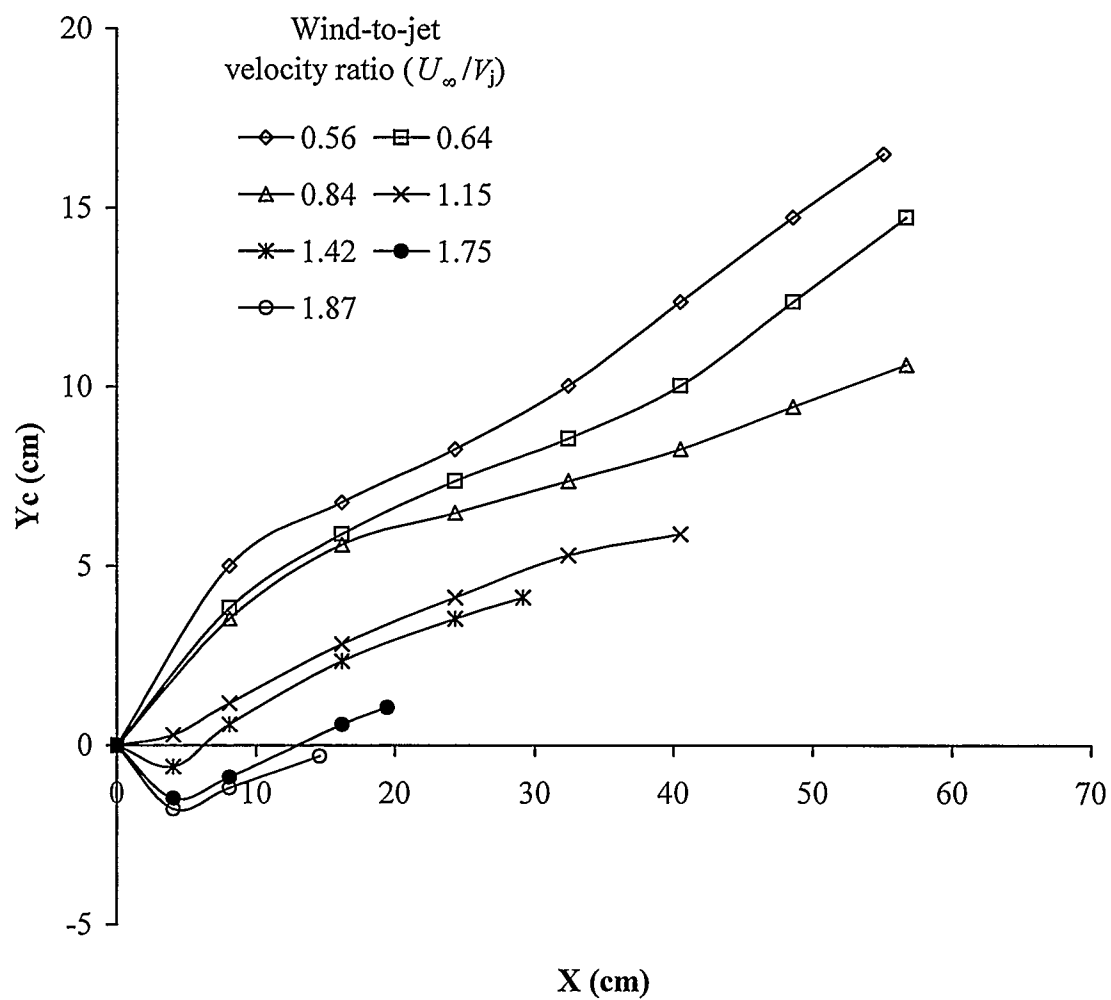


**Figure 4.13** Flame trajectory from the circular nozzle with a discharge area of  $30.4 \text{ mm}^2$  (fuel jet velocity of  $5.5 \text{ m/s}$ ).

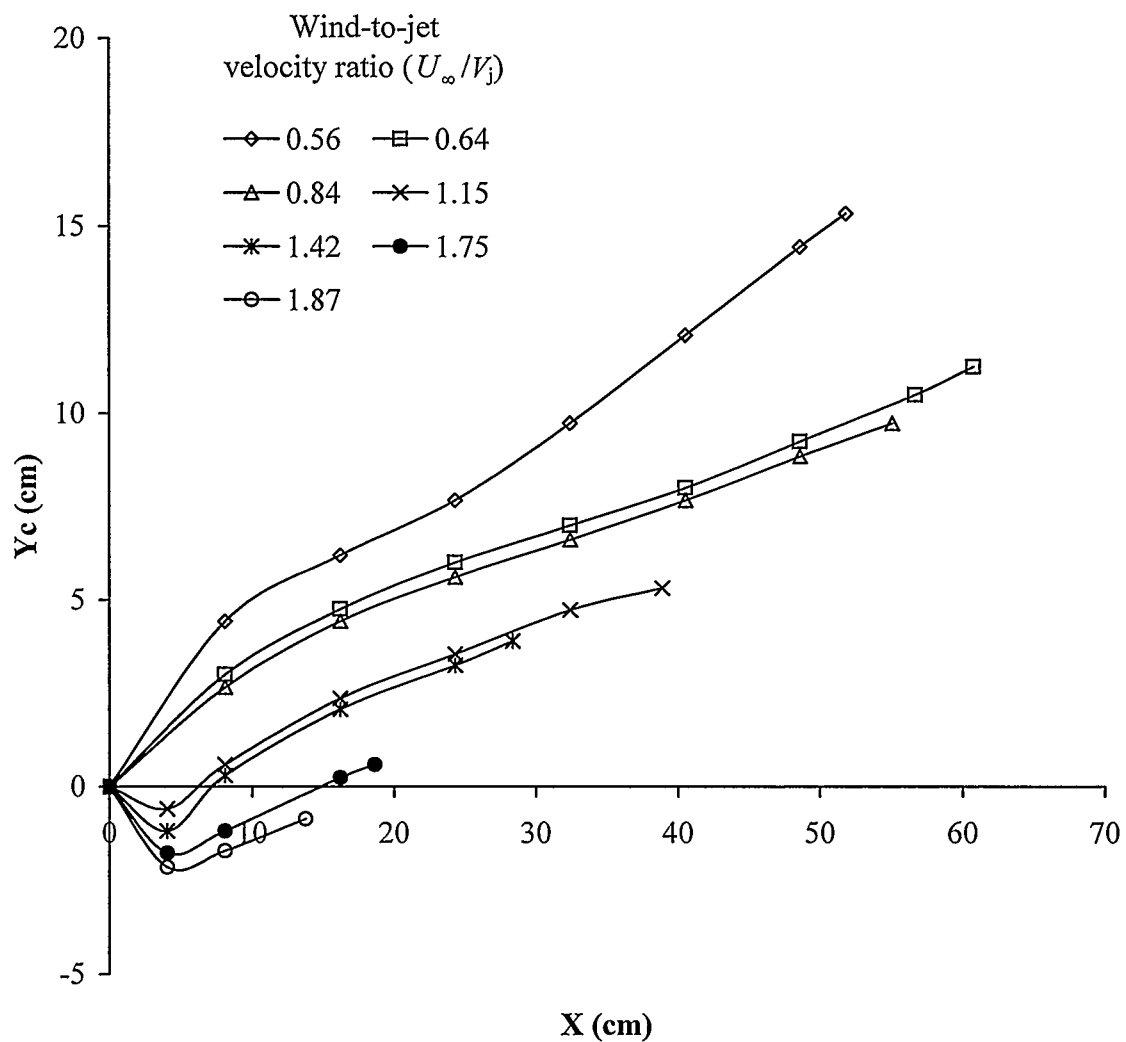


**Figure 4.14** Flame trajectory from the elliptical nozzle with aspect ratio of 2.5 (nozzle discharge area of  $30.4 \text{ mm}^2$ , major axis normal to cross wind, fuel jet velocity of  $5.5 \text{ m/s}$ ).

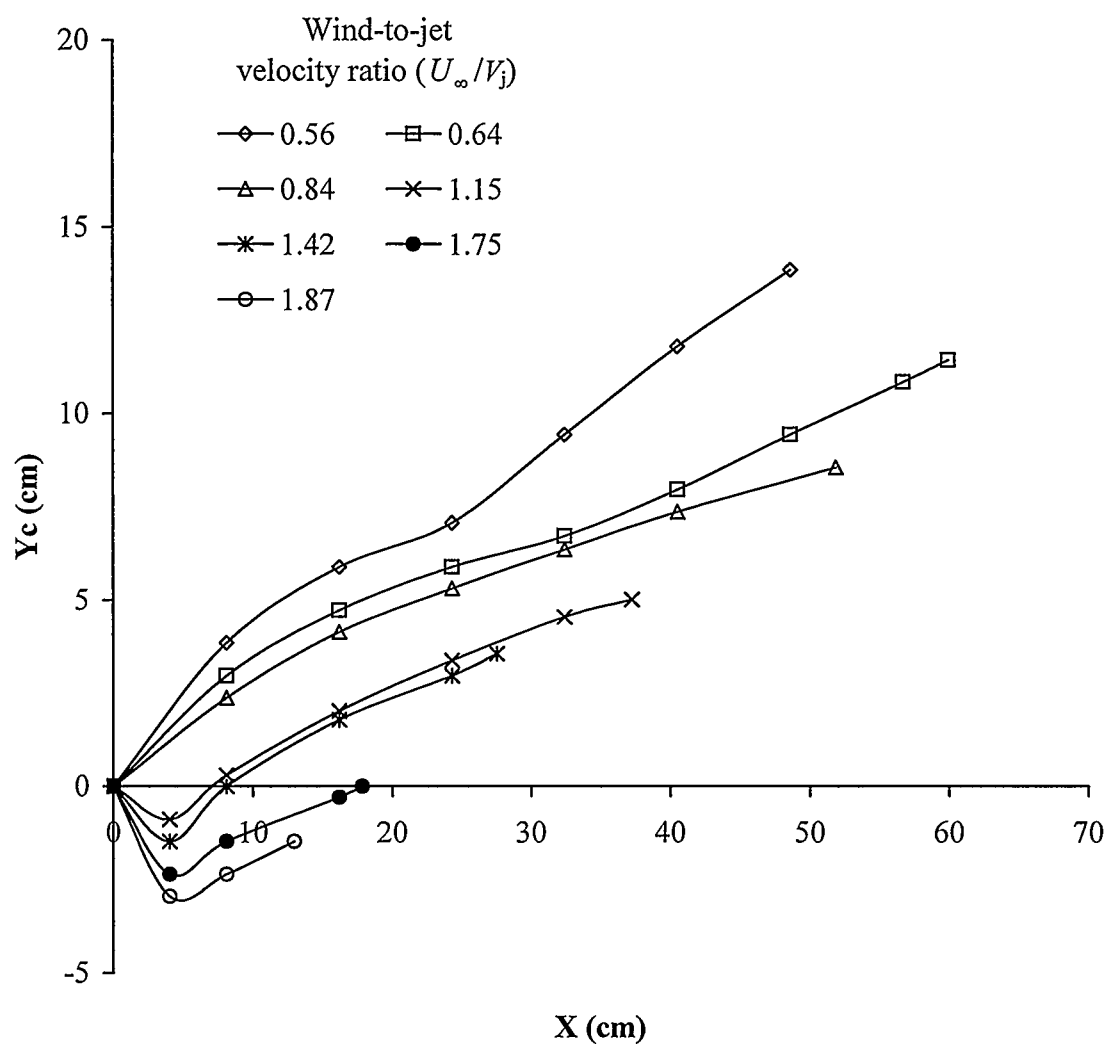


**Figure 4.15** Flame trajectory from the elliptical nozzle with aspect ratio of 3.2 (nozzle discharge area of  $30.4 \text{ mm}^2$ , major axis normal to cross wind, fuel jet velocity of  $5.5 \text{ m/s}$ ).

#### 4.3.4 Comparison of the flame trajectories from different nozzles

**Nozzles with discharge area of  $93.7 \text{ mm}^2$ .** Comparisons of the flame trajectories from circular and elliptical nozzles with discharge areas of  $93.7 \text{ mm}^2$  are shown in **Figure 4.16** to **Figure 4.22** for different cross-flow conditions. In these figures, the flame length and trajectory are compared between the circular and elliptical nozzles. The flames from elliptical nozzles are slightly shorter and, from flame visualization studies, wider than those from the circular nozzle, but the flames from the circular nozzle were more vertical than those from the elliptical nozzles. That is, the greater the aspect ratio, the smaller the angle between the flame trajectory contour line and horizontal cross-wind directions. With an increase in the cross-flow velocity, the flames angled further towards the horizontal until they were completely in the recirculation zone, in the wake of the stacks.

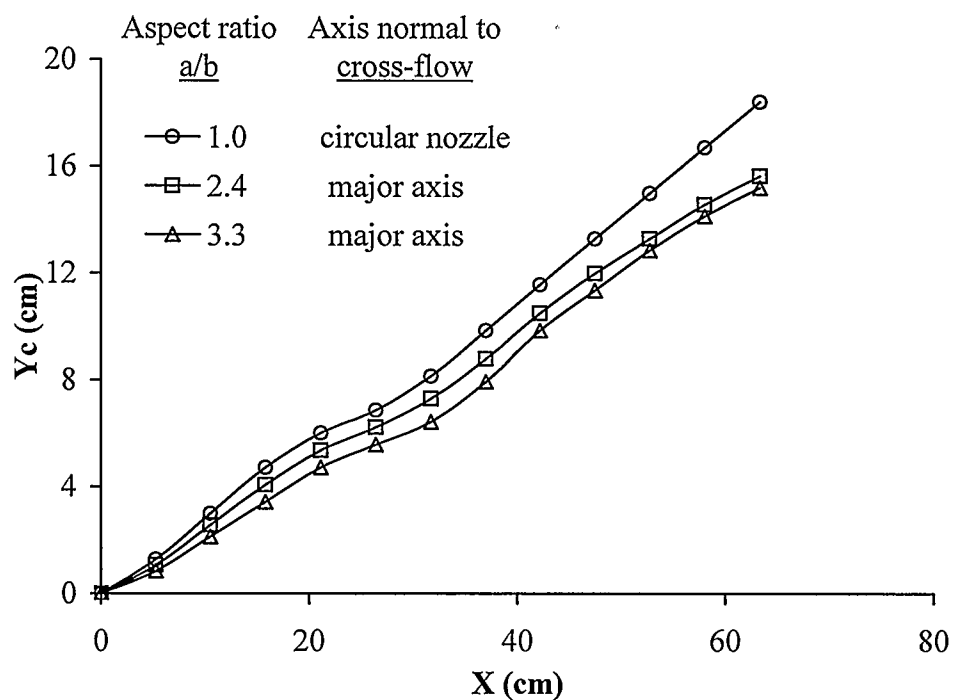


**Figure 4.16** Comparison of flame trajectories from different nozzles (discharge area of  $93.7 \text{ mm}^2$ , fuel jet velocity 4 m/s, cross-wind 3.1 m/s).

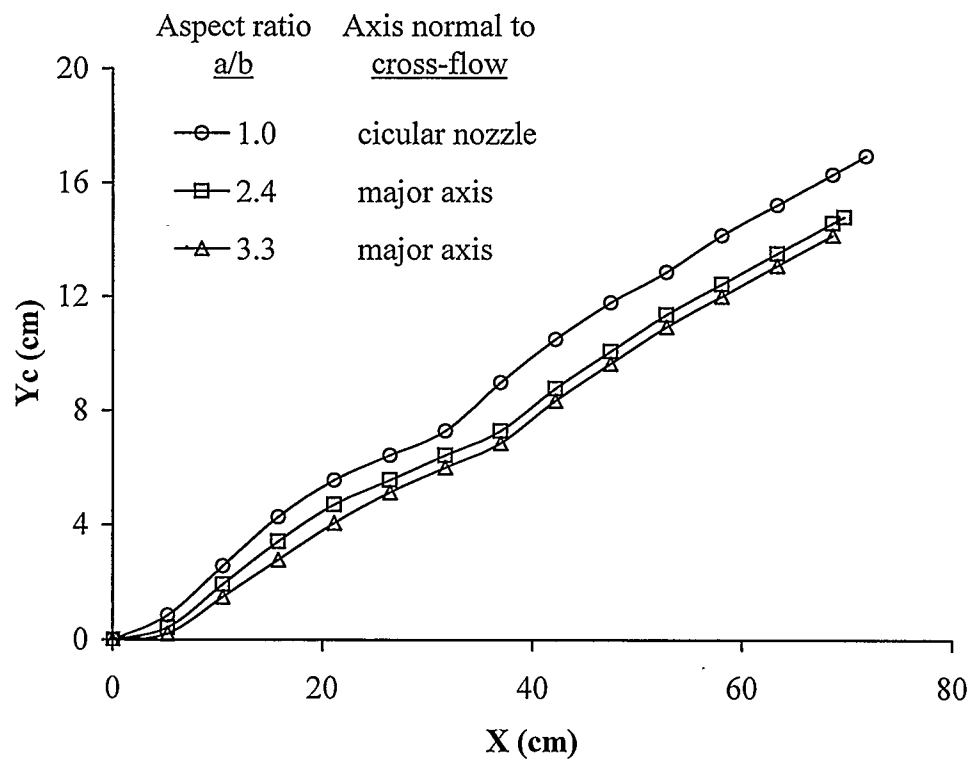


**Figure 4.17** Comparison of flame trajectories from different nozzles (discharge area of  $93.7 \text{ mm}^2$ , fuel jet velocity 4 m/s, cross-wind 3.5 m/s).

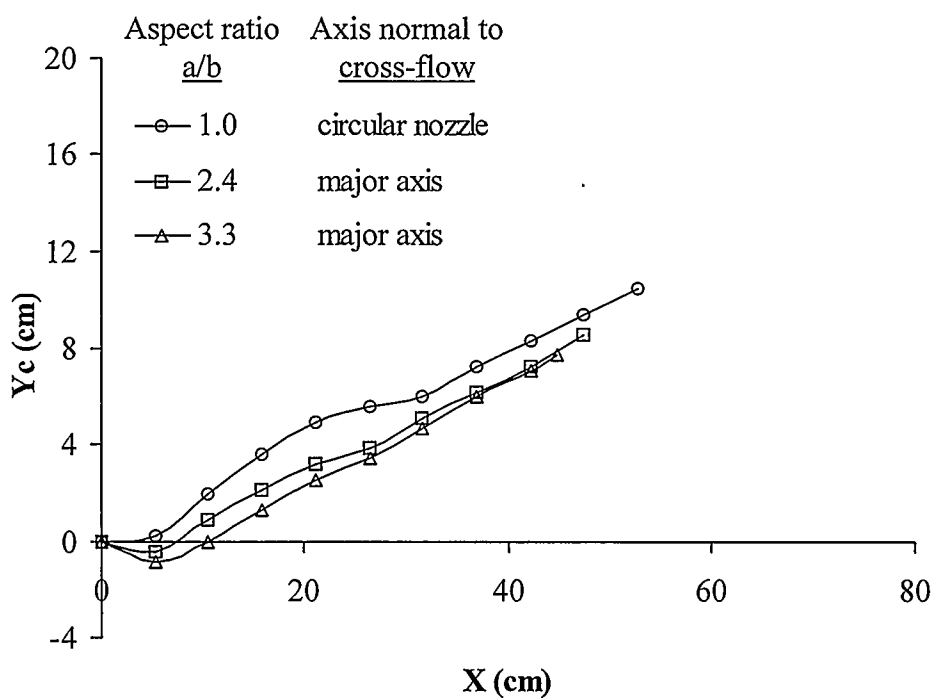


**Figure 4.18** Comparison of flame trajectories from different nozzles (discharge area of  $93.7 \text{ mm}^2$ , fuel jet velocity 4 m/s, cross-wind 4.6 m/s).

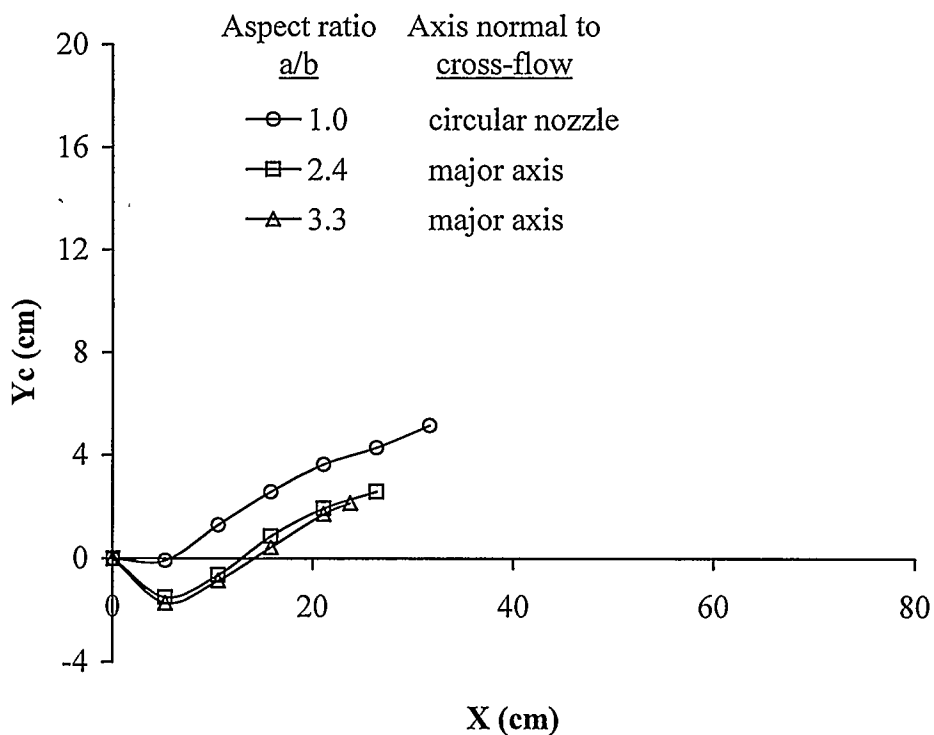


**Figure 4.19** Comparison of flame trajectories from different nozzles (discharge area of  $93.7 \text{ mm}^2$ , fuel jet velocity 4 m/s, cross-wind 6.3 m/s).

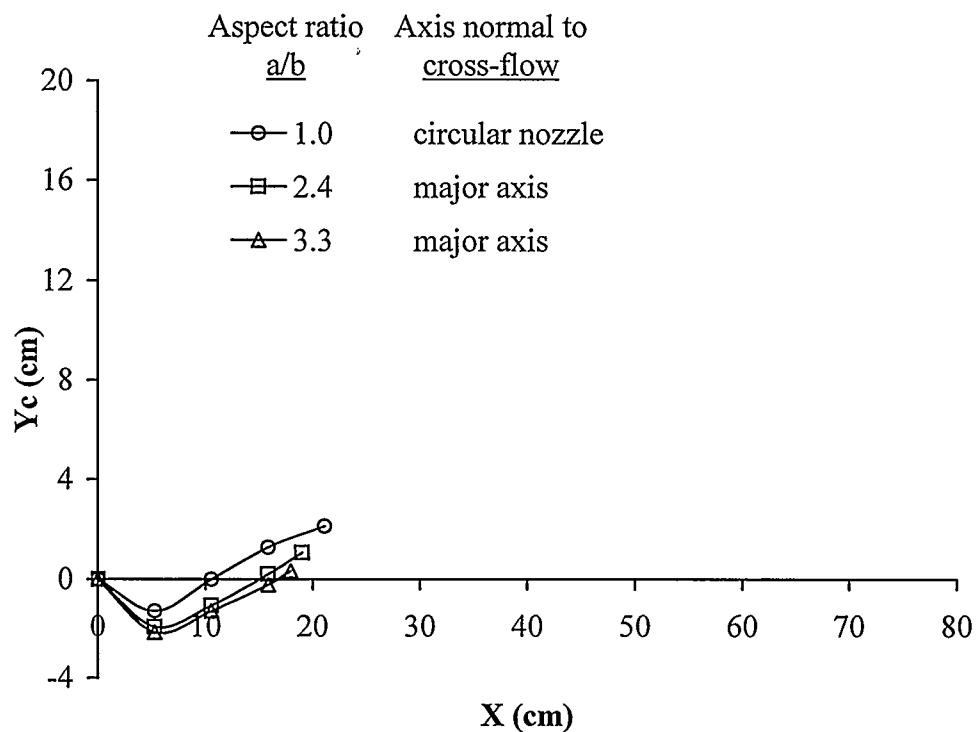


**Figure 4.20** Comparison of flame trajectories from different nozzles (discharge area of  $93.7 \text{ mm}^2$ , fuel jet velocity 4 m/s, cross-wind 7.8 m/s).

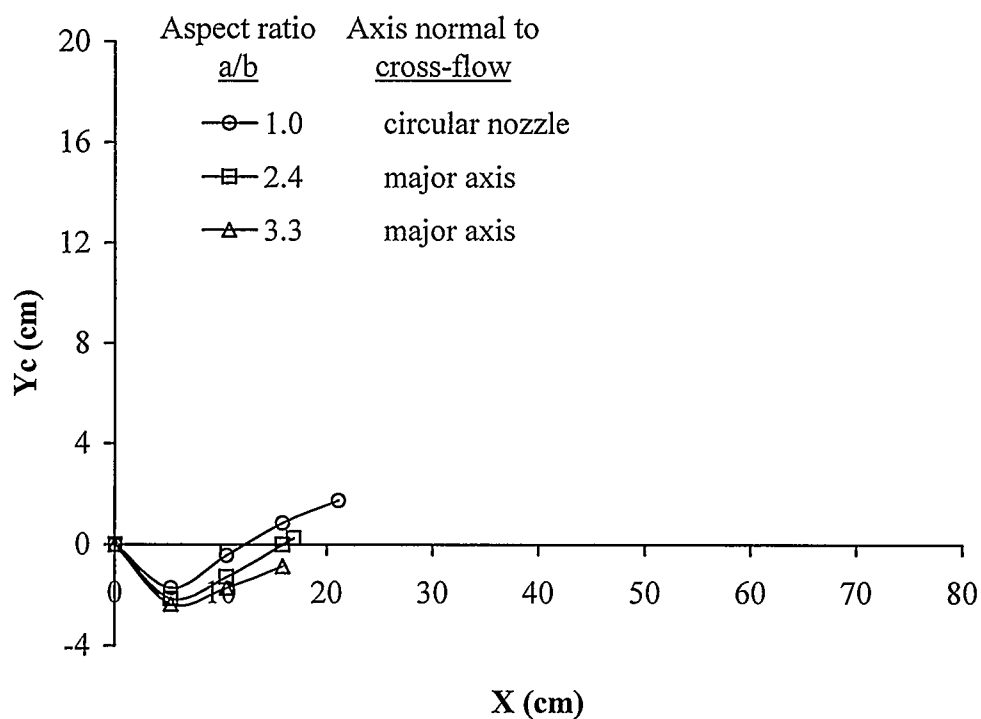


**Figure 4.21** Comparison of flame trajectories from different nozzles (discharge area of  $93.7 \text{ mm}^2$ , fuel jet velocity 4 m/s, cross-wind 9.6 m/s).

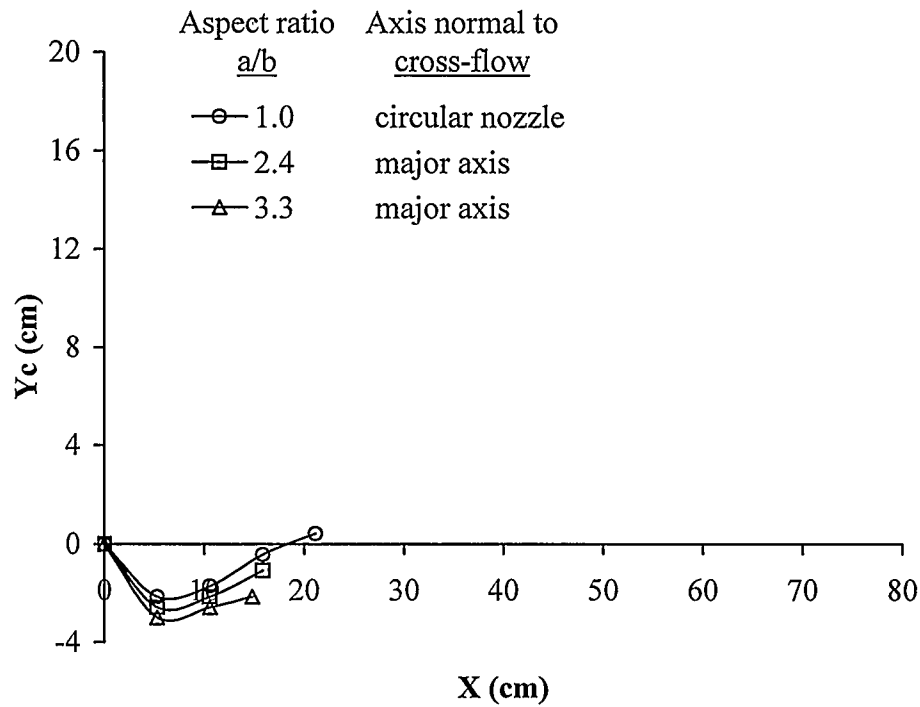


**Figure 4.22** Comparison of flame trajectories from different nozzles (discharge area of  $93.7 \text{ mm}^2$ , fuel jet velocity  $4 \text{ m/s}$ , cross-wind  $10.3 \text{ m/s}$ ).

**Nozzles with discharge area of  $30.4 \text{ mm}^2$ .** Comparisons of flame trajectories from the nozzles with discharge areas of  $30.4 \text{ mm}^2$  are shown in **Figure 4.23** to **Figure 4.29** for different cross-flow conditions. Similar trends to those from nozzles with discharge area of  $93.7 \text{ mm}^2$  were observed for these smaller nozzles. However, for the smaller discharge area nozzles, because of the smaller projected area in the lee-side of the stack, the effects of nozzle shapes on the flame length were not as pronounced as the nozzles with discharge area of  $93.7 \text{ mm}^2$ .



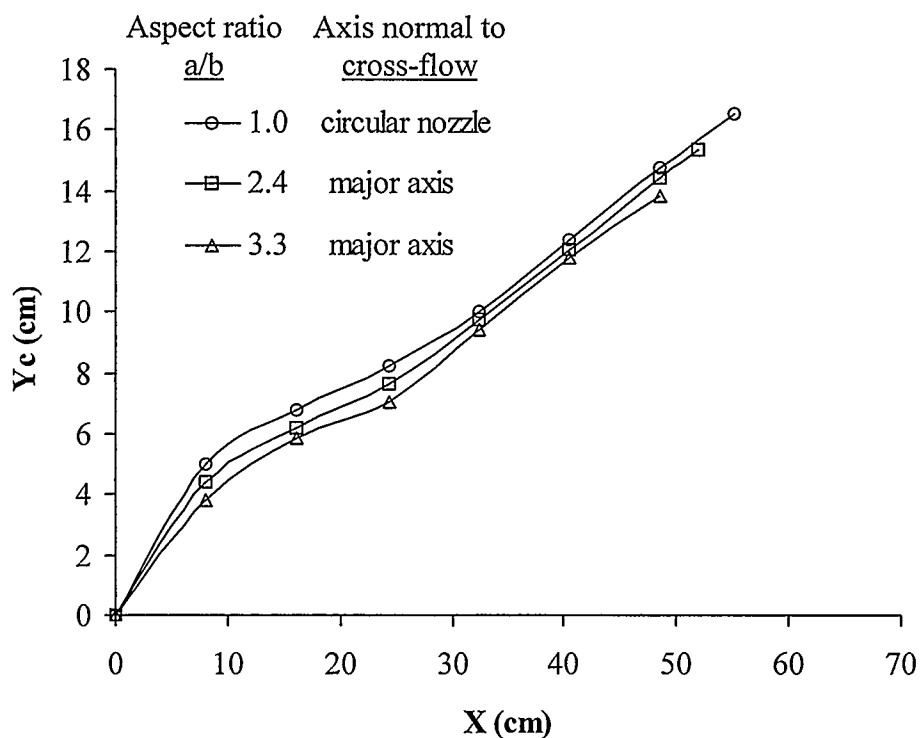


**Figure 4.23** Comparison of flame trajectories from different nozzles (discharge area of  $30.4 \text{ mm}^2$ , fuel jet velocity  $5.5 \text{ m/s}$ , cross-wind  $3.1 \text{ m/s}$ ).

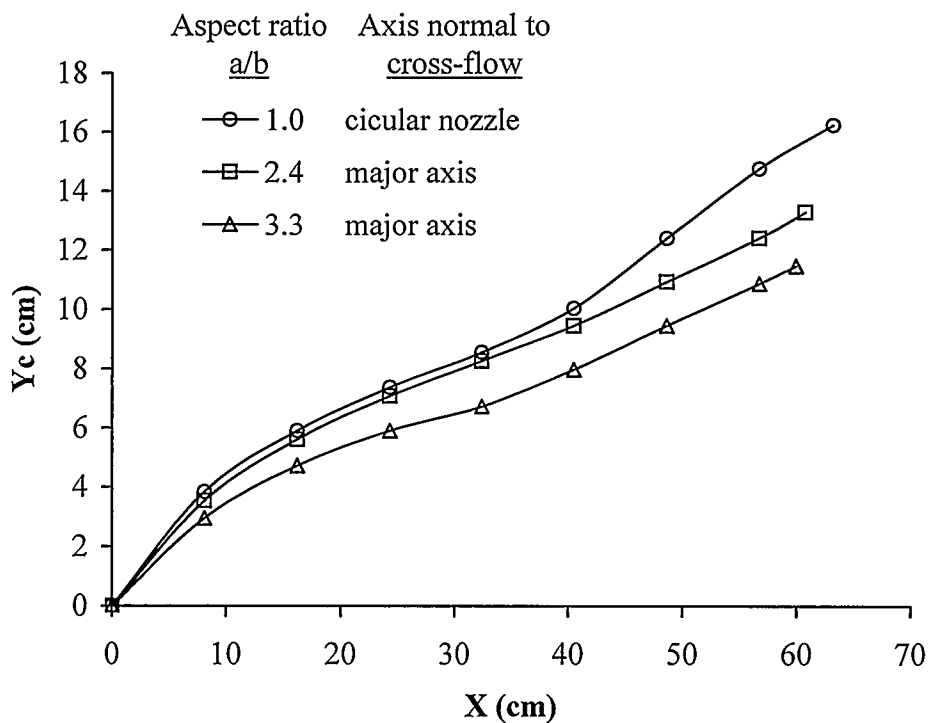


**Figure 4.24** Comparison of flame trajectories from different nozzles (discharge area of  $30.4 \text{ mm}^2$ , fuel jet velocity  $5.5 \text{ m/s}$ , cross-wind  $3.5 \text{ m/s}$ ).

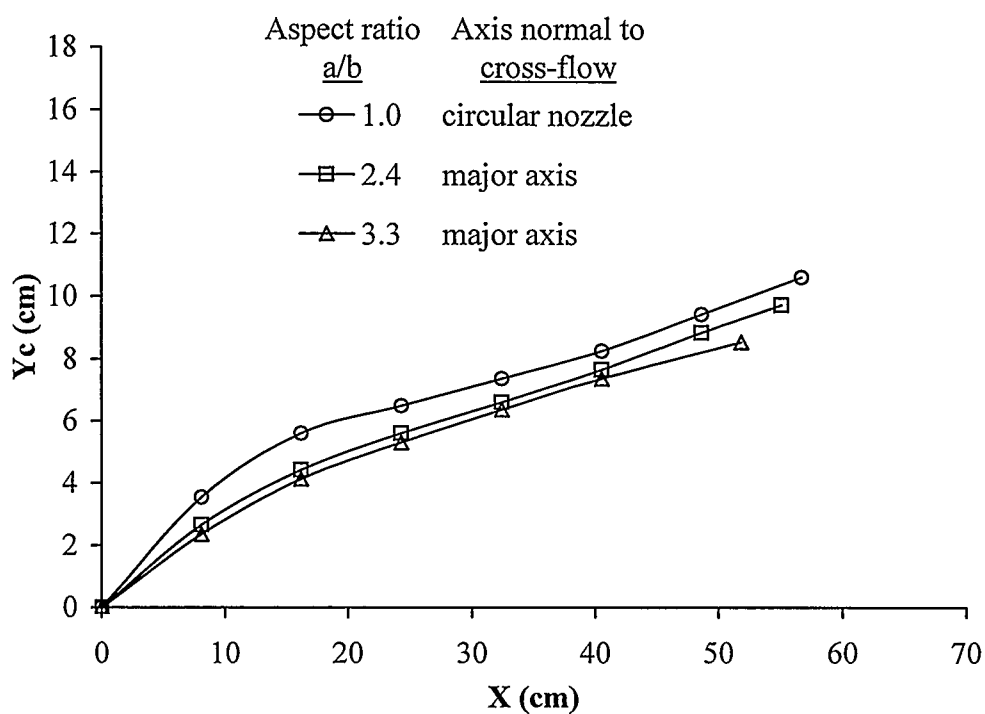


**Figure 4.25** Comparison of flame trajectories from different nozzles (discharge area of  $30.4 \text{ mm}^2$ , fuel jet velocity  $5.5 \text{ m/s}$ , cross-wind  $4.6 \text{ m/s}$ ).

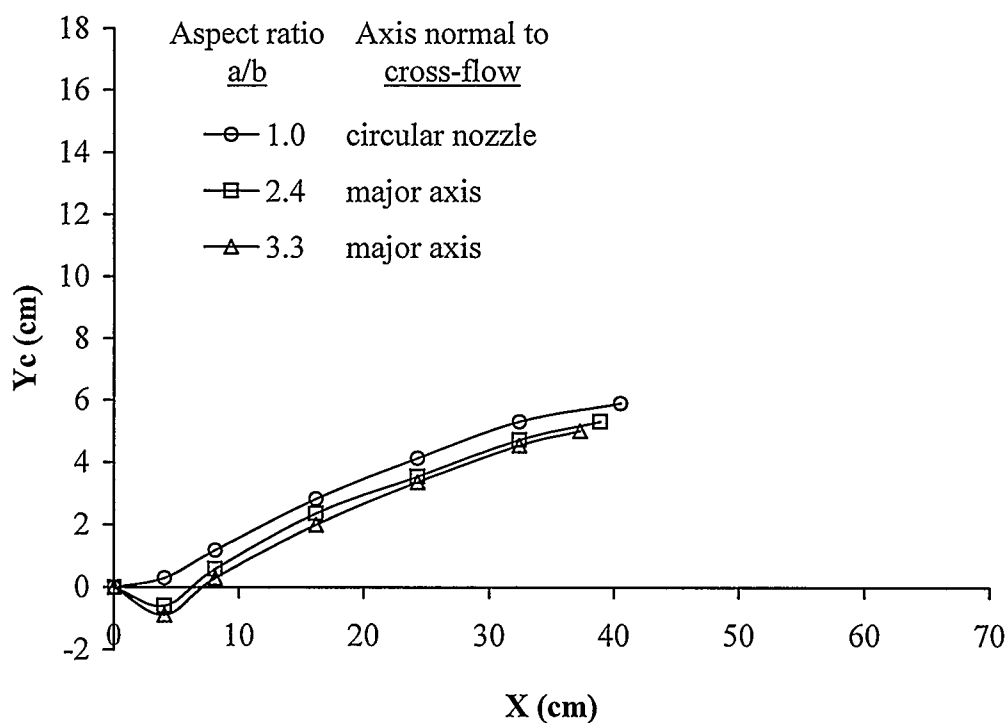


**Figure 4.26** Comparison of flame trajectories from different nozzles (discharge area of  $30.4 \text{ mm}^2$ , fuel jet velocity  $5.5 \text{ m/s}$ , cross-wind  $6.3 \text{ m/s}$ ).

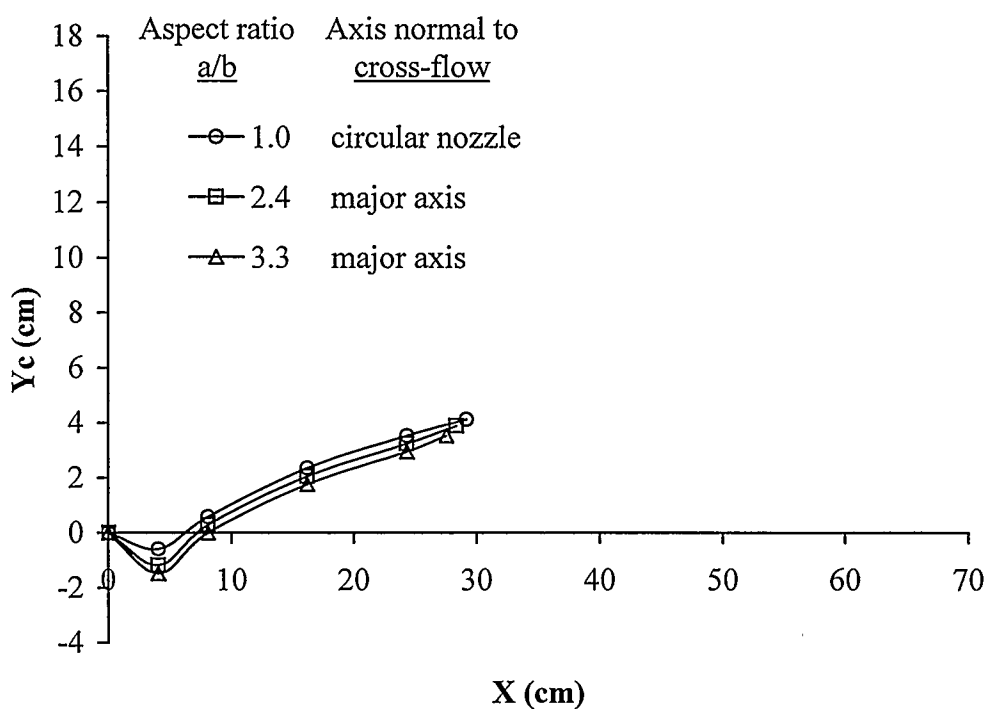


**Figure 4.27** Comparison of flame trajectories from different nozzles (discharge area of  $30.4 \text{ mm}^2$ , fuel jet velocity  $5.5 \text{ m/s}$ , cross-wind  $7.8 \text{ m/s}$ ).

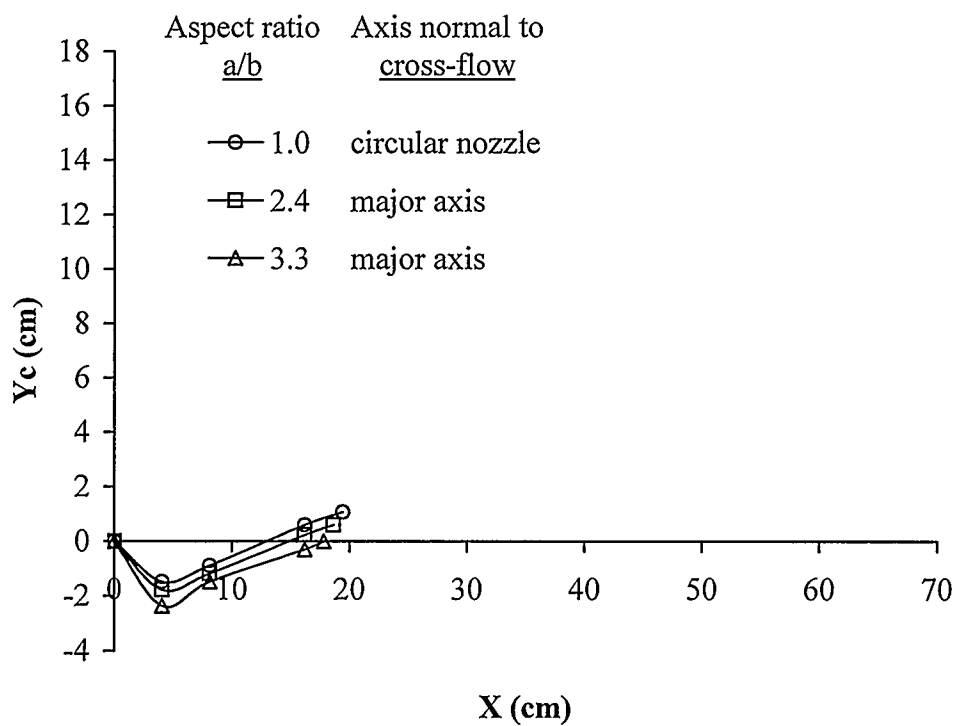


**Figure 4.28** Comparison of flame trajectories from different nozzles (discharge area of  $30.4 \text{ mm}^2$ , fuel jet velocity  $5.5 \text{ m/s}$ , cross-wind  $9.6 \text{ m/s}$ ).

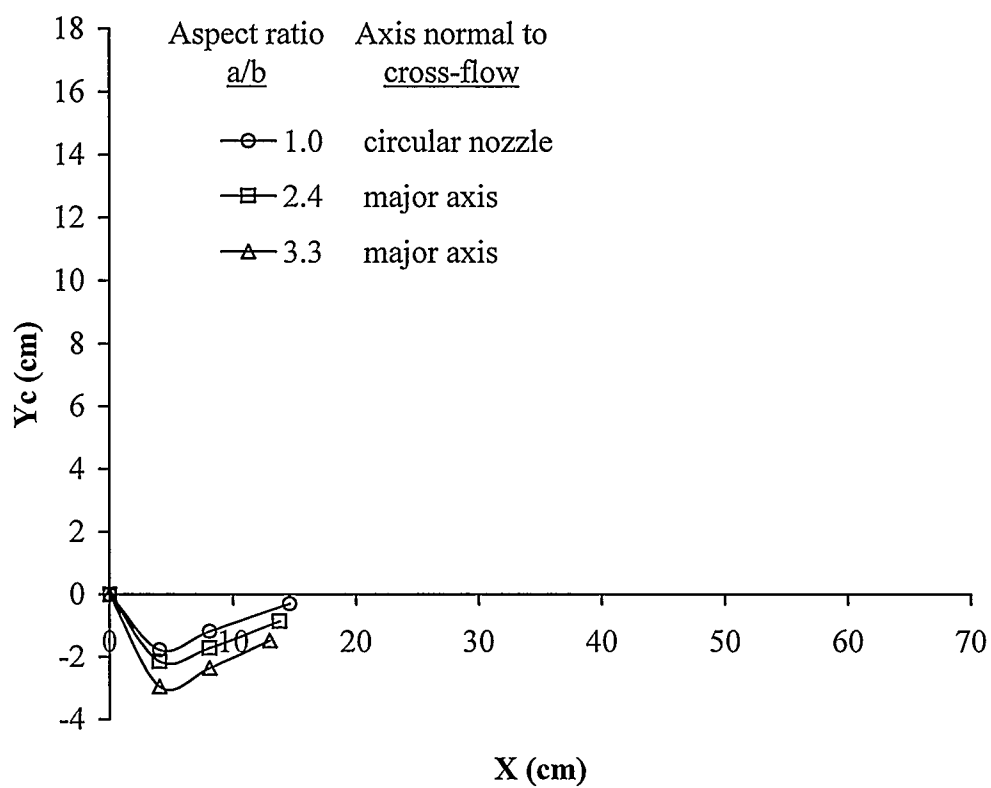


**Figure 4.29** Comparison of flame trajectories from different nozzles (discharge area of  $30.4 \text{ mm}^2$ , fuel jet velocity  $5.5 \text{ m/s}$ , cross-wind  $10.3 \text{ m/s}$ ).

#### 4.4 Mean flame lengths

##### 4.4.1 Nozzles with discharge area of 93.7 mm<sup>2</sup>

**Figure 4.30** and **Figure 4.31** show the effect of the mean flame lengths for nozzles with discharge area of 93.7 mm<sup>2</sup> as a function of the wind-to-jet velocity ratio ( $U_{\infty}/V_j$ ) and wind-to-jet momentum flux ratio ( $R_{\infty} = 1/R_j$ ), respectively. From these figures, it can be seen that at low cross-wind velocities, an increase in the cross-flow velocity increased the flame length. The flame length reached a maximum at  $U_{\infty}/V_j = 0.875$ , and  $R_{\infty} = 0.2$  beyond which further increases in the cross-flow velocities shortened the flame. This trend is consistent with the work of Gollahalli et al (1975) and Majeski et al (1999a, b). At relatively low cross-wind velocities, the cross-wind momentum pushes the flame in the downstream direction; however, the entrainment of the air into the fuel jet is not significant enough to improve the mixing of the fuel and air. Therefore, the flame is still yellowish and sooty (e.g. images in row **B** in **Figure 4.7**). With a further increase of the wind velocity ( $U_{\infty}/V_j$  varied from 0.875 to 2; and  $R_{\infty}$  varied from 0.2 to 1), the flame lengths are shortened drastically. This is due to the enhanced mixing of the fuel and air as a result of an increase in the turbulence intensity. This is consistent with flame visualization studies in which the flame became more bluish with increasing cross-wind velocities (images in rows **B** to **E** in **Figure 4.7**). At high cross-wind velocities ( $U_{\infty}/V_j$  ranging from 2 to 2.6;  $R_{\infty}$  ranging from 1 to 1.7), the flame lengths reached an asymptotic value as the flame stabilized and burned in the recirculation zone of the stack.

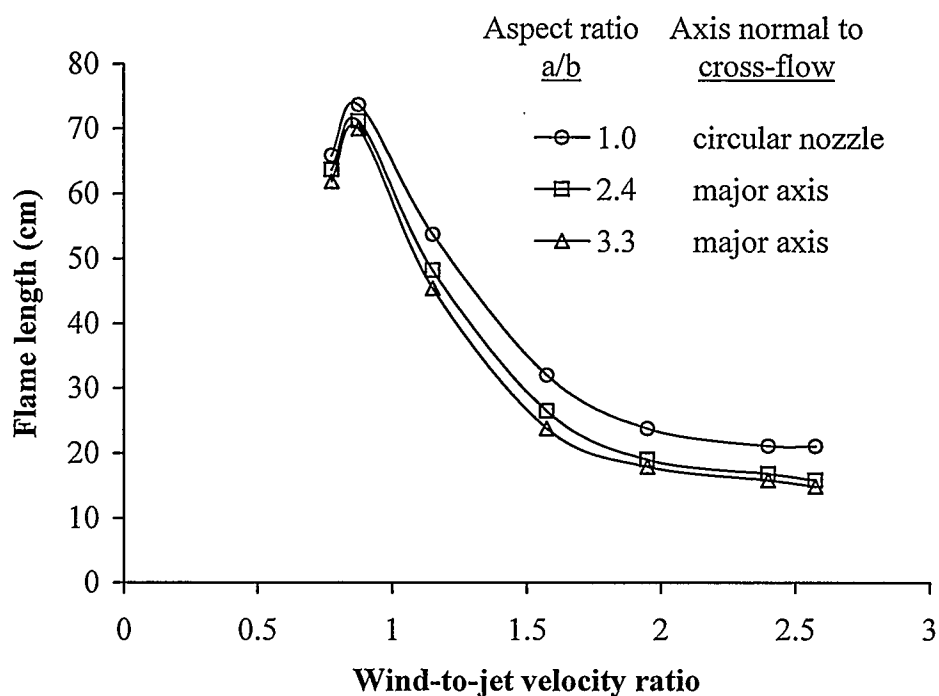


**Figure 4.30** Flame lengths as a function of wind-to-jet velocity ratio  $U_{\infty}/V_j$  (nozzle discharge area of  $93.7 \text{ mm}^2$ , fuel jet velocity 4 m/s).

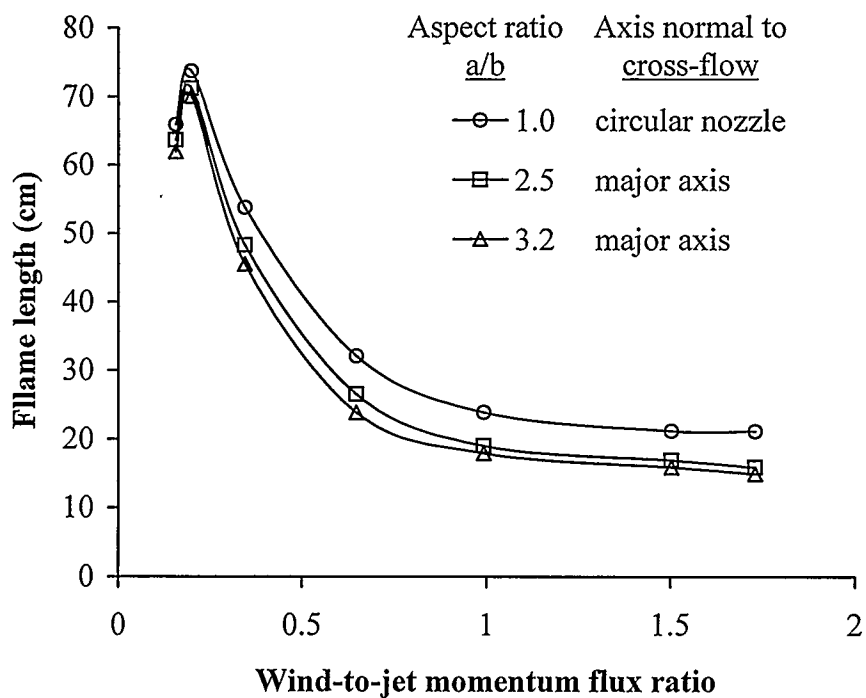


**Figure 4.31** Flame lengths as a function of wind-to-jet momentum flux ratio  $R_{\infty}$  (nozzle discharge area of  $93.7 \text{ mm}^2$ , fuel jet velocity 4 m/s).

#### 4.4.2 Nozzles with discharge area of 30.4 mm<sup>2</sup>

The mean flame lengths for nozzles with a discharge area of 30.4 mm<sup>2</sup> are shown in **Figure 4.32** and **Figure 4.33** as a function of the wind-to-jet velocity ratio ( $U_{\infty}/V_j$ ), and wind-to-jet momentum flux ratio ( $R_{\infty}$ ), respectively. Similar trends as those of nozzles with a discharge area of 93.7 mm<sup>2</sup> were observed; however, the maximum flame length, and range of the wind-to-jet velocity ratio ( $U_{\infty}/V_j$ ) and wind-to-jet momentum flux ratio ( $R_{\infty}$ ) at which the flame length increased or decreased is different. When  $U_{\infty}/V_j$  from 0.56 to 0.64, and  $R_{\infty}$  from 0.08 to 0.1, the flame lengths increased. With a further increase of the cross-wind velocity (i.e.,  $U_{\infty}/V_j$  from 0.64 to 1.4, and  $R_{\infty}$  from 0.1 to 0.52), the flame lengths shortened significantly. At high cross wind velocities (i.e.,  $U_{\infty}/V_j$  from 1.4 to 1.87, and  $R_{\infty}$  from 0.52 to 0.91), the flames lengths for these smaller nozzles decreased more significantly than those for nozzles with a discharge area of 93.7 mm<sup>2</sup>, and an asymptotic value was not approached. With a smaller diameter stack, the recirculation zone was smaller and the flame at high cross-wind velocities could not be sustained in the wake of the stack like in the case of the large discharge area nozzle. Therefore, the flame length continued to decrease with an increase in the cross-wind.

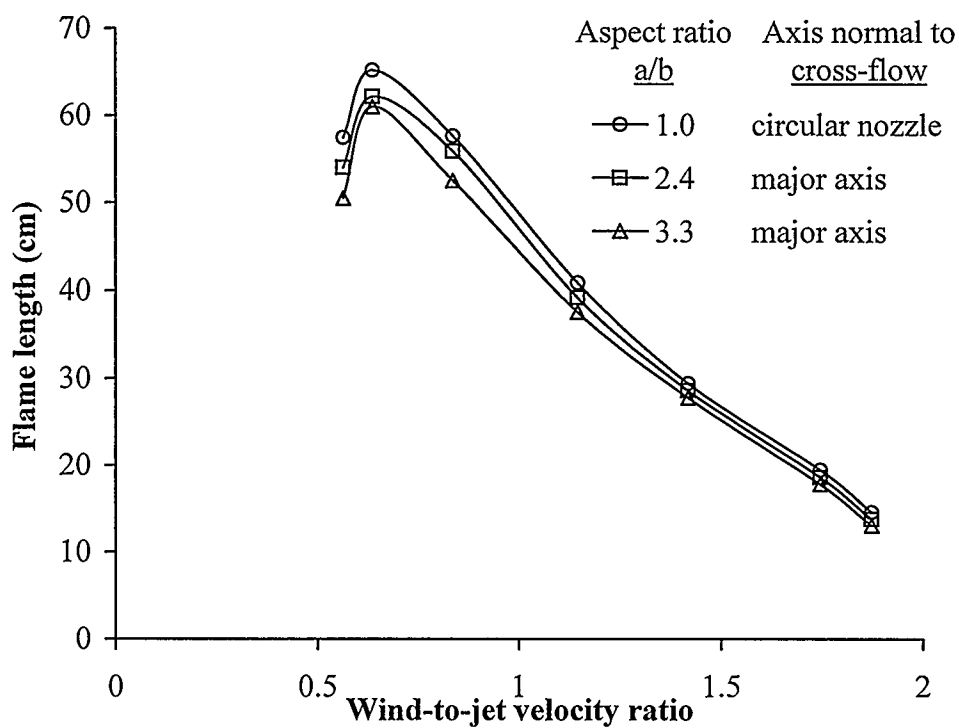


**Figure 4.32** Flame lengths as a function of wind-to-jet velocity ratio  $U_{\infty}/V_j$  (nozzle discharge area of  $30.4 \text{ mm}^2$ , fuel jet velocity  $5.5 \text{ m/s}$ ).

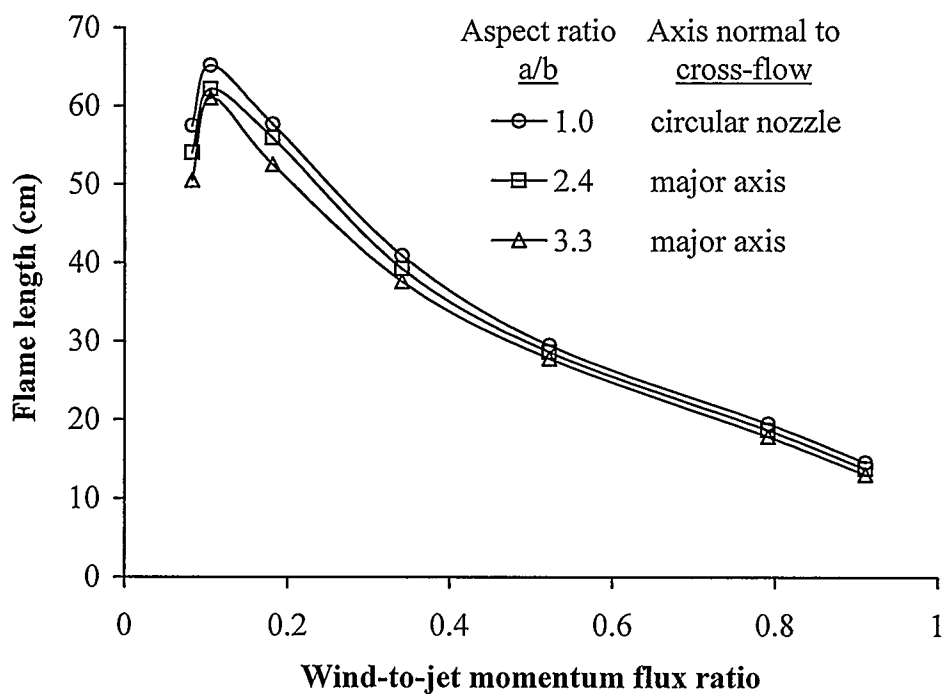


**Figure 4.33** Flame lengths as a function of wind-to-jet momentum flux ratio  $R_{\infty}$  (nozzle discharge area of  $30.4 \text{ mm}^2$ , fuel jet velocity  $5.5 \text{ m/s}$ ).



## CHAPTER FIVE: CONCLUSIONS AND RECOMMENDATIONS

### 5.1 Conclusions

From the discussions and the results presented in this thesis, the following conclusions are made:

- An elliptical jet has the potential to increase the blowout velocity depending on its orientation to the cross-flowing air stream and aspect ratio. The blowout limits of the elliptical jet were improved when the major axis was perpendicular to the cross-flow due to the greater recirculation zone created immediately downstream of the stack which acts as a flame holder. This holds true, especially in the higher wind velocities. However, when the minor axis was perpendicular to the flow, the blowout limits were found to be lower than its major axis counterpart and were sometimes even lower than that of the circular jet.
- The improvement of the blowout limits with elliptical nozzles was higher with larger discharge area nozzles. In all the nozzles used, the aspect ratio of 3.2 with the discharge area of  $93.7 \text{ mm}^2$  (largest discharge area used in this study) had the highest blowout limits.
- The greater recirculation zone created by the larger projected area in the leeside of the stack with the elliptical nozzles improved the blowout limits compared to those of circular nozzles.
- At low cross-wind velocities (i.e., high momentum flux ratio,  $R_j$ ), the flames were attached to the nozzle rim and angled into the downstream direction; the flames were highly radiative and sooty. The flame was blue in color in the near-field

region of the nozzle, with a luminous yellow color region in mid-flame and an orange-red region in the far-field.

- At low cross-wind velocities, an increase in the cross-wind velocity (i.e., decrease in  $R_j$  value) increased the overall flame length and flame was stabilized in the wake of the stack. In the vicinity of the stack, a small luminous yellow region was observed due to the condensed fuel pyrolysis. This luminous region appeared earlier in elliptical nozzles than in the circular nozzle, and the size of the luminous regions increased with an increase in the aspect ratio of nozzles.
- With a further increase in the cross-flow velocity, the flames angled closer to the horizontal and still remained anchored at the wake of the stack. The luminous region on the leeside of the stack became larger, especially for elliptical nozzles and this recirculation region increased further down along the stack. At this point, the length of the flame shortened and the color of the flame was primary blue. At even higher cross-wind velocities, the main tail of the flame was no longer present and the combustion of the fuel occurred exclusively in the recirculation zone on the downstream side of the flare stack.
- Flames from elliptical nozzles were slightly shorter but wider and sootier than those from the circular nozzle under the same operating conditions. This may be the result of the axis-switching phenomenon associated with elliptical nozzles, counter-rotating vortex shedding, and the recirculation zone.
- Flame necking occurred under high cross-wind velocities for small aspect ratio nozzles; for larger aspect ratio elliptical nozzles, necking did not occur in all of the experimental conditions.

- The flame trajectory was a function of the cross-flow velocity ( $U_{\infty}$ ) and fuel jet velocity ( $V_j$ ). At lower wind-to-jet velocity ratios, the flames were bent in the downstream direction of the cross-flow. The flame trajectories were dominated by the initial jet momentum in the near-nozzle region of the flames, and buoyancy effects came into play in the far field region. With an increase in the wind-to-jet velocity ratios, the recirculation zone at the leeside of the stack increased and buoyancy effects were not significant as the flame stabilized in the larger recirculation zone.
- The flame lengths increased with an increase in the cross-wind velocities; however, a local maximum was reached under certain wind-to-jet velocity ratios. Beyond this maximum, the flame lengths decreased significantly with increasing cross-flow velocities. An asymptotic value was reached for the largest discharge area nozzle (i.e., 93.7 mm<sup>2</sup>) at high cross-wind velocities: flames issuing from these larger nozzles were stabilized predominantly in the recirculation zone in the wake of the stack.

## 5.2 Future recommendations

Further investigations are recommended to understand the combustion characteristics of diffusion flames in a cross-flow. These include:

- Studying the effect of low calorific value fuels on the stability limits of diffusion flames is recommended since diluents are frequently present in solution gas flaring at well sites. The use of elliptical jets as a means of improving the combustion of such gases needs to be validated.

- An investigation of emissions from flames issuing from elliptical nozzles is required to verify quantitatively its effectiveness in reducing emissions as well as enhancing combustion efficiency.
- An investigation on the effects of liquids in the gaseous fuels on flame stability and exhaust emissions is recommended since flares in industry frequently burn solution gases.
- Additional improvements of the testing chamber is required for taking images of the cross-section of the flame and for allowing more data to be obtained to analyze the effects of the recirculation zone.
- Temperature and concentration measurements of the flame would assist in qualifying the degree of mixing of fuel and cross-wind flow.
- Laboratory experiments are useful in giving a qualitative understanding of the combustion and fluid dynamic processes involved in flares. However, due to scaling effects, laboratory measurements can not frequently be extrapolated to full scale flares. Therefore, scaling effects should be further studies. This may be achieved by testing a range of nozzles with different discharge areas and deriving a dimensionless formula for interpreting the relationship between the nozzle diameter and the parameters of interest (e.g., cross-wind velocity).
- Nozzles with controlled stream-wise vortex generators (e.g. azimuthal perturbation methods, including corrugated, lobed, or indented nozzle edges, vortex generators, or other nozzle shaping concepts) could be used to explore other methods for the enhancement of mixing of the fuel and air.

## REFERENCES

- Adler, D., and Baron, A., "Prediction of a Three-Dimensional Circular Turbulent Jet in Cross Flow," *AIAA Journal*, Vol. 17, 1979, pp. 168-174.
- Albayrak, Kahraman, "Design of a Low-Speed Axisymmetric Wind Tunnel Contraction," *Journal of Wind Engineering and Industrial Aerodynamics*, Vol. 37, 1991, pp. 79-86.
- Alberta Energy and Utility Board (EUB) News Release 29 July, 1999.
- Askari, A., Bullman, S.J., Fairweather, M., and Swaffield, F., "The Concentration Field of a Turbulent Jet in a Cross-Wind," *Combustion Science and Technology*, Vol. 73, 1990, pp. 463-478.
- Bandaru, Ramarao V., and Turns, Stephen R., "Turbulent Jet Flames in a Cross-flow: Effects of Some Jet, Cross-flow, and Pilot-Flame Parameters on Emissions," *Combustion and Flame*, Vol. 121, 2000, pp. 137-151.
- Barrett, R. V., "Design and Performance of a New Low Turbulence Wind Tunnel at Bristol University," *Aeronautical Journal*, March 1984, pp. 86-90.
- Becher, H.A., Liang, D., and Downey, C.I., "Effect of Burner Orientation and Ambient Airflow on Geometry of Turbulent Free Diffusion Flames," *Eighteenth Symposium (International) on Combustion*, The Combustion Institute, Pittsburgh, 1981, pp. 1061-1071.
- Birch, A.D., Brown, D.R., Fairweather, M. and Hargrave, G.K., "An Experimental Study of a Turbulent Natural Gas Jet in a Cross-Flow", *Combustion Science and Technology*, Vol. 66, 1989, pp. 217-232.

- Bossel, Hartmut H., "Computation of Axisymmetric Contractions," *AIAA Journal*, Vol. 7, No. 10, 1969, pp. 2017-2020.
- Botros, P. E., and Bruzustowski, T. A., "An Experimental and Theoretical Study of the Turbulent Diffusion Flame in Cross-Flow." *Seventeenth Symposium (International) on Combustion*, the Combustion Institute, Pittsburgh, 1978, pp. 389-398.
- Bourguignon, E., Johnson, M. R., and Kostiuk, L. W., "The Use of a Closed-Loop Wind Tunnel for Measuring the Combustion Efficiency of Flames in a Cross Flow," *Combustion and Flame*, Vol. 119, 1999, pp. 319-334.
- Bruzustowski, T.A., Gollahalli, S.R., and Sullivan, H.F., "The Turbulent Hydrogen Diffusion Flame in a Cross-Wind," *Combustion Science and Technology*, Vol. 11, No. 1-2, 1975, pp. 29-33.
- Cook, D.K., "An Integral Model of Turbulent Non-Premixed Jet Flames in a Cross-Flow," *Twenty-Third Symposium (International) on Combustion*, The Combustion Institute, Pittsburgh, 1990, pp. 653-660.
- Crabb, D., Durao, D.F.G., and Whitelaw, J.H., "Round Jet Normal to a Cross Flow," *Journal of Fluids Engineering*, Vol. 103, No.1, 1981, pp. 142-153.
- Chen, Dan-Zhi, "A Modeling Theory of Combustion Chambers," *Combustion Science and Technology*, Vol. 24, 1981, pp. 221-226.
- Ellzey, J.L., Berbee, J.G., Tay, Z.F., and Forster, D.E., "Total Soot Yield from a Propane Diffusion Flame in Cross-Flow," *Combustion Science and Technology*, Vol. 71, 1990, pp. 41-52.

Escudier, M.P., "Aerodynamics of a Burning Turbulent Gas Jet in a Cross-Flow,"

*Combustion Science and Technology*, Vol. 4, 1972, pp. 293-301.

Fairweather, M., Jones, W.P., and Lindstedt, R.P., "Prediction of Radiative Transfer from a Turbulent Reacting Jet in a Cross-Wind," *Combustion and Flame*, Vol. 88, 1992, pp. 45-63.

Fairweather, M., Jones, W.P., Lindstedt, R.P., and Marquis, A.J., "Prediction of a Turbulent Reacting Jet in a Cross-Flow," *Combustion and Flame*, Vol. 84, 1991, pp. 361-375.

Fearn, R., and Weston, R.P., "Vorticity Associated With a Jet in a Cross Flow," *AIAA Journal*, Vol. 12, 1974, pp. 1666-1671.

Fric, T.F., and Roshko, A., "Vortical Structure in the Wake of a Transverse Jet," *Journal of Fluid Mechanics*, Vol. 279, 1994, pp. 1-47.

Gollahalli, S. R., "Aerodynamic and Diluent Effects on the Emission of Nitrogen Oxides from Hydrocarbon Diffusion Flame," *Canadian Journal of Chemical Engineering*, Vol. 56, 1978, pp. 510-514.

Gollahalli, S.R., "Flame Structure and Pollutant Emission Characteristics of Elliptic Laminar Gas Jet Diffusion Flames," Presented at the Energy Sources Technology Conference and Exhibition, ASME, 1999

Gollahalli, S.R., Bruzustowski, T.A., and Sullivan, H.F., "Characteristics of a Turbulent Propane Diffusion Flame in a Cross-Wind," *Transaction of Canadian Society of Mechanical Engineering*, Vol. 3, No. 4, 1975, pp. 205-214.

- Gollahalli, S.R., Khanna, T. and Prabhu, N., "Diffusion Flames of Gas Jets Issued From Circular and Elliptic Nozzles," *Combustion Science and Technology*, Vol. 86, 1992, pp. 267-288.
- Gollahalli, S.R., and Prabhu, N., "Differences of the Structure of Lifted Gas Jet Flames with Laminar Base over Circular and Elliptic Nozzles," Presented at the Energy-source Technology Conference and Exhibition, New Orleans, LA, January 14-18, 1990.
- Gutmark, E., and Grinstein, F.F., "Flow Control with Noncircular Jets," *Annual Reviews in Fluid Mechanics*, Vol. 31, 1999, pp. 239-272.
- Gutmark, E., and Ho, C.M., "Visualization of a Forced Elliptic Jet," *AIAA Journal*, Vol. 24, No. 4, 1985, pp. 684-685.
- Gutmark, E., Schadow, K.C., Parr, T.P., Hanson-Parr, D.M., and Wilson, K.J., "Noncircular Jets in Combustion System," *Experiments in Fluids*, Vol. 7, 1989, pp. 248-258.
- Gutmark, E., Schadow, K.C., and Wilson, K.J., "Noncircular Jet Dynamics in Supersonic Combustion," *Journal of Propulsion*, Vol. 5, No. , Sep.-Oct., 1989.
- Gutmark, E., Schadow, K.C., and Wilson, K.J., "Subsonic and Supersonic Combustion Using Noncircular Injectors," *Journal of Propulsion*, Vol. 7, No. 2, 1991.
- Hernandez, J., Crespo, A., and Duijm, N. J., "Numerical Modeling of Turbulent Jet Diffusion Flames in the Atmospheric Surface Layer," *Combustion and Flame*, Vol. 101, No. 1-2, 1995, pp. 113-131.
- Ho, C.M., and Gutmark, E., "Vortex Induction and Mass Entrainment in a Small-Aspect-Ratio Elliptic Jet," *Journal of Fluid Mechanics*, Vol. 179, 1987, pp. 383-405.



- Houghton, J.T., Meira Filho, L.G., Callander, B.A., Harris, N., Kattenberg, A., and Maskell, K., "Climate Change 1995: the Science of Climate Change," *IPCC (International Panel on Climate Change)*, Cambridge University Press, Cambridge, U.K., 1996
- Huang, R.F. and Chang, J.M., "The Stability and Visualized Flame and Flow Structures of a Combusting Jet in Cross-Flow," *Combustion and Flame*, Vol. 98, 1994, pp. 267-278.
- Huang, R.F. and Wang, S.M., "Characteristic Flow Modes of Wake-Stabilized Jet Flames in a Transverse Air Stream," *Combustion and Flame*, Vol. 117, 1999, pp. 59-77.
- Huang, R.F. and Yang, M.J., "Thermal and Concentration Fields of Burner-Attached Jet Flames in Cross Flow," *Combustion and Flam*, Vol. 105, 1996, pp. 211-224.
- Hussain, F., and Husain, H.S., "Elliptic Jets. Part1. Characteristics of Unexcited and Excited Jets," *Journal of Fluid Mechanics*, Vol. 208, 1989, pp. 257-320.
- Johnson, M.R. and Kostiuk, L.W., "Effects of a Fuel Diluent on the Efficiencies of Jet Diffusion Flames in Crosswind," Presented at the Combustion Institute, Canadian Section, 1999 Spring Technical Meeting, Edmonton, Alberta, May 16-19, 1999.
- Johnson, M.R. and Kostiuk, L.W., "Effects of Low-Momentum Jet Diffusion Flames in Crosswinds," *Combustion and Flam*, Vol. 123, 2000, pp. 189-200.
- Johnson, M.R., Majeski, A.J., Wilson, D.J., and Kostiuk, L.W., "The Combustion Efficiency of a Propane Jet Diffusion Flame in Cross-Flow," Presented at the Fall Meeting of the Western States Section of the Combustion Institute, Seattle, Washington, October 26-27, 1998.

- Johnson, M.R., Zastavniuk, O., Wilson, D.J., and Kostiuk, L.W., "Efficiency Measurements of Flares in a Cross-Flow," Presented at Combustion Canada 1999, Calgary, Alberta, May 26-28, 1999.
- Johnson, M.R., Zastavniuk, O., Dale, J.R. and Kostiuk, L.W., "The Combustion Efficiency of Jet Diffusion Flames in Cross-Flow," Presented at the Joint Meeting of the United States Section, the Combustion Institute, Washington, D. C., March 15-17, 1999.
- Kalghatgi, G.T., "Blow-Out Stability of Gaseous Jet Diffusion Flames. Part I: In Still Air," *Combustion Science and Technology*, Vol. 26, 1981, pp. 233-239.
- Kalghatgi, G.T., "Blow-Out Stability of Gaseous Jet Diffusion Flames. Part II: Effect of Cross Wind," *Combustion Science and Technology*, Vol. 26, 1981, pp. 241-244.
- Kalghatgi, G.T., "Blow-Out Stability of Gaseous Jet Diffusion Flames. Part III: Effect of Burner Orientation to Wind Direction," *Combustion Science and Technology*, Vol. 28, 1982, pp. 241-245.
- Kalghatgi, G.T., "The Visible Shape and Size of a Turbulent Hydrocarbon Jet Diffusion Flame in a Cross-wind," *Combustion and Flame*, Vol. 52, 1983, pp. 91-106.
- Kamotani, Y., and Greber, I., "Experiments on a Turbulent Jet in a Cross Flow," *AIAA Journal*, Vol. 10, No. 11, November 1972, pp. 1425-1429.
- Karagozian, A.R., "Analytical Model for the Vorticity Associated With a Transverse Jet," *AIAA Journal*, Vol. 24, No.3, 1986, pp. 429-436.
- Karagozian, A.R., and Nguyen, T.T., "Effects of Heat Release and Flame Distortion in the Transverse Fuel Jet," *Twenty-First Symposium (International) on Combustion*, the Combustion Institute, Pittsburgh, 1986, pp. 1271-1279.

Karim, G. A. and Klat, S. R., "The Measurement of the Mass Flow Rate of Diffusion Gases Using a Choked Nozzle," Laboratory practice, University of Calgary.

Kibrya, M.G. "An Experimental and Analytical Examination of Jet Diffusion Flames in Non-Quiescent Environments of Fuel and Air" Ph. D Dissertation, Department of Mechanical Engineering, University of Calgary, Calgary, January, 1987.

Lam, K. and Pomfret, M.J., "Design and Performance of a Low Speed Wind Tunnel," *International Journal of Mechanical Engineering Education*, Vol. 13, No. 3, 1984, pp. 161-172.

Majeski, Adrian J., Wilson, David J., and Kostiuk, Larry W., "Local Maximum Flare Length of Flares in a Crosswind," Presented at the Canadian Section of the Combustion Institute, Edmonton, Alberta, May 16-19, 1999.

Majeski, Adrian J., Wilson, David J., and Kostiuk, Larry W., "Size and Trajectory of a Flare in a Cross Flow," Presented at Combustion Canada 1999, Calgary, Alberta, May 26-28, 1999.

Mehta, R.D. and Bradshaw, P., "Design Rules for Small Low Speed Wind Tunnels," *Aeronautical Journal*, November 1979, pp. 443-449.

Mikhail, M.N., "Optimum Design of Wind Tunnel Contractions," *AIAA Journal*, Vol. 17, No. 5, May 1979, pp. 471-477.

Morel, T., "Design of Two-Dimensional Wind Tunnel Contractions," Presented by the Fluids Engineering Division of The American Society of Mechanical Engineers at the Winter Annual Meeting, New York, N. Y., December 5, 1975.

- Papanikolaou, N. and Wierzbza, I., "Effect of Burner Geometry on the Blowout Limits of Jet Diffusion Flames in a Co-flowing Oxidizing Stream," *Transactions of the ASME*, Vol. 118, June, 1996, pp. 134-139.
- Papanikolaou, N. and Wierzbza, I., "The Effects of Burner Geometry and Fuel Composition on the Stability of a Jet Diffusion Flame," *Journal of Energy Resources Technology*, Vol. 119, December, 1997, pp. 265-270.
- Papanikolaou, N., "An Experimental Investigation of the Flow Structure and Stability Limits of Jet Diffusion Flames in a Co-flowing Oxidizing Stream," Ph. D Dissertation, Department of Mechanical Engineering, University of Calgary, Calgary, May, 1998.
- Pohl, J.H., Lee, J., Payne, R., and Tichenor, B.A., "Combustion Efficiency of Flares," *Combustion Science and Technology*, Vol. 50, 1986, pp. 217-231.
- Popovic, B., Thomson, M.J., and Lightstone, M.F., "The Combustion Efficiency of Furnace Exhaust Gas Combustors: A Study of Jet Mixing in a Reacting Cross Flow," *Combustion Science and Technology*, Vol. 155, 2000, pp. 31-49.
- Poudenx, P. and Kostiuk, L.W., "An Investigation of the Mean Plume Structures of a Flare in a Crosswind," Presented at the Canadian Section of the Combustion Institute, Edmonton, Alberta, May 16-19, 1999.
- Prabhu N. and Gollahalli, S.R., "Effect of Aspect ratio on Combustion Characteristics of Elliptic Nozzle Flames" *Emerging Energy Technology*, ASME, Vol. 36, 1991.
- Prybysh, Roberta, "The Production of Toxic Emissions from Reaction Diffusion Jet Flames in a Cross-flow," Master's Dissertation, Department of Mechanical Engineering, University of Alberta, Edmonton, Spring, 2002.

- Quinn, W. R., "Passive Near-field Mixing Enhancement in Rectangular Jet Flows," *AIAA Journal*, Vol. 29, No. 4, April 1991, pp. 515-519.
- Ramsey, J.W., and Goldstein, R.J., "Interaction of a Heated Jet with a Deflecting Stream," *Journal of Heat Transfer*, Vol. 93, 1971, pp. 365-372.
- Rao, V.K., and Bruzustowski, T.A., "Tracer Studies of Jets and Diffusion Flames in Cross-Flow," *Combustion Science and Technology*, Vol. 28, No. 5-6, 1982, pp. 229-239.
- Reeder, M.F. and Samimy, M., "The Evolution of a Jet with Vortex-Generating Tabs: Real-Time Visualization and Quantitative Measurements," *Journal of Fluid Mechanics*, Vol. 311, 1996, pp. 73-118.
- Reeder, M.F., Samimy, M., and Elliott, G.S., "Investigation of the Effect of Tabs on Supersonic Jets Using Advanced Diagnostics," *Journal of Propulsion and Power*, Vol. 12, No. 4, July-August 1996, pp. 742-751.
- Schadow, K.C., Wilson, K.J., Lee, M.J., and Gutmark, E., "Enhancement of Mixing in Ducted Rockets with Elliptic Gas-Generator Nozzles," *AIAA paper* 84-1260, 1984.
- Schadow, K.C., Wilson, K.J., Lee, M.J., and Gutmark, E., "Enhancement of Mixing in Reacting Fuel-rich Plumes Issued form Elliptic Nozzles," *Journal of Propulsion*, Vol. 3, No. 2, March-April, 1987, pp.145-149.
- Schadow, K.C., Gutmark, E., Wilson, K.J., and Parr, D.M., "Mixing Characteristics of a Ducted Elliptic Jet," *Journal of Propulsion*, Vol. 4, No. 4, July-August, 1988, pp. 328-333.

Smith, S.H., and Mungal, M.G., "Mixing, Structure and Scaling of the Jet in Cross-flow,"

*Journal of Fluid Mechanics*, Vol. 357, 1998, pp. 83-122.

Stoy, R.L., and Ben-Haim, Y., "Turbulent Jets in a Confined Cross flow," *Journal of*

*Fluids Engineering, Transactions of the ASME*, Vol. 95, 1973, pp. 551-556.

Stroscher, M., "Investigations of Flare Gas Emissions in Alberta," Environmental Technologies, Alberta Research Council Report, November 1996.

Stroscher, M., "Characterization of Emissions from Diffusion Flare Systems" *Journal of the Air and Waster Management Association*, Vol. 50, October, 2000

University of Alberta Flare Research Project – Interim Report, November 1996 – June 2000, December 1, 2000

Urson, H., Lightstone, M.F., and Thomson, M.J., "A Numerical Study of Jets in a Reacting Cross-flow," *Numerical Heat Transfer*, Part A, Vol. 40, 2001, pp. 689-714.

Verma, S.B. and Rathakrishnan, E., "Studies of Elliptic Jets with Passive Control," 1996 *Fluids Engineering Division Conference*. Vol. 2, ASME 1996.

Yoo, U. D. and Shin, D. D., "An Experimental Study of Jet Diffusion Flames in Cross Air-Flow," *Journal of the Institute of Energy*, Vol. 67, September 1994, pp. 121-127.

Zaman, K.B.M.Q., "Axis Switching and Spreading of an Asymmetric Jet: the Role of Coherent Structure Dynamics," *J. Fluid Mech.* Vol. 316, 1996, pp. 1-27.

Zaman, K.B.M.Q., Reeder, M.F., and Samimy, M., "Control of an Axisymmetric Jet Using Vortex Generators," *Physical of Fluids*, Vol. 6, No. 2, February 1994, pp. 778-793.

Zaman, K.B.M.Q., Steffen, C.J., and Reddy, D.R., "Entrainment and Spreading Characteristics of Jets From Asymmetric Nozzles," 28<sup>th</sup> *AIAA* Fluid Dynamics Conference, 4<sup>th</sup> *AIAA* Shear Flow Control Conference, Snowmass Village, CO., June 29-July 2, 1997.

**Appendix A: Calibration of choked nozzles used in the experiments**

There are five types of choked nozzles used in the experiments with diameters of 2.26, 1.32, 1.09, 0.91, and 0.64 mm. The calibration curves of these nozzles are shown in the following **Figure A.1**.

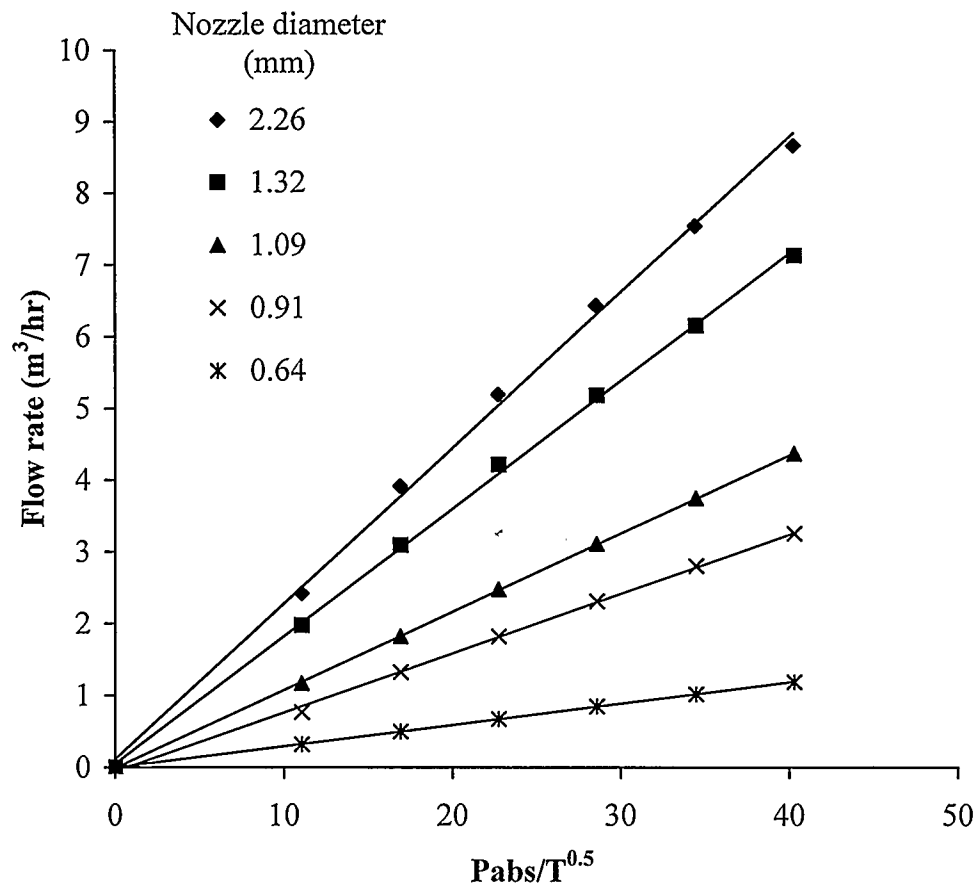


**Figure A.1** Calibration curves for the choked nozzles used in the experiments.



**Appendix B:** Calculations of the major and minor diameters for elliptical nozzles

**1. Series one:**  $D_o = 12.7$  mm (OD) diameter circular nozzle and elliptical nozzles with same discharge area of  $93.7 \text{ mm}^2$ :

i). Area of the circular nozzle:

$$A_c = (3.14 * D_i^2)/4$$

Where,  $D_i$  = inner diameter of the circular nozzle, for  $D_o = 12.7$  mm (OD) circular nozzle with  $\Delta = 0.89$  mm wall thickness,  $D_i = 10.9$  mm

$$A_c = 93.7 \text{ mm}^2$$

ii). Area of the elliptical nozzle:

$$A_e = 3.14 * (a-0.89) * (b-0.89)$$

Where,  $a = \frac{1}{2}$  major diameter (mm),  $b = \frac{1}{2}$  minor diameter (mm)

iii). Area of the circular nozzle = Area of the elliptical nozzle

$$D_i^2/4 = (a-0.89) * (b-0.89)$$

(a). For elliptical nozzle of aspect ratio of 2.5:

$$a = 2.5 * b, \quad D_i^2/4 = (2.5 * b - 0.89) * (b - 0.89)$$

$$b = 4.1 \text{ mm}, a = 10.2 \text{ mm},$$

$$\text{Major diameter} = 2 * a = 8.2 \text{ mm}, \text{ minor diameter} = 2 * b = 20.4 \text{ mm}$$

Similarly, (b) for elliptical nozzle of aspect ratio 3.2: major diameter =  $2 * a = 7.3$  mm, minor diameter =  $2 * b = 23.4$  mm

**2. Similarly, in series two:**  $D_o = 8$  mm (OD) diameter circular nozzle and elliptical nozzles with same discharge area of  $30.4 \text{ mm}^2$  ( $\Delta = 0.89$  mm wall thickness):

(a). For elliptical nozzle of aspect ratio of 2.4:

$$\text{Major diameter} = 12.7 \text{ mm}, \text{ minor diameter} = 5.3 \text{ mm}$$

(b). For elliptical nozzle of aspect ratio of 3.3:

Major diameter = 15.3 mm, minor diameter = 4.6 mm

**3. Similarly, in series three:**  $D_o = 6.35$  mm (OD) diameter circular nozzle and elliptical nozzles with same discharge area of  $16.4 \text{ mm}^2$  ( $\Delta = 0.89$  mm wall thickness):

(a). For elliptical nozzle of aspect ratio of 1.3:

Major diameter = 7.3 mm, minor diameter = 5.6 mm

(b). For elliptical nozzle of aspect ratio of 1.6:

Major diameter = 8.1 mm, minor diameter = 5.1 mm

### Appendix C: Results for the wind tunnel uniformity measurements

Three velocities, 2.4 m/s, 6.7 m/s, and 10.3 m/s, were chosen to test the uniformities in the wind tunnel. The distribution of cross-wind velocity and variance uniformities are listed below.

#### 1. Distribution of velocity uniformity when the average velocity was 2.4 m/s

##### Horizontal positions 1 to 10

Vertical positions 1 to 16	2.2610	2.3260	2.3620	2.3870	2.3000	2.2150	2.2110	2.3120	2.2910	2.1560
	2.3800	2.3820	2.3740	2.3790	2.3600	2.3620	2.2970	2.4040	2.2900	2.1440
	2.3720	2.3670	2.3700	2.4020	2.3820	2.3570	2.3360	2.4260	2.2860	2.1850
	2.3850	2.3720	2.3860	2.3850	2.3920	2.3590	2.3310	2.4520	2.3150	2.1680
	2.3450	2.3710	2.3820	2.3800	2.3580	2.3590	2.3530	2.4750	2.3800	2.2940
	2.2940	2.2880	2.3780	2.3930	2.3860	2.3780	2.3780	2.4790	2.4020	2.3870
	2.3090	2.3040	2.3730	2.3760	2.4030	2.3980	2.3800	2.4990	2.4030	2.4080
	2.3410	2.3500	2.3740	2.3800	2.3880	2.3960	2.3940	2.4720	2.3900	2.4240
	2.3240	2.3570	2.3960	2.3810	2.3930	2.4050	2.3950	2.4440	2.3860	2.4440
	2.3860	2.3700	2.4010	2.3940	2.4050	2.4150	2.4030	2.4380	2.3970	2.4270
	2.3770	2.3890	2.4140	2.4170	2.3970	2.4030	2.4120	2.4250	2.4170	2.4400
	2.3770	2.3640	2.4170	2.4300	2.4060	2.4260	2.4330	2.4570	2.4020	2.4200
	2.3910	2.3760	2.4020	2.4230	2.4300	2.4360	2.4350	2.4240	2.4060	2.4240
	2.3870	2.3860	2.4020	2.4120	2.4080	2.4130	2.4250	2.4360	2.4070	2.3000
	2.3850	2.3870	2.4040	2.3910	2.4050	2.3960	2.4180	2.4380	2.3880	2.3270
	2.2640	2.2880	2.3470	2.3370	2.3010	2.3030	2.2350	2.2520	2.2630	2.3270

Maximum = 2.4990    minimum = 2.1440    average = 2.3725

## 2. Distribution of variance when the average velocity was 2.4 m/s

**Horizontal positions 1 through 10**

Vertical positions 1 to 16	0.4110	0.4330	0.4760	0.4840	0.4360	0.3580	0.3530	0.4090	0.4070	0.2920
	0.4600	0.4740	0.4850	0.4760	0.4510	0.4230	0.3980	0.4550	0.4000	0.2850
	0.4840	0.4570	0.4780	0.4610	0.4970	0.4410	0.3850	0.4490	0.3920	0.3160
	0.4780	0.4730	0.4740	0.4780	0.4610	0.4340	0.4010	0.4560	0.4070	0.2990
	0.4510	0.4780	0.4890	0.4590	0.4720	0.4390	0.4010	0.4840	0.4820	0.4040
	0.4160	0.4170	0.4780	0.4590	0.5030	0.4640	0.4280	0.4860	0.4740	0.4190
	0.4450	0.4310	0.4700	0.4820	0.4930	0.4640	0.4510	0.5070	0.4550	0.4270
	0.4710	0.4750	0.4530	0.4760	0.4810	0.4560	0.4320	0.4790	0.4640	0.4010
	0.4670	0.4700	0.4690	0.4430	0.4890	0.4360	0.4230	0.4740	0.4850	0.3920
	0.4790	0.4570	0.4900	0.4650	0.4920	0.4370	0.4260	0.4580	0.4650	0.3890
	0.4840	0.4910	0.5080	0.4650	0.4570	0.4480	0.4410	0.4560	0.4880	0.4200
	0.4800	0.4950	0.4990	0.4740	0.4900	0.4780	0.4210	0.5010	0.4950	0.4790
	0.4630	0.4760	0.4890	0.4760	0.4520	0.4670	0.4250	0.4610	0.4860	0.5370
	0.4740	0.4940	0.4700	0.4770	0.4710	0.4760	0.3960	0.4570	0.4890	0.5260
	0.4680	0.5250	0.4720	0.4920	0.4540	0.4620	0.4660	0.4660	0.4720	0.5590
	0.4300	0.4600	0.4620	0.4540	0.4350	0.4380	0.3440	0.3590	0.4230	0.5590

Maximum =0.5590    minimum =0.2850    average =0.4540

### 3. Distribution of velocity uniformity when the velocity was 6.7 m/s

#### Horizontal positions 1 through 10

Vertical positions 1 to 16	5.9810	6.3490	6.4610	6.5340	6.4110	6.4500	6.2230	6.3340	6.3210	5.9370
	6.5820	6.6210	6.7000	6.6910	6.6640	6.5550	6.5710	6.5450	6.5710	6.1350
	6.6210	6.6140	6.7180	6.7330	6.7010	6.6880	6.6820	6.6580	6.6190	6.3960
	6.4660	6.6340	6.7030	6.7000	6.7540	6.7110	6.7220	6.6750	6.6800	6.3980
	6.5830	6.6890	6.6770	6.7330	6.7630	6.7710	6.6990	6.6690	6.5650	6.4140
	6.6680	6.6700	6.7010	6.7300	6.7240	6.7060	6.6970	6.6680	6.7040	6.2490
	6.7050	6.6750	6.6620	6.7460	6.7340	6.7020	6.6740	6.6590	6.6650	6.2420
	6.6520	6.6590	6.7040	6.7170	6.7770	6.7190	6.7260	6.6710	6.6690	6.5430
	6.6610	6.6800	6.7100	6.7710	6.7500	6.7770	6.7440	6.7220	6.7450	6.4300
	6.6620	6.6790	6.6750	6.7870	6.7530	6.7680	6.8030	6.7780	6.7500	6.5500
	6.6900	6.7070	6.7240	6.7040	6.7710	6.7400	6.7470	6.7980	6.7840	6.5720
	6.7010	6.7070	6.7010	6.6620	6.7680	6.7830	6.8020	6.8190	6.7840	6.6460
	6.7130	6.7100	6.7130	6.7200	6.7280	6.7570	6.7790	6.7620	6.7690	6.5310
	6.7240	6.7060	6.7000	6.7180	6.7590	6.7370	6.7560	6.7710	6.6970	6.4330
	6.7090	6.7510	6.7280	6.7410	6.7330	6.7200	6.7660	6.6680	6.5270	6.3970
	6.3190	6.3010	6.5400	6.5430	6.5940	6.5640	6.3700	6.1570	5.9390	5.6980

Maximum = 6.8190    minimum = 5.6980    average = 6.6290

## 4. Distribution of variance when the velocity was 6.7 m/s

**Horizontal positions 1 through 10**

Vertical positions 1 to 16	0.7660	0.6850	0.5810	0.5210	0.5360	0.5100	0.5870	0.5610	0.5310	0.7780
	0.5120	0.4910	0.5000	0.4280	0.4900	0.4510	0.4380	0.4570	0.4430	0.8100
	0.5070	0.4760	0.4610	0.4260	0.4370	0.4800	0.4410	0.4150	0.4150	0.7080
	0.5920	0.5020	0.4410	0.4170	0.4000	0.3950	0.4200	0.4040	0.4620	0.6570
	0.5860	0.5060	0.4550	0.4340	0.4700	0.4460	0.4220	0.4260	0.4820	0.7060
	0.5470	0.5220	0.5860	0.4500	0.4870	0.4460	0.4900	0.4930	0.4530	0.7860
	0.5750	0.5030	0.5410	0.5160	0.4600	0.4270	0.4450	0.4720	0.5130	0.7470
	0.5450	0.5360	0.5300	0.5010	0.4520	0.5040	0.4770	0.4840	0.5380	0.6680
	0.5630	0.5060	0.5000	0.4660	0.4810	0.5240	0.4480	0.4320	0.4870	0.7080
	0.5830	0.4880	0.5560	0.5070	0.5400	0.4990	0.5440	0.5120	0.4810	0.7320
	0.5410	0.4820	0.5380	0.4870	0.5060	0.5570	0.4850	0.4190	0.4880	0.7230
	0.5350	0.4800	0.5190	0.5380	0.5230	0.5720	0.4170	0.3590	0.4700	0.6580
	0.4740	0.5160	0.4880	0.5110	0.4720	0.4820	0.3920	0.3870	0.4390	0.7100
	0.4770	0.4450	0.4740	0.5200	0.4950	0.4490	0.4430	0.3960	0.4490	0.7940
	0.5210	0.4450	0.4540	0.4060	0.4420	0.4060	0.3820	0.4140	0.5240	0.7420
	0.7040	0.6230	0.5350	0.5240	0.4760	0.4800	0.5740	0.6950	0.7600	1.0650

Maximum = 1.0650    minimum = 0.3590    average = 0.5187

## 5. Distribution of velocity uniformity when the velocity was 10.3 m/s

**Horizontal positions 1 through 10**

Vertical positions 1 to 16	10.261	10.316	10.326	10.339	10.335	10.323	10.308	10.282	10.233	9.670
	10.344	10.335	10.338	10.321	10.338	10.336	10.340	10.336	10.332	10.214
	10.332	10.328	10.322	10.318	10.327	10.329	10.337	10.326	10.329	10.264
	10.322	10.314	10.295	10.300	10.314	10.313	10.312	10.336	10.307	10.275
	10.300	10.312	10.291	10.304	10.329	10.314	10.298	10.299	10.298	10.168
	10.291	10.289	10.314	10.318	10.326	10.327	10.297	10.271	10.226	9.907
	10.286	10.305	10.317	10.331	10.325	10.327	10.316	10.277	10.092	9.713
	10.292	10.319	10.325	10.342	10.343	10.329	10.337	10.279	10.238	10.044
	10.295	10.325	10.311	10.309	10.322	10.329	10.333	10.316	10.309	10.079
	10.310	10.313	10.320	10.318	10.313	10.328	10.331	10.329	10.312	10.136
	10.307	10.305	10.329	10.330	10.331	10.319	10.315	10.320	10.326	10.244
	10.254	10.298	10.295	10.317	10.337	10.332	10.324	10.325	10.322	10.269
	10.150	10.244	10.304	10.314	10.318	10.338	10.327	10.335	10.316	10.289
	10.255	10.282	10.306	10.307	10.332	10.322	10.325	10.324	10.307	10.275
	10.270	10.326	10.331	10.341	10.331	10.331	10.328	10.328	10.306	10.211
	10.091	10.128	10.260	10.290	10.274	10.291	10.291	10.224	9.939	9.283

Maximum = 10.3440    minimum = 9.2830    average = 10.2801

## 6. Distribution of variance when the velocity was 10.3 m/s

**Horizontal positions 1 through 10**

Vertical positions 1 to 16	0.0710	0.0300	0.0220	0.0120	0.0160	0.0310	0.0440	0.0830	0.1120	0.6090
	0.0100	0.0130	0.0130	0.0310	0.0130	0.0140	0.0120	0.0180	0.0220	0.1270
	0.0190	0.0190	0.0230	0.0260	0.0220	0.0210	0.0140	0.0260	0.0190	0.0760
	0.0240	0.0290	0.0470	0.0420	0.0360	0.0350	0.0360	0.0150	0.0490	0.0710
	0.0480	0.0260	0.0530	0.0410	0.0220	0.0370	0.0470	0.0470	0.0500	0.2010
	0.0460	0.0510	0.0310	0.0290	0.0240	0.0280	0.0460	0.0800	0.1190	0.5660
	0.0580	0.0370	0.0270	0.0160	0.0250	0.0210	0.0310	0.0710	0.2340	0.5440
	0.0530	0.0250	0.0230	0.0100	0.0120	0.0240	0.0140	0.0620	0.0880	0.2600
	0.0460	0.0350	0.0380	0.0400	0.0420	0.0250	0.0180	0.0300	0.0330	0.2540
	0.0300	0.0450	0.0290	0.0300	0.0410	0.0220	0.0250	0.0180	0.0290	0.2430
	0.0390	0.0460	0.0200	0.0200	0.0190	0.0320	0.0520	0.0290	0.0200	0.0940
	0.0980	0.0610	0.0460	0.0310	0.0130	0.0190	0.0290	0.0210	0.0230	0.0720
	0.1930	0.0950	0.0370	0.0310	0.0270	0.0130	0.0220	0.0140	0.0290	0.0480
	0.0820	0.0600	0.0360	0.0360	0.0170	0.0270	0.0230	0.0220	0.0330	0.0580
	0.0710	0.0200	0.0150	0.0100	0.0160	0.0160	0.0190	0.0190	0.0320	0.1120
	0.2180	0.1960	0.0700	0.0580	0.0690	0.0500	0.0540	0.1400	0.4390	0.7680

Maximum =0.7680    minimum =0.0100    average =0.0646